UNIVERSITI TEKNOLOGI MARA

EFFECTS OF SMALL ANGULAR VARIATIONS IN IMPLANT POSITIONING ON STABILITY OF CEMENTED TOTAL HIP ARTHROPLASTY

ZAITUL ASYIKIN BINTI AZNAN

MSc

June 2026

UNIVERSITI TEKNOLOGI MARA

EFFECTS OF SMALL ANGULAR VARIATIONS IN IMPLANT POSITIONING ON STABILITY OF CEMENTED TOTAL HIP ARTHROPLASTY

ZAITUL ASYIKIN BINTI AZNAN

Thesis submitted in fulfilment
of the requirements for the degree of
Master in Science
(Mechanical Engineering)

Faculty of Mechanical Engineering

June 2026

CONFIRMATION BY PANEL OF EXAMINERS

I certify that a Panel of Examiners has met on 28 October 2025 to conduct the final examination of Zaitul Asyikin binti Aznan on her Masters of Science thesis entitled "Effects Of Small Angular Variations In Implant Positioning On Stability Of Cemented Total Hip Arthroplasty" in accordance with Universiti Teknologi MARA Act 1976 (Akta 173). The Panel of Examiner recommends that the student be awarded the relevant degree. The Panel of Examiners was as follows:

Mohamed Azly Abdul Aziz, PhD
Associate Professor
Faculty of Mechanical Engineering
Universiti Teknologi MARA
(Chairman)

Eli Nadia Abdul Latip, PhD
Senior Lecturer
Faculty of Mechanical Engineering
Universiti Teknologi MARA
(Internal Examiner)

Muhammad Hazli Mazlan, PhD
Senior Lecturer
Faculty of Electrical and Electronic
Engineering
Universiti Tun Hussien Onn Malaysia
(External Examiner)

PROFESSOR DR HJH ZURAEDA BINTI IBRAHIM
Dean
Institute of Postgraduates Studies
Universiti Teknologi MARA
Date: 8 June 2026

AUTHOR'S DECLARATION

I declare that the work in this thesis was carried out in accordance with the regulations of Universiti Teknologi MARA. It is original and is the results of my own work, unless otherwise indicated or acknowledged as referenced work. This thesis has not been submitted to any other academic institution or non-academic institution for any degree or qualification.

I, hereby, acknowledge that I have been supplied with the Academic Rules and Regulations for Post Graduate, Universiti Teknologi MARA, regulating the conduct of my study and research.

Name of Student	:	Zaitul Asyikin binti Aznan
Student ID. No.	:	2022650466
Programme	:	Master of Science (Mechanical Engineering) – CEEM750
Faculty	:	Mechanical Engineering
Thesis Title	:	Effects Of Small Angular Variations In Implant Positioning On Stability Of Cemented Total Hip Arthroplasty
Signature of Student	:	…………………. ………………………..
Date	:	June 2026

ABSTRACT

Total Hip Arthroplasty (THA) is a widely performed surgical procedure in which an artificial prosthesis replaces a diseased or fractured hip joint. An important factor in determining primary stability and long-term mechanical performance in cemented total hip arthroplasty is implant orientation. This study aims to predict the effects of implant positioning at varus and sagittal to implant stability in hip arthroplasty. Using finite element analysis (FEA), this study examined how sagittal and varus angular positioning affected the stress, strain, and deformation responses of a cemented THA. Computed tomography (CT) data was used to reconstruct a three-dimensional femur model, and Abaqus was used to model a cemented THA assembly that included an femur (σ_y= 115 MPa), cement mantle (σ_y= 29 MPa), and hip implant (σ_y= 205 MPa). The findings show that even little variations in implant placement have a significant impact on cement mantle stress and deformation. Maximum stress and deformation occurred at 0.3° (24.62 MPa and 10.29 µm, respectively) in sagittal positioning and -0.25° (20.19 MPa and 10.33 µm) in varus positioning during stair climbing. Implant stability is reflected in the mechanical reaction of the cement mantle, which mediates load transfer between the implant and bone. Although stresses remained below the PMMA yield strength, misalignment of implants may still increase fatigue-related risk, potentially compromising stability.

ACKNOWLEDGEMENT

Firstly, I wish to thank God for giving me the opportunity to embark on my Master and for completing this long and challenging journey successfully. I would like to express my deepest gratitude to all those who have supported me throughout the journey of completing this thesis.

First and foremost, I wish to extend my sincere thanks to my supervisor, Assoc. Prof. Ts. Dr. Abdul Halim Abdullah for his invaluable guidance, expert advice, and constant encouragement throughout this research. His insightful feedback and constructive criticism have been essential in shaping this work.

I would also like to acknowledge Assoc. Prof Dr. Mohd Fairudz Bin Mohd Miswan and Ts. Dr. Shahrul Hisyam Marwan for their support and thoughtful suggestions during the course of this study.

A special thank you to the staff of College of Engineering Postgraduate Studies for providing all the necessary resources and assistance required for this research. Their help has been vital in facilitating my work.

I would like to express my gratitude to my family and friends for their unwavering support, patience, and understanding. Without their encouragement, love, and sacrifices, this achievement would not have been possible.

TABLE OF CONTENTS

LIST OF TABLES

LIST OF FIGURES

LIST OF SYMBOLS

Symbols

°	Degree
E	Young Modulus
N	Newton
ν	Poisson's Ratio
σ_y	Yield Strength
ε	Strain

LIST OF ABBREVIATIONS

Abbreviations

BMI	Body Mass Index
CT	Computed Tomography
DICOM	Digital Imaging and Communications In Medicine
FEA	Finite Element Analysis
HRQoL	Health-Related Quality of Life
OA	Osteoarthritis
PJI	Prosthetic Joint Infection
PMMA	Polymethylmethacrylate
QoL	Quality of Life
TCIA	The Cancer Imaging Archive
THA	Total Hip Arthroplasty
TKA	Total Knee Arthroplasty
VMS	Von Mises Stress

CHAPTER 1
INTRODUCTION

1.1 Research Background

The hip is the joint where the femur and acetabulum meet. It is a ball-and-socket joint that permits flexible and multidirectional movement (Chen et al., 2023). The femur, also called the thigh bone is the largest and longest human bone (Gupta & Ming Tse, 2013).

Osteoarthritis is commonly known as "wear-and-tear" arthritis, age-linked arthritis, or degenerative joint disorder. It entails a gradual deterioration of articular cartilage, the development of subchondral cysts, the formation of osteophytes, the loosening of periarticular ligaments, muscle weakening, and potential inflammation of the synovial lining. This condition impacts the major joints of the lower limbs, such as the hips, which can lead to decreased mobility and significant physical limitations. This can result in a decline in self-sufficiency and a greater reliance on healthcare resources (Lespasio et al., 2018).

Meanwhile, osteoporosis is a condition affecting the skeletal system, marked by the deterioration of bone tissue's microarchitecture and a reduction in bone mass (Clynes et al., 2020). It weakens bone strength and increases the risk of fracture (Cosman et al., 2014). Among elderly individuals, the forearm, hip, and vertebrae are the locations most prone to experiencing fractures (Clynes et al., 2020). It not only affected the quality of life but also increased the financial burden (Carey et al., 2022).
Total hip arthroplasty (THA) involves replacing the hip joint with femoral components that simulate a ball and socket joint in order to reconstruct the hip joint (Marwan et al., 2017). The femoral component consists of the femoral head, neck and shaft segments (Thejeel & Endo, 2022a). It helps to restore function and to improve the quality of life (Zhang et al., 2021). It offers a cost-effective way to make improvements and relieve discomfort (Aznan et al., 2020).

Primary stability is initial fixation and secure attachment of the implant within the surrounding bone immediately after surgery. It is crucial for the long-term success of the implant as well as the overall function of the joint. Dislocation of the implants which commonly occurs in early post-operative is caused by surgical approach, the integrity of the soft tissue envelope and component design (Thejeel & Endo, 2022b). Implant stability in THA influenced by the implant positioning and orientation during primary fixation between the long axis of femur and prosthesis stem. (Yusof et al., 2021). One of the dislocation factors is component malposition (Meneghini, 2018). According to Wera et al., the malposition could occur at the acetabular and femoral components (Wera et al., 2012). The current study will be focusing on two types of malposition which are sagittal and varus. In the hip arthroplasty context, varus malposition refers to the alignment of the implant components in such a way that the femoral component deviates inward or medially from the vertical axis of the femur as shown in Figure 1.1. Sagittal malposition refers to improper alignment or positioning of the components of the implant in the sagittal plane as shown in Figure 1.2.

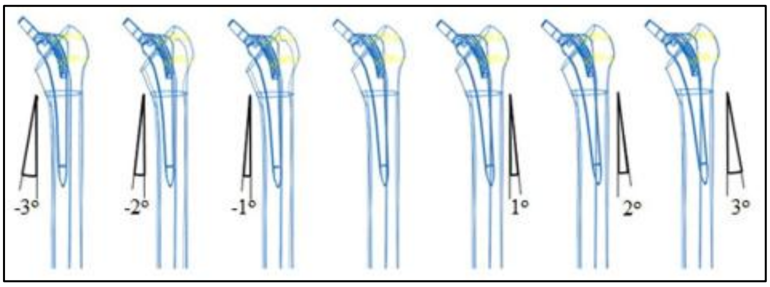

Figure 1.1 Implant Malposition at Varus Plane with Different Angles (Yusof et al.,2021).

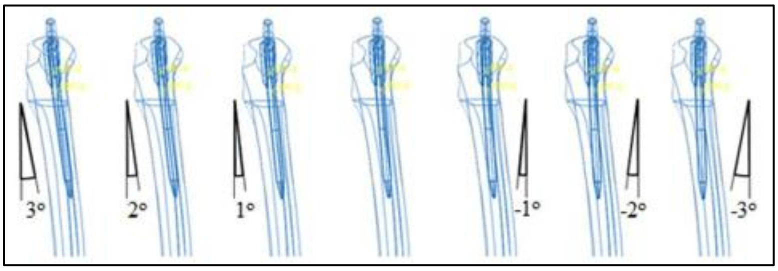

Figure 1.2 Implant Malposition at the Sagittal Plane with Different Angles (Yusof et al., 2021).

There are two types of fixations which are cemented and cementless fixation. Polymethylmethacrylate (PMMA) is used in cemented THA as a grout to create an interlocking fit between the prosthesis and cancellous bone. Meanwhile, bone is biologically fixed to a surface layer of the prosthesis in uncemented hips (Maggs & Wilson, 2017). The current study will focus on cemented fixation. Blythe et al. found the cemented fixation of THA is more cost-effective compared to uncemented (Blythe et al., 2020).

Moarrefzadeh et al found that the Health-Related Quality of Life (HRQoL) is noticeably improved after half and a year after THA, especially when compared to before THA. The analysis of the findings suggests that during the initial six months following THA, enhancements in the physical component of HRQoL were primarily responsible for improving elderly individual life. In the subsequent 12 months post-THA, improvement in both the mental and physical aspects of HRQoL contributed to the overall enhancement of life quality after the surgery (Moarrefzadeh et al., 2022)

1.2 Motivation for This Work

The finding of this study will help to reduce the risk of dislocation as well as the revision of total hip arthroplasty. A study by Khan et al. found that the surgeon experiences more physiological stress during performing revision THA and total knee arthroplasty (TKA) compared to primary THA and TKA. The findings also help to improve the surgical technique and increase the lifespan of the implant. Also, indirectly reducing the cost spent by the patients.

1.3 Problem Statement

Total Hip Arthroplasty (THA) is a surgical procedure that replaces the diseased hip joint with a hip implant. This procedure helps relieve pain, restore normal hip joint function, and improve quality of life. The procedure has shown an increasing trend over the years for treating hip joint diseases reflecting its effectiveness in improving patient mobility.

While this procedure is typically effective, THA is associated with its own set of risks and potential complications such as dislocation, instability, aseptic loosening and infection. Instability can occur due to various factors such as improper positioning of the component, inadequate soft tissue tension, lack of experience and incorrect surgical technique of surgeon. Hip implant instability can lead to discomfort, pain and reduced mobility. This condition leads to the revision of THA which is more complex compare to the initial hip replacement surgery. Also, revision THA procedure requires the patient to make additional financial commitments. To ensure positive long-term outcomes, lower the risk of problems, and improve the overall functionality of the implanted joint, excellent primary stability must be attained.

In the THA scenario, the stability of implant position can be defined as the capability of the implanted femoral component to withstand the mechanical environment under physiological loading, with minimal micromotion at the implant-cement or cement-bone interfaces. The primary stability is commonly determined by analysing the stress and strain distribution in the cement mantle and the surrounding bone under physiological loading conditions. It is crucial to assess implant orientation at the sagittal and varus planes because various orientations affect load transmission and stress-strain distribution.

The goal of providing a highly stable implant position, especially in cemented THA procedures, is critical to ensure effective implant function. This can be attained through a tight fit of the implant at the cement-bone interface.

Despite advances in surgical procedures and implant designs, inconsistencies in implant orientation during hip arthroplasty have been noted, which may compromise the implant's initial stability. The influence of small variations in implant orientation on primary stability remains a subject of ongoing investigation. To address this gap, this study will use finite element analysis to investigate how small deviations in implant orientation affect the implant’s initial stability by analysing the stress and strain distribution in the cement mantle of cemented total hip arthroplasty.

1.4 Research Objectives

The objectives of the study are:

i. To develop a 3D model of femoral bone from the Computed Tomography (CT) scan images.
ii. To reconstruct a finite element model of cemented Total Hip Arthroplasty.
iii. To predict the effects of small variation of angles at varus and sagittal to implant stability in hip arthroplasty.

1.5 Significance of Study

This study is important because it investigates the effects of implant placement on load transfer and stress distribution in cemented hip replacement. Important information is offered to enhance surgical results by analyzing the effects of minor changes in implant angles in the sagittal and varus planes. Improved implant designs and surgical methods may result from the findings, which would increase hip implant longevity and lower the possibility of problems like wear or loosening. Additionally, this study contributes to the field of biomedical engineering by deepening the understanding of stress mechanics in orthopaedic implants, paving the way for future research and clinical advancements.

1.6 Limitation

i) Computed Tomography (CT) scan data was obtained from The Cancer Imaging Archive (TCIA). The data belongs to 60 years old male, has a weight of 78kg and height of 170cm.

ii) This study represents two types of positioning which are varus and sagittal. In the sagittal plane, the implant angles are set at -0.3°, -0.2°, -0.1°, 0.1°, 0.2°, and 0.3°. In the varus plane, the implant angles are -0.75°, -0.5°, -0.25°, 0.25°, 0.5° and 0.75°.

iii) The models are assumed to be homogeneous, isotropic and linear elastic material.

iv) Walking and stair climbing are considered as loading conditions in this study.

1.7 Thesis Scope

The scope of this thesis focuses on investigating the effects of implant positioning on stress distribution and load transfer in cemented hip arthroplasty. It utilizes finite element analysis (FEA) software, specifically Abaqus, to simulate and assess how different implant angles in the sagittal and varus planes influence biomechanical outcomes. Key variables such as stress components (S), Mises equivalent stress (MISES), and translations/rotations (U) are analyzed to provide insights into how implant positioning can impact the performance and longevity of the hip implant.

CHAPTER 2
LITERATURE REVIEW

2.1 Clinical Background

The hip joint is a vital anatomical structure in the human body, consisting of a ball-and-socket assembly created by the rounded head of the femur and the concave acetabulum of the pelvis (Zaghloul, 2018). It allows for a wide range of movements essential for daily activities and physical functions. These movements include six primary plane motions such as flexion, extension, abduction, adduction, internal rotation, and external rotation, as well as various combinations and successive movements (Aghayan & Lee, 2014). Figure 2.1 shows the cross-sectional view of the normal hip joint. Figure 2.2 illustrated the part of the femur which consists of the proximal, shaft and distal. The proximal region is divided into 3 zones, which are A is trochanteric, B is neck and C is head. The femur is the longest and most robust bone in the human body. The length correlates with a striding motion, whereas the strength relates to weight and muscle forces. It consists of an upper end, a shaft, and a lower end. The proximal femur comprises the head, neck, greater trochanter, and lesser trochanter (Singh et al., 2023).

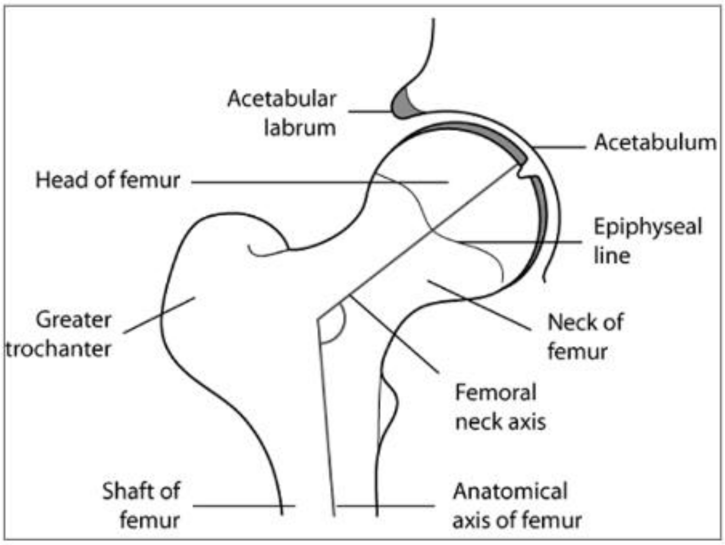

Figure 2.1 Cross-sectional View of the Normal Hip Joint (Zaghloul, 2018)

Figure 2.2 Part of the Femur (Chang et al., 2018).

The Gruen zone system is a widely adopted clinical protocol for evaluating implant status, dividing the bone-implant interface into seven distinct zones as shown in Figure 2.3. Currently, clinicians manually identify these zones and the implant boundary, a process that is time-consuming and prone to errors and inconsistencies. Automating this process could improve efficiency, accuracy, and patient outcomes. Although some studies have attempted to automate hip implant segmentation, there is currently no research focused on automating the identification of Gruen landmarks specifically in radiographs of total hip arthroplasty (Alzaid et al., 2024). Zone 1 refers to the top of the stem in bone down to the inferior point and Zone 2 refers to the end of Zone 1 to halfway to the tip point. Zone 3 refers to the end of Zone 2 to the tip point meanwhile below the tip point refers as Zone 4. Zone 5 is the opposite of Zone 3 meanwhile Zone 6 is the opposite of Zone 2. Zone 7 is opposite to Zone 1. Alzaid et al introduced the new landmark of each zone as shown in Figure 2.4.

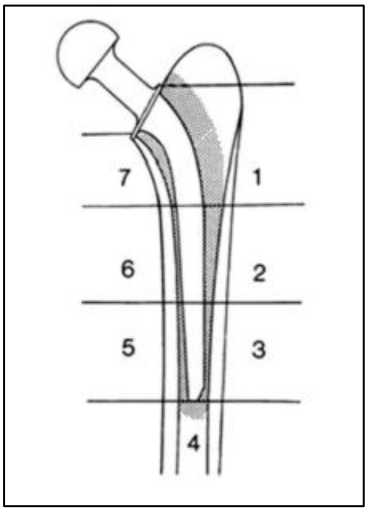

Figure 2.3 Gruen Zones of Femur (Alzaid et al., 2024)

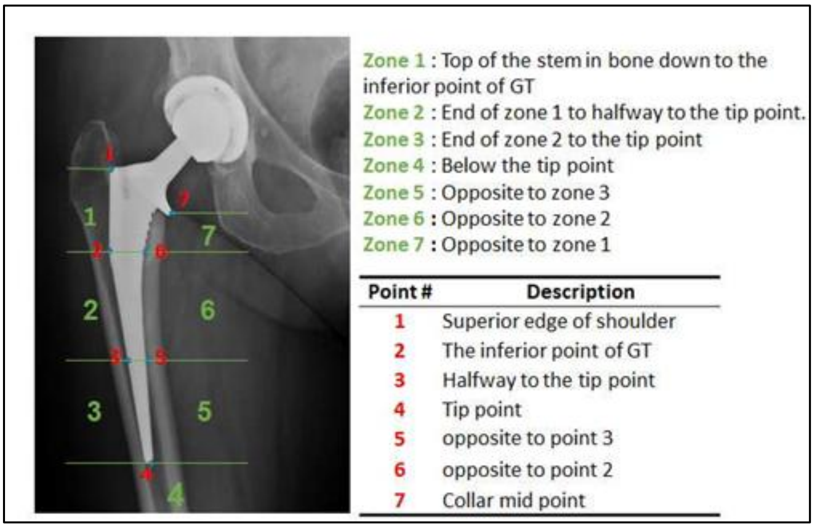

Figure 2.4 Modified Definition of Gruen Zone (Alzaid et al., 2024)

The Total Hip Arthroplasty (THA) is a surgical technique in which an artificial hip implant prosthesis completely replaces the diseased or broken hip. It involves an acetabular and a femoral component that need secure attachment to the pelvic and femoral bones. The primary goal is to achieve optimal positioning for the effective functionality of the prosthesis. The acetabular component, referred to as the acetabular cup, may consist of a single piece adhered with cement to the acetabulum, or it may comprise two parts: an outer dome secured by impaction (known as "press fit") and/or screws, along with an inner component (referred to as "liner" or "insert") housed within the outer component. As for the femoral component, it typically consists of a stem that can be cemented or press-fitted without cement, and a head that attaches to the stem. (Torini et al., 2023). Total hip arthroplasty is indicated for patients with hip osteoarthritis, femoral head necrosis, and refractory joint pain, with factors influencing the need for surgery including patient characteristics like age, body mass index (BMI), and comorbidities (Panwar et al., 2023). THA typically occurs in elderly individuals (Gómez Alcaraz et al., 2021; Moarrefzadeh et al., 2022). However, previous study found that THA is becoming more prevalent among a younger demographic, specifically individuals aged between 40 and 60 years, with a rising demand and low revision rates, especially in those with osteoarthritis and higher surgeon volumes (A. G. Chen et al., 2023). Due to rising accident rates and unhealthful lifestyle choices, the rate of total hip prostheses is likewise rising in modern society (Belwanshi et al., 2022). Shichman et al. predict an increase in THA procedures of 176% by 2040 and 659% by 2060 (Shichman et al., 2023). Understanding femur anatomy and Gruen zone is important to determine the load transfer and mechanical stability.

2.2 Implant & Stability

Implant fixation is defined as the techniques employed to securely affix a medical implant to bone or adjacent tissue, preserving its stability and functionality within the body. There are two types of fixations which are cemented and cementless. Cement in THA act as a grout to create an interlocking fit between the prosthesis and cancellous bone. Figure 2.5 refers to the schematic of cemented hip illustrating the layered configuration of its components. Polymethylmethacrylate (PMMA) works like a dynamic filler, occupying the space between the implant and bone. It helps to stabilize the implant and allows the load to be smoothly transferred from the implant to the surrounding bone tissue (Douglas et al., 2021). Meanwhile for cementless fixation the bone is biologically fixed to a surface layer of the prosthesis in uncemented hips (Maggs & Wilson, 2017).

Cemented implants can be categorized into taper-slip (force-closed) and composite beam (shape-closed). Taper slim are collarless and have a highly polished surface finish. Cemented sockets are typically polyethylene cups with thick walls. Commonly, they contain grooves on the outer surface to promote stability within the cement mantle and an embedded wire marker to enable positioning to be assessed on postoperative X-rays (Maggs & Wilson, 2017). It is believed that cemented fixation is less risk of periprosthetic fracture, loosening and revision (Thejeel & Endo, 2022a).

Cemented hip stems have the advantage of less rehabilitation time as the patient can walk without help immediately after surgery (Singh & Harsha, 2016).

A study by X. T. Chen et al., shows that cemented fixation in THA is related to lower probabilities of periprosthetic fractures at various postoperative time points which are 30, 90, and 180 days, compared to cementless fixation (X. T. Chen et al., 2023). Additionally, previous research indicates that cemented and hybrid THA procedures result in lower blood loss compared to cementless THA, although this does not necessarily translate to lower transfusion rates (Meißner et al., 2023). As a result, the biomechanical consequences of small deviations in cemented implant orientation and their potential contribution to long-term failure mechanisms remains unclear. This highlights the need for detailed finite element–based analyses to evaluate cement mantle stresses and implant stability under realistic loading conditions. Finite element-based research are necessary to close this knowledge gap since the impact of these variances on the distribution of cement mantle stress and long-term implant stability under functional loading conditions has not been fully examined.

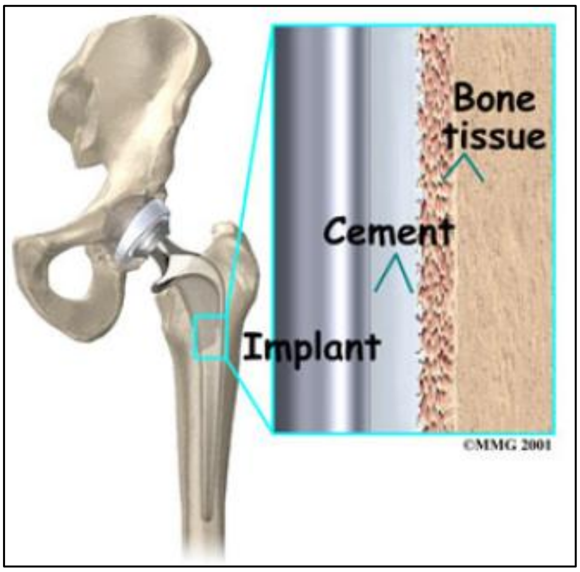

Figure 2.5 Schematic of Cemented Hip Arthroplasty (Hung et al., 2019)

Revision of THA is a technique in which an implanted hip prosthesis is removed and replaced with a new one. The number of revision THA procedures performed each year grew by 28% from 2012 to 2018 (Upfill-Brown et al., 2021). While THA is performed with great success, there are risks with the procedure; PJI occurs from 0.6% to 2.2%, which can lead to serious complications and possible revision surgery (Fowler et al., 2019). Previous studies have identified instability as one of the common indications of revision of total hip arthroplasty (Shichman et al., 2022; Upfill-Brown et al., 2021). Although, according to Shichman et al., aseptic loosening is the main common indication of revision hip arthroplasty, followed by the dislocation and instability of implants. (Shichman et al., 2022). Additionally, patients with osteonecrosis, post-traumatic osteoarthritis, and femoral neck fractures are more likely to have revision within five years of original THA, with infection and instability being prominent causes (Oltean-Dan et al., 2022).

A study by Patel et al. found the most frequent cause of revision of THA appears to be dislocation and instability (21.8%), followed by mechanical loosening (19.74%), mechanical complications (17.38%) and infection (15.10%). The findings were influenced by the demographic and comorbidity profile of the patients. Most patients (42.33%) required revision of all components, which is the most common type of revision (Patel et al., 2023). Experience and surgical techniques of surgeons also contribute to implant failure (Anil et al., 2022). Ravi et al. concluded that patients were more likely to experience dislocation and early revision if their operation was performed by a surgeon who had performed 35 or fewer similar procedures in the year prior to the index procedure (Ravi et al., 2014). There are many THAs performed each year which now exceeds one million world-wide, which makes it important to look at these complications, and find ways to improve surgical technique in order to provide a higher quality of life for patients (Fontalis et al., 2021; Fowler et al., 2019).

There is a study that investigates the unstable of total hip arthroplasty. The contributing factors of the implant dislocation are including component malposition, extra-prosthetic impingement, polyethylene wear, abductor muscle incompetence, altered neurologic or proprioception about the hip from neurologic disease or spinal disease, and less frequently an adverse local tissue reaction from metal hypersensitivity or infection (Meneghini, 2018). This study uses a CT scan to access the acetabular and femoral positions which are acetabular abduction angle, anteversion, and femoral component anteversion. However, the current study will predict the implant malposition at the varus and sagittal position.

According to Sirignano at al., instability at the one-year mark subsequent to primary total hip arthroplasty saw a decrease from around 4% in the year 2000 to 2.3% in 2010 and further down to 1.6% in 2018. The primary reason behind the need for revision surgery was identified as infection (18.6%), followed by periprosthetic fracture (14%), mechanical loosening (11.5%), and instability (9.4%). Groups at higher risk for instability post-total hip arthroplasty continue to encompass individuals of older age, those with elevated Charlson index scores, individuals with obesity, patients with lumbar spine issues, as well as those with neurocognitive disorders (Sirignano et al., 2023).

Dislocation commonly occurs during the early phase of THA. It happens when the forces on the implant head, which are mostly generated by impingement, exceed the soft tissue tension or resistance helping to limit the head's excessive motion. Patient, surgical technique and implant are the possible cause of dislocation (Kobayashi & Yukizawa, 2023). Dislocation is a recognised complication which can negatively affect health-related QoL, and this effect is especially true for patients undergoing primary THA, as patient-reported outcomes suggest that hip-related QoL worsens after dislocation (Hermansen et al., 2022). In addition, dislocation increases healthcare costs and resource utilization with median costs significantly increasing for patients who require revision surgery (Galvain et al., 2022). Additionally, several studies have established that dislocation can negatively impact patient-reported outcomes, given the need to implement effective management strategies (Galvain et al., 2022; Hermansen et al., 2022).

Anil et al. focus on aseptic loosening in THA. Aseptic loosening is the failure of the fixation of a prosthetic component in the absence of infection. Aseptic loosening is caused by ineffective initial fixation, as well as mechanical and biological loss of fixation (Anil et al., 2022). A long-term follow-up of an uncemented hydroxyapatite coated femoral stem reported a survival rate of 98.4% at 20 years for aseptic loosening with a single case revised for this reason. (Yee et al., 2024). The trabecular oriented pattern (top) acetabular cup had a 90.5% survival rate with aseptic loosening being a leading cause of revision (Mosconi et al., 2021). In a study of tapered titanium femoral components, the survivorship for aseptic loosening was exceptionally high at 30 years (99%) (Mclaughlin et al., 2023).

Misalignment is one of the causes of total hip arthroplasty failure. The seminal contribution has been made by Yusof et al. in promoting implant stability by predicting the effects of varus and sagittal positioning. It has been shown that the stress in varus positioning is higher than in sagittal positioning during stair-climbing condition (Yusof et al., 2021). A critical open question is whether the cemented hip arthroplasty will have the same result in both positioning.

Marwan et al. also investigated the stress distribution in cementless THA femur during walking and stair climbing at straight, varus +3° and varus -3° malposition. This study also found the maximum Von-misses in intact femur is higher during stair climbing, compared to walking conditions. Misalignment of the stems can lead to increased deformation around the fixation site, particularly in cases with a varus angulation of -3˚ (Marwan et al., 2017). However, the effects of stem malalignment due to sagittal orientation parameters, particularly with regard to the stresses in the cement mantles, on cemented THA implants are not well clarified biomechanically.

Another previous study is focusing on two types of misalignments which are retroversion and anteversion on cemented hip arthroplasty (Aznan et al., 2020). Loading condition that has been investigated in this study includes walking that (normal), and stair climbing (highest force activities). This study shows that retroversion has the highest magnitude of stress during walking and stair climbing. Stair climbing has the highest stress magnitude as compared to walking because the activity requires more force. The highest stress distribution is located at the distal region due to highly concentrated loading applied in hip joint contact. This study was limited to extraversion and anteversion conditions. The similarity with the current study is both studies are focusing on the cemented THA.

As has been reported in the previous literature (Belaïd et al., 2022), the stress decreased as the valgus angle (positive angle) increased meanwhile, the stress increased when the varus angle (negative angle) increased. The mean maximum principal stress at the proximal femur was 12.56MPa (SD=±4.14), 9.44MPa (SD=±3.24) and 6.48MPa (SD=±2.49) for -10°, 0° and +10° respectively. Meanwhile, the mean minimum principal stress was 17.11MPa (SD=±4.59), 15.11MPa (SD=±4.08) and 12.69MPa (SD=±3.5) for -10°, 0° and +10° respectively. Hwang et al also performed finite element analysis to find the maximum principal stress (MPS) and maximal tensile stress. When the mechanical axis was applied from the valgus to varus alignment, there was an increase in MPS and a distal movement of the femoral weakest point. In addition, this study found that peak strain position and magnitude were influenced by the lower limb geometry (Hwang et al., 2022).

Furthermore, the effects of the deviations, often occurring during surgical practice, with regard to the relatively high precision necessary for implants not initially surpassing the yield abilities of the implant material, have not drawn much attention, although they may contribute to the development of regions with high stresses due to mismatch orientation. Thus, there is a need for a comprehensive finite element analysis on the effects of implant orientation on the cemented THA under high-load activity.

2.3 Loading and Boundaries Conditions

Walking and the act of climbing stairs are biomechanical loading conditions that provide critical insight into the considerations of total hip arthroplasty (THA) research, particularly regarding their consequences on still other conditions, including osteoarthritis (OA) of the hip. As a weight-bearing activity, it is one of the important functional tasks. Studies suggest that performance in doing the task of stair ascent and descent correlates with severity in cases of hip OA thus, influences some decisions regarding THA (Stasi et al., 2023). Such activities are essential for evaluating joint power generation and functional recovery following surgery, as they represent aspects of daily living most affected by hip osteoarthritis (Queen et al., 2019). Furthermore, Yusof et al. considered stair climbing as a loading condition in their analysis to predict how varus and sagittal implant positioning might influence implant stability in cementless hip arthroplasty.(Yusof et al., 2021). Similarly, Aznan et al. considered both loading conditions when estimating the effects of stem malalignment on bone adaptation(Aznan et al., 2020).

Walking and stair climbing are primary activities that influence the wear and tear of total hip arthroplasty (THA) components since various loading conditions will influence micromotion and wear rates. Previous study examined the effects of various factors on hip implant wear rates, highlighting the importance of considering daily life activities in wear predictions (Alpkaya et al., 2024). Stair climbing creates larger micromotion at the proximal and distal ends of hip stems, which may affect implant initial fixation and long-term stability (Kanaizumi et al., 2022). Normal walking along with cycling has been shown to dramatically increase the volumetric wear rates of THA components, with cycling further raising wear by 67% (Toh et al., 2023). Also concerning is stress shielding, whereby the excessive loading of the prosthesis leads to a reduction in bone density, especially in younger patients with a potential need for a second surgery (Gabriele et al., 2022).

While walking and climbing stairs are acknowledged as essential functional loading conditions for assessing the performance of total hip arthroplasty (THA), most research to date has concentrated on cementless implants, wear prediction, or bone adaptation outcomes. Although these activities have been demonstrated to affect micromotion, wear rates, and stress shielding, little is known about their biomechanical effects on cemented THA, especially with regard to cement mantle behaviour and implant stability.

Additionally, while walking and stair-climbing loads have been used to study implant malalignment and positioning, these analyses seldom incorporate the combined effects of everyday activities, cemented fixation mechanics, and minor variations in implant orientation within a single framework. Therefore, it is still unclear how physiologically relevant loading conditions affect implant micromotion, cement mantle stress distribution, and long-term stability in cemented THA.

2.4 Finite Element Analysis

Additionally, there is a review article aimed to identify the major criteria and approaches that Finite Element Analysis (FEA) can implement to obtain superior performance from hip implants (Belwanshi et al., 2022). FEA helped numerous studies in identifying the critical areas where fatigue, fractures, mechanical stresses, and strains are most likely to occur and cause hip implant failure (Belwanshi et al., 2022). Previous study implemented FEA to obtain the maximal principal stress in the proximal femur in varus and sagittal positioning. FEA allows to determine the stress distribution and load transfer in the femoral shaft (Yusof et al., 2021). Belwanshi et al. also emphasizes the benefits of using FEA, such as its ability to optimize the geometry and shape of an implant without compromising its mechanical behaviour or increasing implant weight. Also, FEA helps to perform quick testing of the specimen with different materials (Belwanshi et al., 2022). As for the current study, FEA will be performed to predict the effects of implant malposition at varus and sagittal to implant stability in hip arthroplasty in Abaqus software.

This study utilized InVesalius 3.0 software to convert the 2D CT scan image to 3D model. InVesalius is an open -source software that has user-friendly graphical interface. It allows users to perform the manual segmentation, thresholding and watershed techniques (Paulo Amorim et al., 2015). Previous researches has demonstrated the utilization of InVesalius for the reconstruction of 3D models from DICOM images (Mendonça et al., 2023; Stocco et al., 2022). Moreover, Ruppert et al were using InVesalius to build a hand tracking and gesture recognition system based on the Kinect device. The surgeon is allowed to control this software through hand gestures performed in the air. (Ruppert et al., 2012).

Table 1 shows the comparison the past studies related to the positioning and orientation of femur and THA. The combination effects of small angle variations of hip implant at various varus and sagittal orientation of cemented total hip arthroplasty remain little investigated.

Table 1
Comparison of Previous Studies

Previous studies	(Marwan et al., 2017)	(Yusof et al., 2021)	(Aznan et al., 2020)	(Belaïd et al., 2022)	(Hwang et al., 2022).
Type of positioning	Straight, varus +3° and varus -3°.	varus and sagittal(-1°, -2°, -3°, 1°, 2°, 3°)	normal, anterversion, retroversion	Neutral varus, valgus	neutral, varus, and valgus
Loading condition	Walking & stair climbing	Stair climbing	Walking & stair climbing	Standing	standing
Type of fixation	Cementless	Cementless	Cemented	Femur only	Femur only
Critical area	Medial distal end of femur	Within the hip implant until the distal end of the prosthesis	Cement mantle	Femoral neck	Shaft of femur
Research gap	Limited to cementless THA only without considering the sagittal orientation	Limited to cementless THA without considering the walking activity as loading condition	Considering the cemented THA but different type of orientation	Focusing on varus malaligment on femur only during standing activity	Loading condition limited to walking and stair climbing

CHAPTER 3
RESEARCH METHODOLOGY

3.1 Introduction

This chapter consists of the methodology implemented in this study to achieve all objectives. A three-dimensional (3D) femur model was developed from a computed tomography (CT) scan image. Then, the Finite Element model for the femur, stem prosthesis and cement mantle was reconstructed. The research was conducted in collaboration with the University of Malaya, which provided essential data for the investigation. The research methodology involved multiple phases, including the assembly of all components of cemented hip arthroplasty using advanced simulation software, Abaqus. Finite element analysis (FEA) was then applied to simulate the mechanical behaviour of the hip joint. This approach made it possible to thoroughly investigate stress distribution and pinpoint areas of concern under different loading conditions, providing a comprehensive view of the system's performance. Figure 3.1 shows the flow chart of this study.

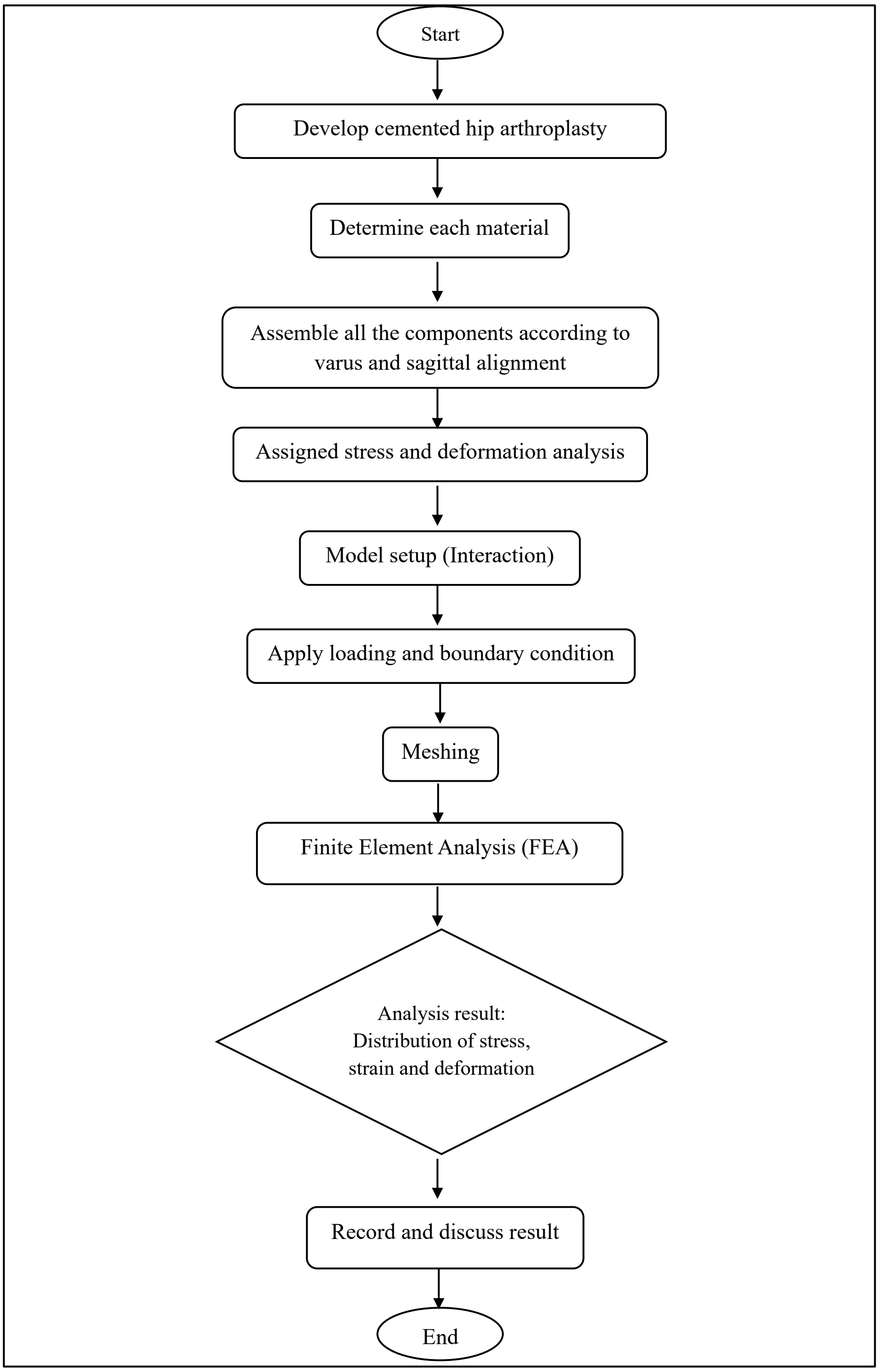

Figure 3.1 Flow Chart

3.2 Generation of Femur Model

InVesalius 3.1, an open-source software, was used to transform 2D CT scan images into detailed 3D models. Figure 3.2 shows a 2D CT image of the whole body. Before creating the 3D model, the femur was isolated through a process called segmentation. Segmentation involves identifying and separating specific parts of the scan, such as bones or organs. This was done by selecting regions based on their brightness or using tools to clearly define the areas of interest. In this case, the focus was on isolating the femur for detailed study which was represented in yellow colour as shown in Figure 3.2.

The final 3D model of the femur, shown in Figure 3.3, represents the segmented area in a clear and refined form. To ensure accuracy, the model's surface has been smoothed, and any unwanted artifacts from the segmentation process have been removed. These adjustments help create a clean and precise representation of the femur, making it more suitable for visualization and analysis. Figure 3.3 shows the model of intact femur with an approximate length of 454 mm.

This process highlights how InVesalius effectively converts medical imaging data into 3D models, providing a better way to study and understand anatomical structures.

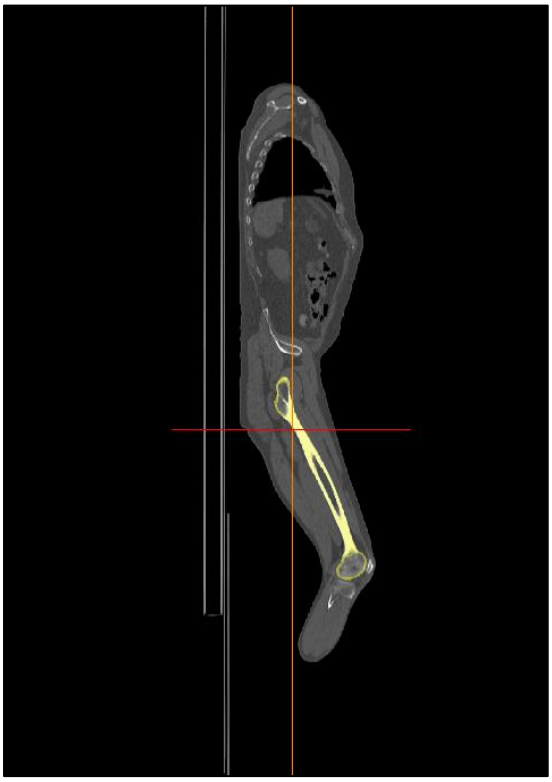

Figure 3.2 Segmentation of Femur.

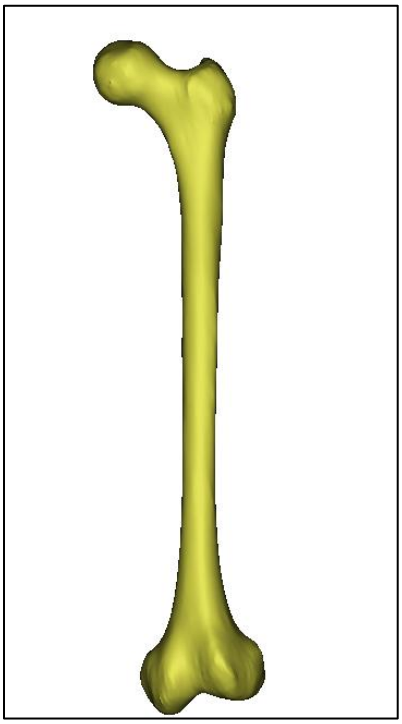

Figure 3.3 3D Model of Intact Femur

3.2.1 Validation of Femur

The femoral model employed in this study was validated against the experimental findings reported by Simoes et al (Simões et al., 2000). Model validation was achieved by comparing the strain distribution within the intact femur to that observed in the experimental study. The loading (X= -263.8N, Y= -1841.3N, Z= -433.8N) and boundary conditions were applied as shown in Figure 3.4(a). The measurement locations have been assigned as M1-M5 and L1-L5 in the medial and lateral planes respectively as shown in Figure 3.4(b). The half of the femur was used to reduce the time of analysis. The similarity of strains and its magnitude at points of interest indicates the credibility of the created model to represent the biomechanical behaviour of the femur.

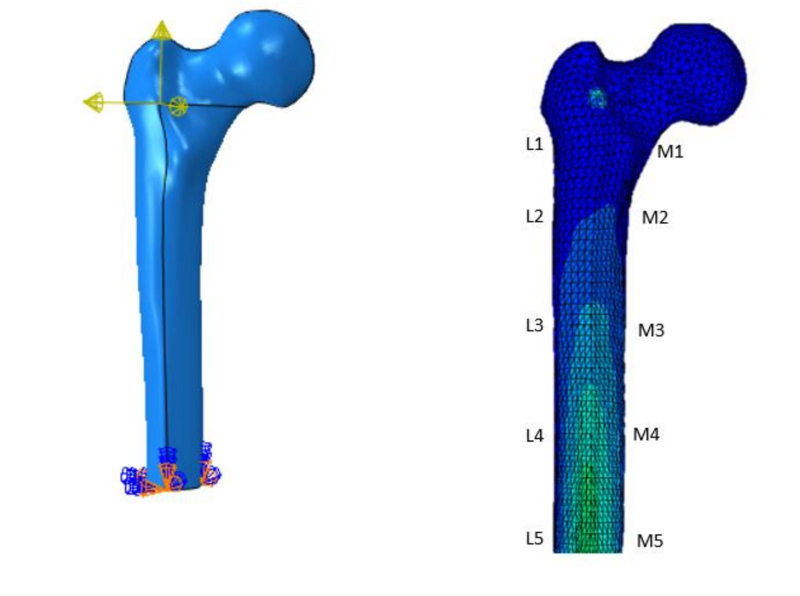

(a) (b)

Figure 3.4 (a) Location of Loading and Boundary Condition. (b) Measurement Location of Strain Distribution.

3.2.2 Convergence Study

A convergence study was conducted to ensure the accuracy and reliability of the finite element analysis (FEA) in evaluating stress distribution in the femur of Total Hip Arthroplasty (THA). In finite element analysis (FEA), greater precision in the solution is achieved with the utilization of finer mesh elements. Nevertheless, this comes at the cost of increased computational time, necessitating a convergence analysis to determine the optimal mesh size for accurate FEA results (Mohamad Azmi et al., 2024).

To achieve this, models with element sizes of 4 mm, 4.5 mm, 5 mm, 5.6 mm, and 6 mm were analyzed. The FEA focused on evaluating the Von Mises Stress, with specific node groups extracted from each model to assess convergence, as illustrated in Figure 3.5. Convergence was determined by comparing the percentage difference in stress values at each node between consecutive mesh sizes. If this difference was below 5%, the model was considered converged. As shown in Figure 3.6 , the results exhibited a consistent trend across all element sizes, with stress values decreasing progressively from node 1 to node 6. The mesh convergence analysis confirmed that the percentage differences between 4.5 mm and 5 mm were below 5%, leading to the selection of 5 mm as the optimal element size. This ensures that the analysis achieves a balance between computational efficiency and result accuracy, providing reliable insights into stress distribution, bone remodelling and implant stability.

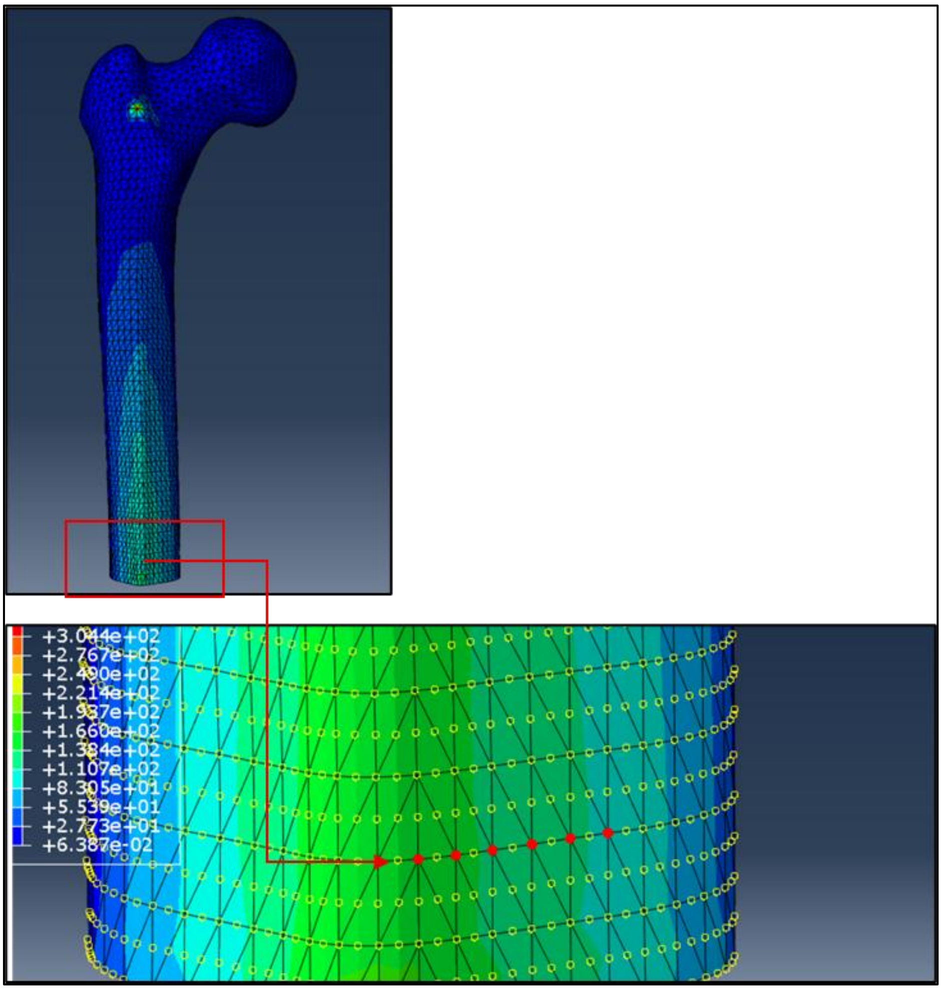

Figure 3.5 Group of Nodes

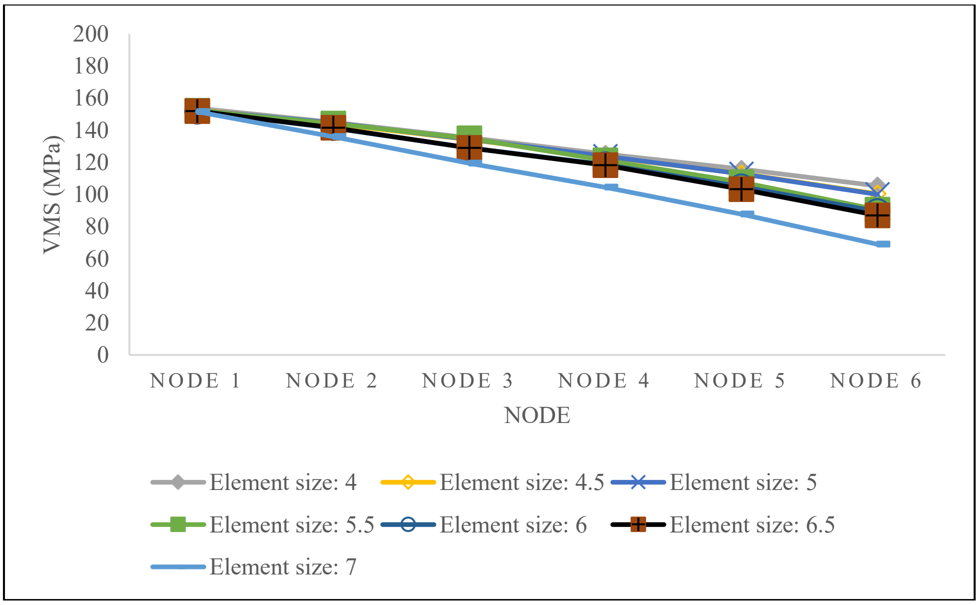

Figure 3.6 Magnitude of Equivalent Von Miss Stress for 6 Selected Nodes

3.3 Generation of Cemented Total Hip Arthroplasty of Finite Element Model

After the development of 3D model, finite element model was reconstructed in Abaqus software. CAD model was imported into the software. As shown in Figure 3.7, this study used a cemented THA model that consisted of three main components, which are hip implant, cement mantle, and femur with approximate length of 166.15mm, 148.29 mm and 243.06 mm, respectively. In this study, only the upper region of the femur was utilized to minimize analysis time. The femoral head was removed in order to allow for the accurate insertion of the hip implant into the femoral canal. For this study, CT scan data was obtained from The Cancer Imaging Archive (TCIA). The bone cement model has a distal thickness of 20 mm and a surrounding thickness of 2 mm (Ahmad et al., 2020).

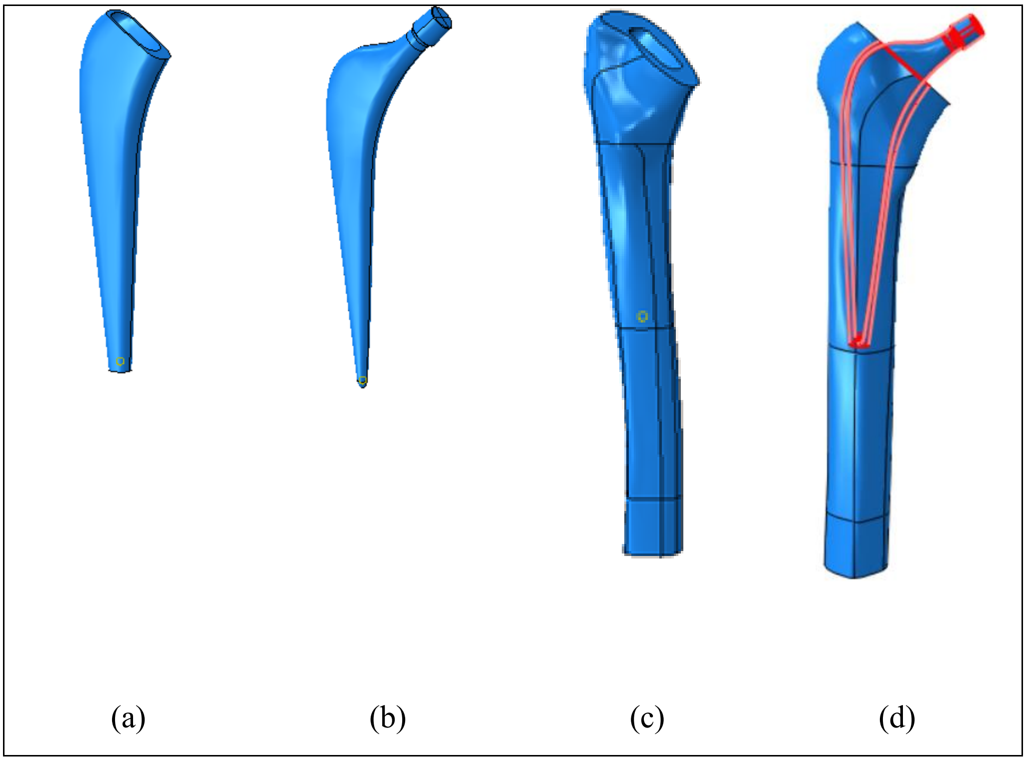

Figure 3.7 (a) Cement Mantle (b) Implant (c) Femur (d) Assembled of THA

.

3.3.1 Material Properties

To achieve an accurate model, material attributes were designated for each component. In this study, the femur was made of cortical bone, whereas polymethyl methacrylate (PMMA) material was used for the cement mantle (Ahmad et al., 2020). The hip implant was assumed to be made of biocompatible stainless steel, which was known for its remarkable resistance to corrosion and superior strength (Olugbade, 2022). All materials were assumed to be homogenous, isotropic and linear elastic. Table 1 shows the material properties that will be used in the finite element model.

Table 2
Material Properties (Lamvohee et al., 2014).

Component	Materials	E(GPa)	Poisson Ratio, ν	Yield Strength, σ_y (MPa)
Femur	Cortical bone	17	0.3	115
Cement Mantle	PPMA	2	0.3	29
Hip Implant	Stainless steel	200	0.28	205

3.3.2 Mesh

Generate the mesh for the complete hip arthroplasty model to ensure that the computational algorithms yield robust and reliable numerical results (Yusof et al., 2021). By integrating global and local seed parameters and employing tetrahedral elements, the meshing process is designed to generate an optimized mesh that accurately represents the structural complexities and loading conditions of the cemented hip arthroplasty model.

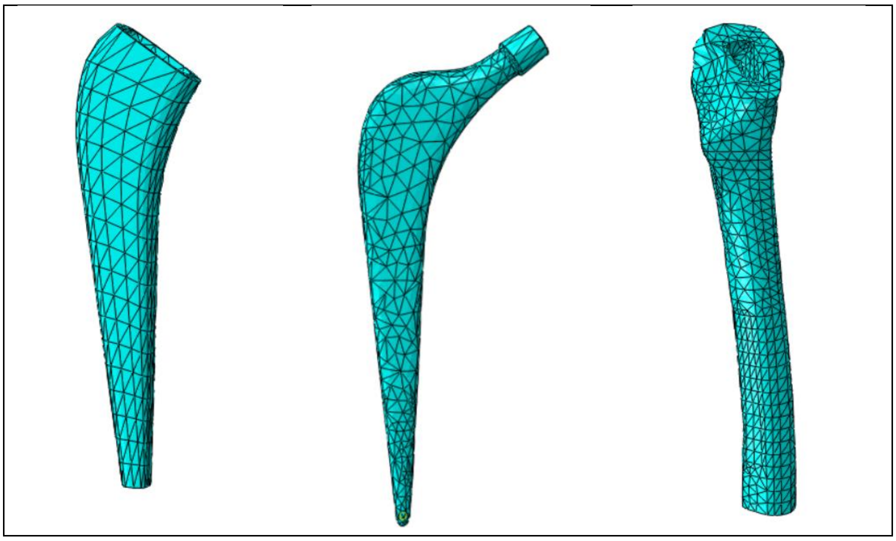

Figure 3.8 Meshing of (a) Cement Mantle (b) Hip Implant (c) Half Femur

3.3.3 Assembly & Interaction

The femur, cement mantle, and implant were combined using the Assembly feature in Abaqus. Based on Figure 3.9, an instance is created for each model component and a dependent part instance was selected. These instances are carefully positioned and aligned to replicate the arrangement of the components as they would be during surgery. Coincidence Point Constraint was used to arrange the component.

In the interactions stage, the model setup was defined to iteratively analyze stress distribution and load transfer within the hip model. Surface contact constraints were essential to ensure accurate biomechanical simulations for cemented hip arthroplasty in the finite element analysis (FEA). The "Tie" function in Abaqus was utilized by established surface to surface contact to secure the connections between the femur and cement mantle, as well as between the cement mantle and the hip implant component as shown in Figure 3.10. Figure 3.11 show the combination of individual models that generates the complete THA model.

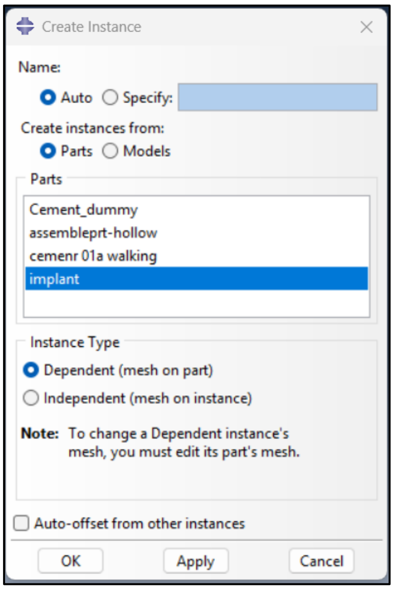

Figure 3.9 Create Instance in Abaqus

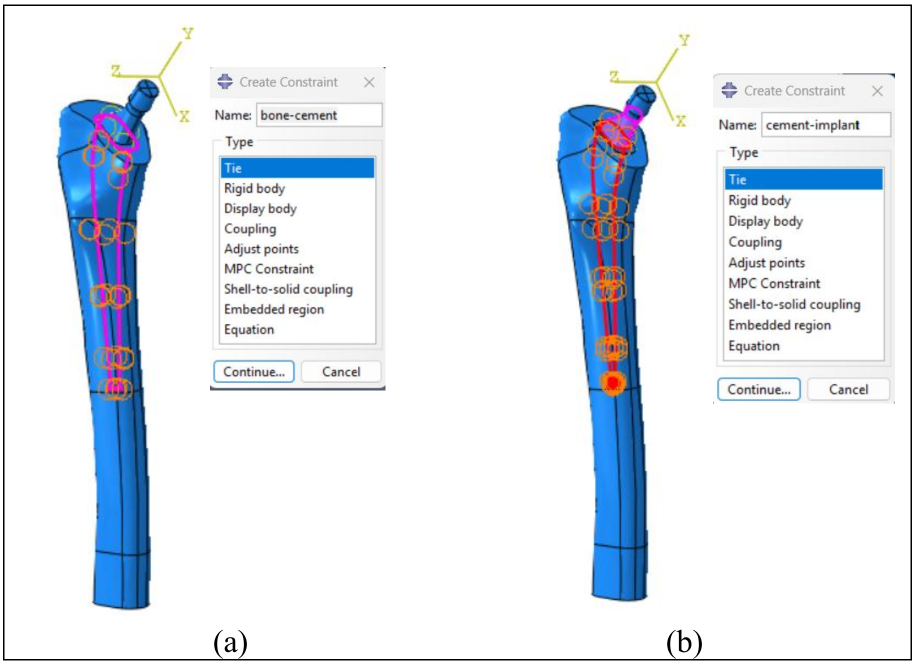

Figure 3.10 Interaction Between (a) Femur and Cement Mantle (b) Cement Mantle and Hip Implant

Figure 3.11 Model of Total Hip Arthroplasty

3.4 Configuration of Different Implant Positioning at Varus and Sagittal Plane

The 'Step' phase employs Abaqus software to assess the effects of implant positioning in cemented hip arthroplasty. Outputs include S (stress components and invariants), MISES (Mises equivalent stress), and U (translations and rotations).

3.4.1 Sagittal and Varus Positioning

Figure 3.12 shows the implant positioning at various angle at the varus plane meanwhile Figure 3.13 refers to the implant positioning at the sagittal plane.

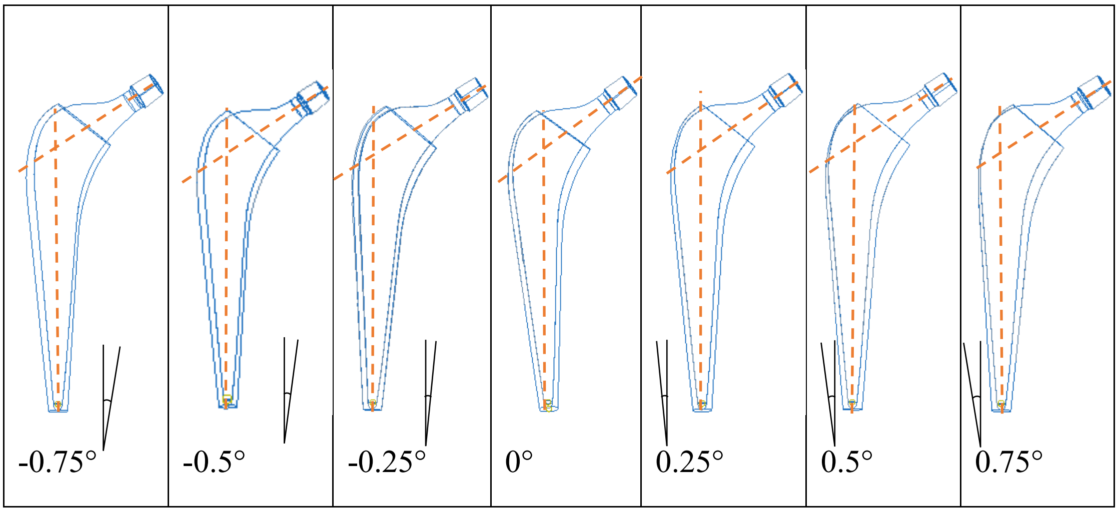

Figure 3.12 Implant Positioning in Different Angles at the Varus Plane (Anterior View).

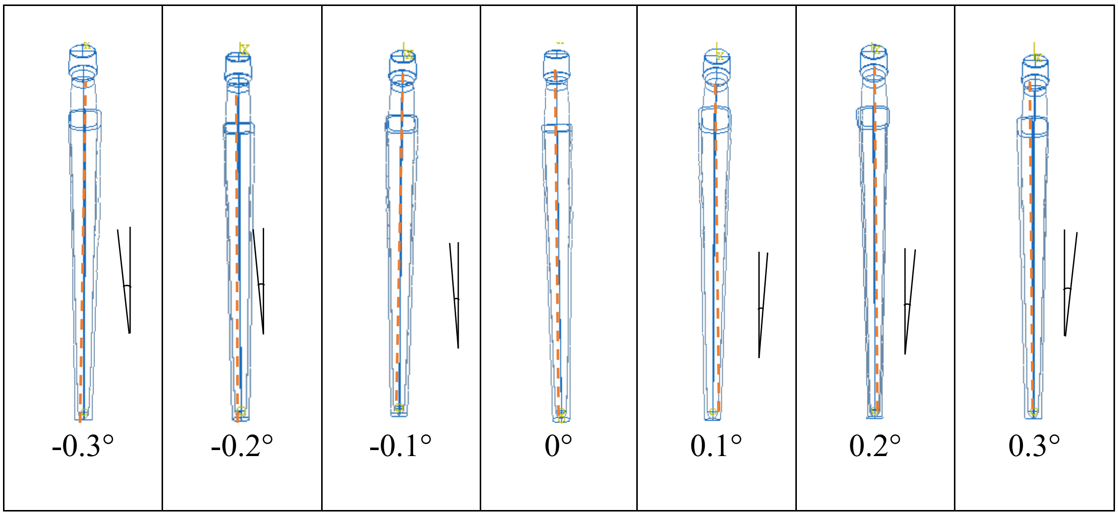

Figure 3.13 Implant Positioning in Different Angles at the Sagittal Plane (Medial View).

3.4.2 Loading and Boundary Conditions

Forces and boundary conditions were implemented by mapping the walking and stair-climbing activity profile onto the hip model. Two forces have been exerted on the femur model, representing hip loading (P1) and muscle reaction (P2), with a fixed load positioned at the lower end as shown in Figure 3.14(a). Table 3 shows the magnitude of force for both loading conditions.

Table 3
Magnitude of Force for Walking and Stair Climbing (Aznan et al., 2020)

Loading condition	Point	Forces (N)	X	Y	Z
Walking	P1	Hip Joint Contact	-263.8 N	-1841.3 N	-433.8 N
	P2	Abductor	34.5 N	695 N	465.9 N
Stair climbing	P1	Hip Joint Contact	-486.8 N	-1898.3 N	-476.4 N
	P2	Abductor	231.4 N	682.1 N	563.1 N

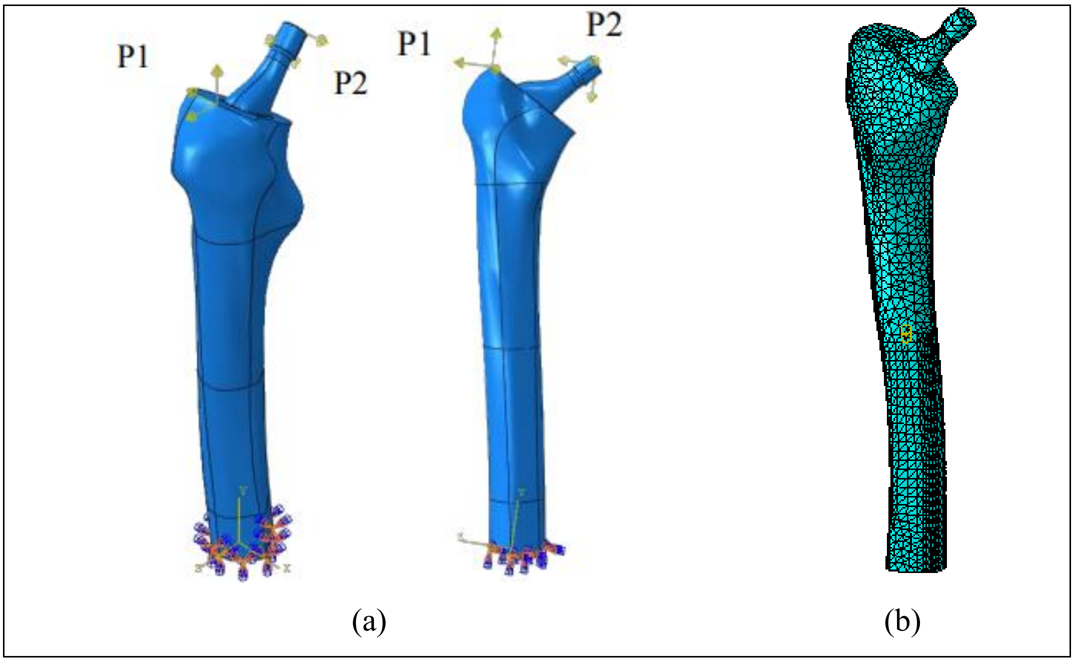

Figure 3.14 (a) Location of Each Loading and Boundary Condition at Different Views and (b) Meshing of Cemented Hip Arthroplasty Model

CHAPTER 4
RESULTS AND DISCUSSIONS

4.1 Introduction

This chapter explored the impact of implant positioning on stress distribution, strain distribution, and deformation. For stress distribution, each model was visually represented with a colour gradient, where grey indicated areas of higher stress concentrations, and blue represented regions with lower stress levels. Similarly, in the strain distribution analysis, the colour gradient ranged from blue for minimum strain to grey for maximum strain. Lastly, for deformation, the colour scale ranged from blue, denoting minimal deformation, to red, representing maximal deformation

4.2 Finite Element Analysis of Femur

The validation of the femur model was determined by analyzing the strain distribution within the femur of the model. The femur model employed in this study was validated against the experimental findings reported by Simoes et al (Simões et al., 2000). Model validation was achieved by comparing the strain distribution within the femur to that observed in the experimental study. To replicate the experimental conditions, an identical loading configuration comprising joint reaction forces and abductor muscle forces was applied, with the distal end of the femur constrained. As shown in Figure 4.1, the strain distribution exhibits a similar pattern despite differences in magnitude. This variation can be attributed to the individual differences in physiological loading conditions (Abdullah et al., 2009).

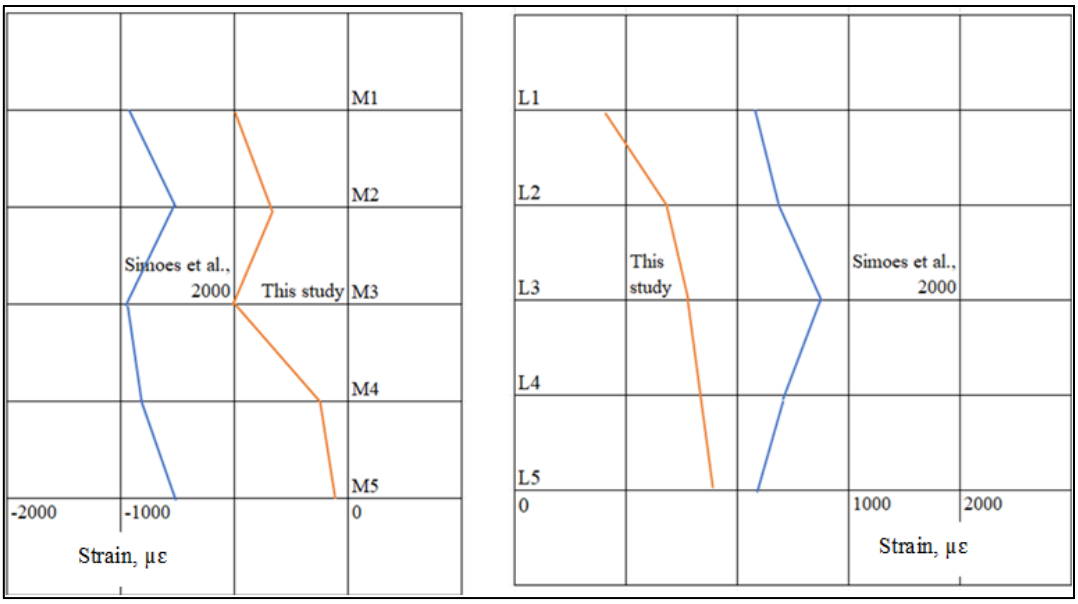

Figure 4.1 Pattern of Strain Distributions at the Medial and Lateral Plane of the Femur

4.3 Effect of Implant Positioning on the Stability of Cemented Total Hip Arthroplasty

4.3.1 Variation in Small Angles at Sagittal Positioning

Sagittal alignment during walking and stair climbing activity was assessed by examining six angles: -0.3°, -0.2°, -0.1°, 0.1°, 0.2°, and 0.3°, with 0° designated as the reference angle.

4.3.1.1 Total Hip Arthroplasty

Figure 4.2 and Figure 4.3 illustrates that the colour consistency suggests the stress pattern remains relatively unchanged across different sagittal angles under walking and stair climbing loading conditions. For both loading conditions, the regions of high stress are located along the medial and lateral aspects of the bone and implant, likely due to the transfer of load from the implant to the femur. The THA model also demonstrates elevated Von Mises stress at the distal end of the cement mantle. A study by Oshkour et al also found that higher stress was exhibited at the distal part of cement mantle which may contributed to an increased risk of cement mantle fracture and fatigue crack propagation (Oshkour et al., 2013). This stress concentration is likely attributed to the high reaction force at the lower cement mantle, resulting from force application at the hip joint contact (Aznan et al., 2020). The elevated stress in these areas raises concerns regarding potential implant failure or bone resorption due to stress shielding.

Figure 4.4 and Figure 4.5 shows the consistent strain pattern across all the tested angles. The strain appears to concentrate along specific regions of the femur, which could indicate areas at higher risk for mechanical failure or stress concentration depending on the implant position. The increased strain observed is likely a result of the load being transferred from the prosthesis to the bone, a common occurrence in proximity to the region where the implant stem is positioned. Moreover, the grey coloration in the area of the cement indicates a region of elevated strain. The relationship between strain and stress is characterized by an increase in strain corresponding to elevated stress levels. During weight-bearing activities, the lower section of the femoral component is exposed to significant strain resulting from bending moments and shear forces. The variations between angles are subtle; however, they may be pivotal in determining the optimal sagittal angle to minimize stress within the cement mantle or the surrounding bone. Stress concentrations frequently occur at interfaces between materials with differing stiffness, such as between the bone cement and the bone or between the implant and the cement. These regions of stress concentration are of particular importance, as they can significantly influence the longevity and stability of the implant within the bone. During the act of climbing stairs, the distribution of strain within the femur rises, especially when using the Muller prosthesis, resulting in elevated stresses and a risk of aseptic loosening. This situation can adversely affect bone health, hasten degenerative changes and require vigilant observation after total hip arthroplasty (Sofuoglu & Cetin, 2015).

Figure 4.6 and Figure 4.7 show the amount of deformation is relatively consistent across the range of angles, showing a similar pattern under both loading conditions with the highest deformation occurred at the top of the component while the least deformation is observed at the base. This phenomenon can be attributed to the cantilever effect, in which the load applied at the hip joint generates the largest moment arm at the superior portion of the implant. Such a result is anticipated, as the superior portion of the implant experiences the greatest deformation under load, given its position as the most distal point relative to the fixed support at the base of the femoral bone. A smooth gradient from grey to blue suggests a consistent stress distribution across all sagittal angles. The deformation patterns are symmetric, with similar effects seen at both negative (-0.3° to -0.1°) and positive (0.1° to 0.3°) angles. This may indicate a more optimal load transmission through all the components and remains unaffected by deformation.

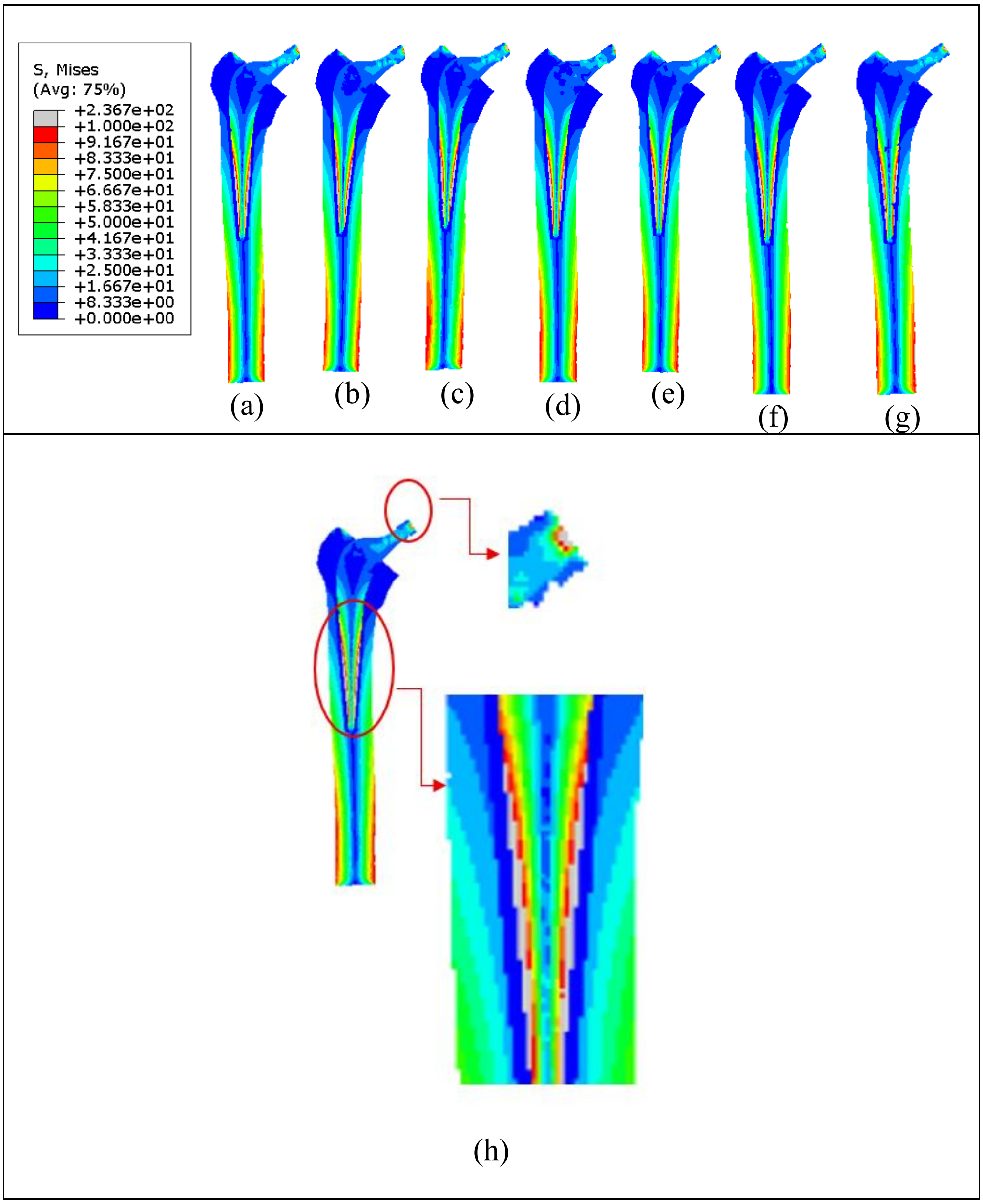

Figure 4.2 Stress Distribution Analysis for All Components at Different Sagittal Angles under Walking Loading Condition (a) -0.3°, (b) -0.2°, (c) -0.1°, (d) 0°, (e) 0.1°, (f) 0.2° and (g) 0.3° (h) Close-up View

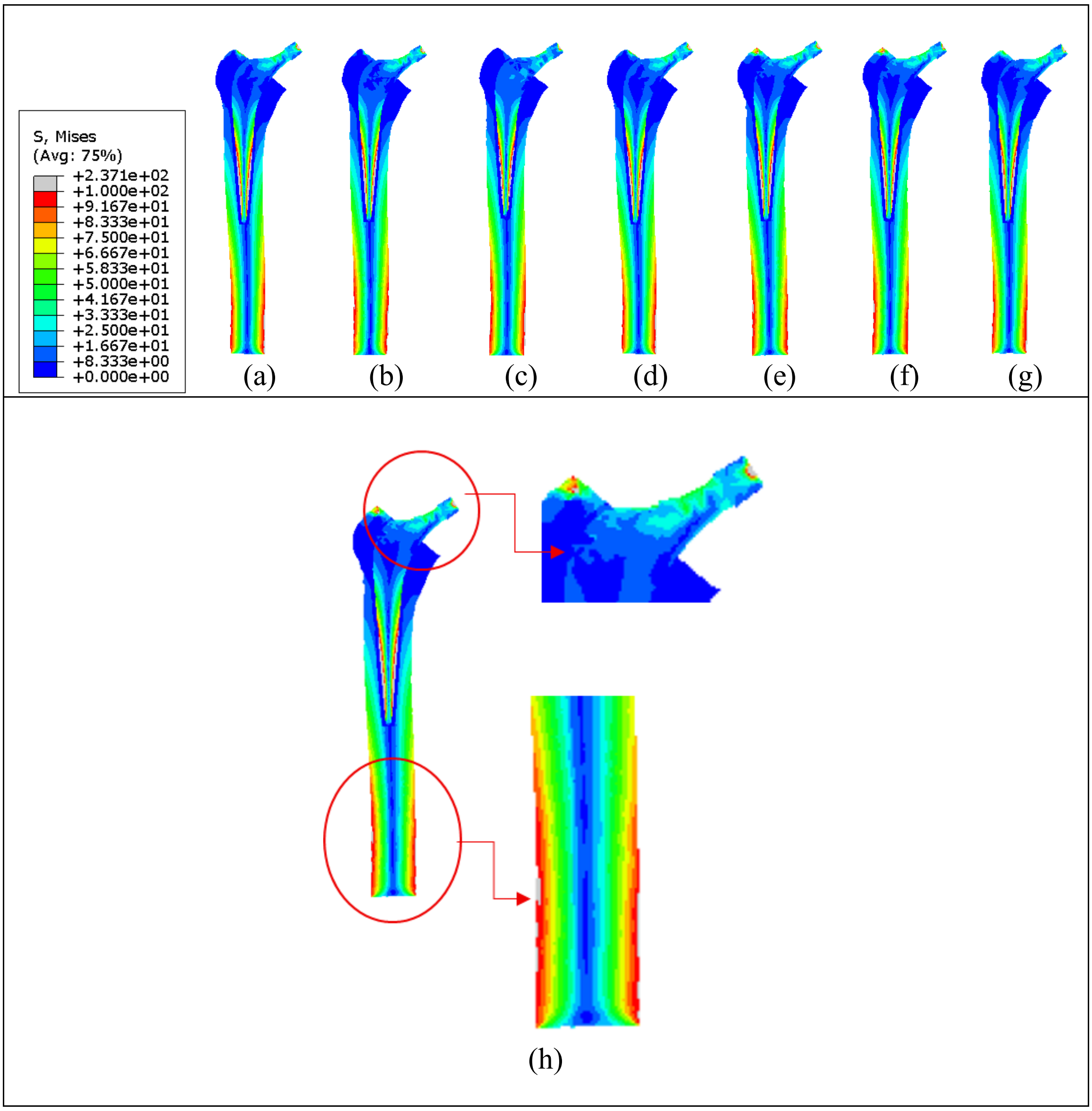

Figure 4.3 Stress Distribution Analysis for All Components at Different Sagittal Angles under Stair Climbing Loading Condition (a) -0.3°, (b) -0.2°, (c) -0.1°, (d) 0°, (e) 0.1°, (f) 0.2° and (g) 0.3° (h) Close-up View

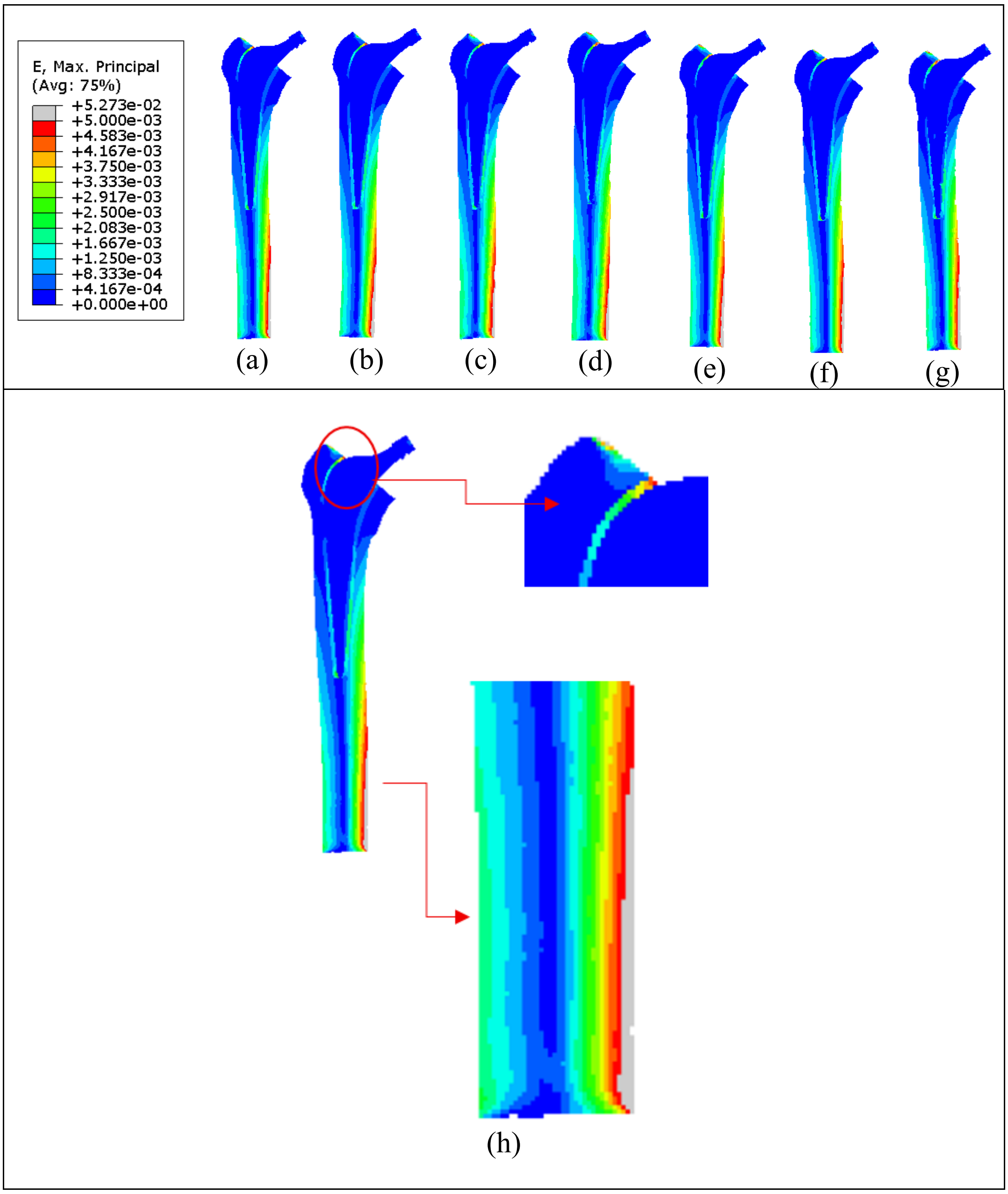

Figure 4.4 Strain Distribution Analysis for All Components at Different Sagittal Angles During Walking (a) -0.3°, (b) -0.2°, (c) -0.1°, (d) 0°, (e) 0.1°, (f) 0.2° and (g) 0.3° (h) Close-up View

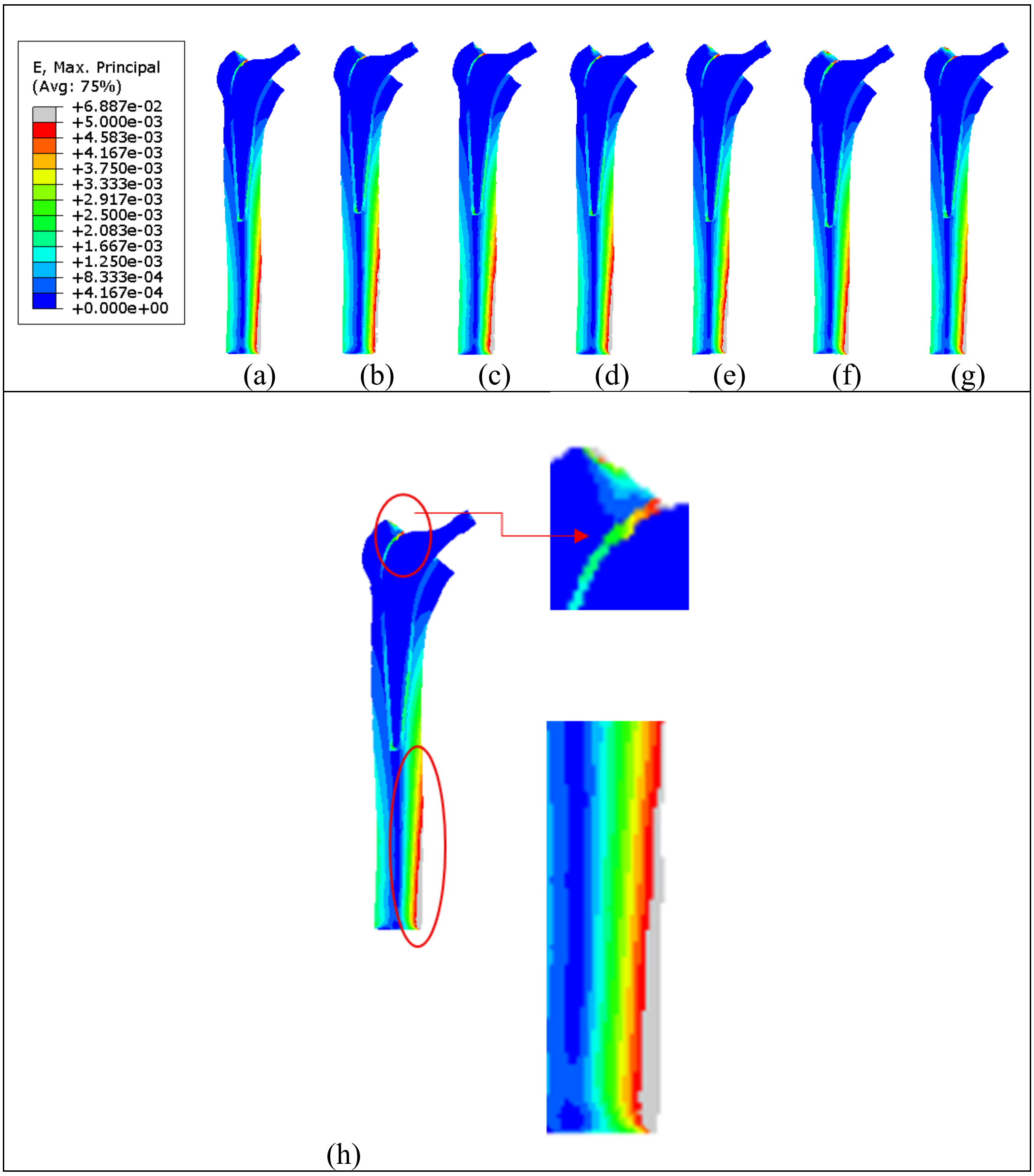

Figure 4.5 Strain Distribution Analysis for All Components at Different Sagittal Angles under Stair Climbing Loading Condition (a) -0.3°, (b) -0.2°, (c) -0.1°, (d) 0°, (e) 0.1°, (f) 0.2° and (g) 0.3° (h) Close-up View

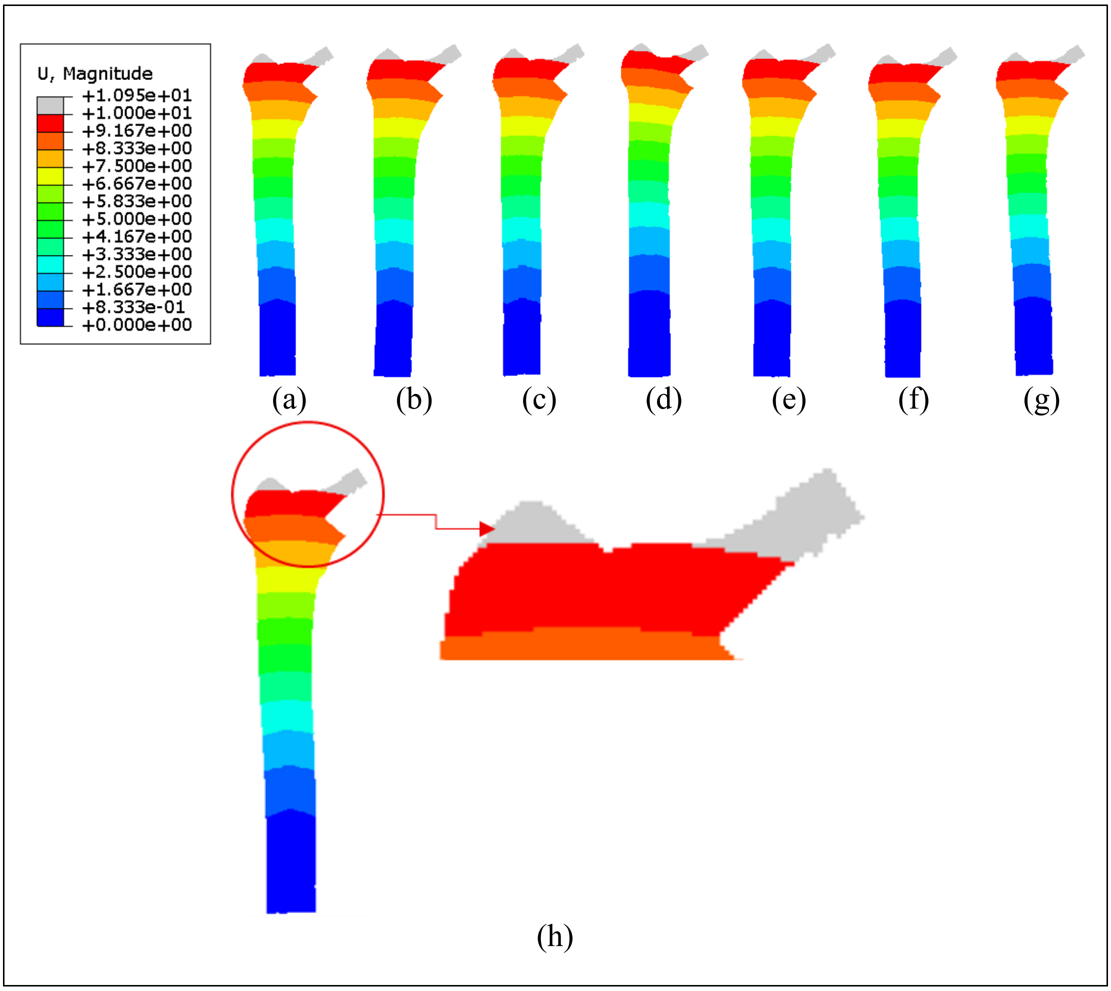

Figure 4.6 Total Deformation Analysis for All Components at Different Sagittal Angles under Walking Loading Condition (a) -0.3°, (b) -0.2°, (c) -0.1°, (d) 0°, (e) 0.1°, (f) 0.2° and (g) 0.3° (h) Close-up View

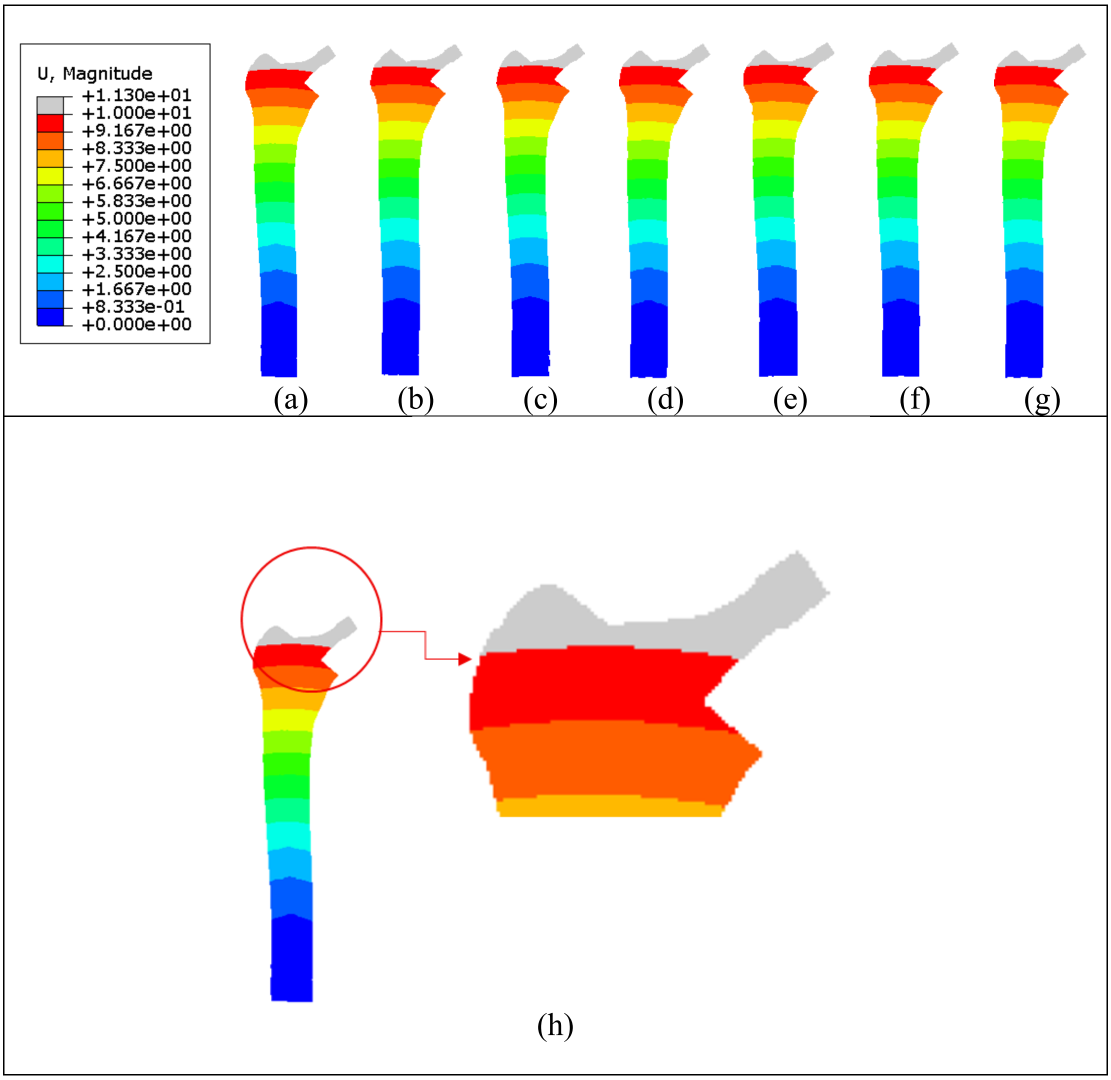

Figure 4.7 Total Deformation Analysis for All Components at Different Sagittal Angles under Stair Climbing Loading Condition (a) -0.3°, (b) -0.2°, (c) -0.1°, (d) 0°, (e) 0.1°, (f) 0.2° and (g) 0.3° (h) Close-up View

4.3.1.2 Half Femur

There is a distinct pattern of distal load transfer noticed in the stress distribution throughout the femur divided into Gruen zones, as shown in the Figure 4.80. In the Gruen zones 1, 2, 6, and 7 located in the proximal area of the femur, most of these stress areas appear blue, indicating very low stress, suggesting that there is a very limited load transfer proximally, leading to probable stress shielding and probably bone resorption in the calcar region, Zone 7 over a prolonged amount of time. Zones 5 and 3, which occupy the mid to distal region, displayed a progressive increase through the stress range, represented by a shift from blue to green and yellow, suggesting a mild stress. Zone 4 is at the distal tip of the stem and contains the highest stress concentration, from yellow to red and grey. This indicates load transfer has become completely distal, and this pattern appears with stiff or long cemented femoral stems. The overall stress distribution in Figure 4.8 indicates a pattern of mechanical load shifting from the proximal femur to the distal femur, and this may have long-term effects on bone remodelling and stability of the implant.

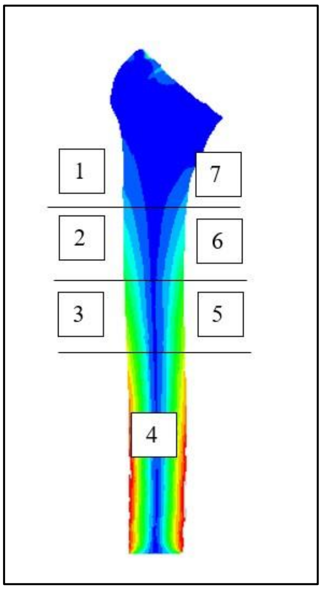

Figure 4.8 Stress Distribution Across the Femoral Gruen Zones

Figure 4.9 and Figure 4.10 show the Von Mises stress for the femoral bone at different sagittal angles under walking and stair climbing loading condition, respectively. The stress distribution does not exhibit significant alterations when subjected to various sagittal alignments. For both loading conditions, high stress is concentrated in the lower regions of the femoral bone, while the upper region (proximal femur) exhibits a lower stress concentration suggesting the implant absorbs and redistributes load, reducing stress on the surrounding bone. This phenomenon is likely associated with the bending moment effect of the femur (Luo et al., 2020). Moreover, the stress distribution remains stable across different activities, such as stair climbing with assistive devices, suggesting that the human body naturally adapts to varying loads without significant shifts in stress patterns (Zhu et al., 2023). Previous studies found femoral neck strains are generally higher during descent, suggesting a greater risk of hip pain and stress fractures in this phase (Deng et al., 2021).

Next, Figure 4.11 and Figure 4.12 illustrates the strain distribution across various angles under walking and stairs climbing loading conditions, respectively. In all models, strain is primarily localized in the distal portion of the femur, particularly along the cortical bone adjacent to the implant or in load-bearing regions, with a more pronounced concentration observed on the right side. This asymmetry may be attributed to variations in loading conditions or differences in bone density, leading to an uneven distribution of strain. The grey colour seems visible near the distal femur and medial cortex. These regions are subjected to greater strain suggesting a higher risk of structural failure under excessive loading. Strain distribution in the femur increases, especially with the Müller prosthesis, resulting in higher stresses that may contribute to aseptic loosening. This can adversely affect bone health, accelerate degenerative changes, and highlight the need for careful post-operative monitoring following total hip arthroplasty (Sofuoglu & Cetin, 2015). The consistency in strain distribution across the different angles suggests that changes in the sagittal angle have a minimal impact on the deformation of the femoral bone under load, which is a positive indication of the implant's stability across the tested range of angles. In contrast to the previous study, both sway-back and forward-flexed postures demonstrated increased stress and deformation as the angle between the femoral axis and the gravity line increased. These findings underscore the significant influence of posture on femoral mechanical behaviour during gait (Belaid & Bouchoucha, 2015). A study from Altai et al. found that during walking, significant variability in peak strains, influenced more by gluteus medius forces than hip joint contact forces (Altai et al., 2021).

Moreover, Figure 4.13 and Figure 4.14 demonstrate the degree of deformation diminishes from proximal to distal, indicating that the proximal femur undergoes the greatest deformation due to load transfer and its relative flexibility. Both loading conditions demonstrate consistent patterns, with no significant variation in magnitude observed. The femoral bone’s response to loading remains stable across the various sagittal alignments analyzed, indicating a consistent behavior under the tested conditions. Understanding total deformation in total hip arthroplasty is essential for evaluating implant stability and long-term success. It plays a key role in determining the risk of complications like dislocation and the need for revision surgery However, in Figure 4.14, deformation appears slightly larger in the femoral head region. The gradient seems more uneven which suggests increased structural displacement

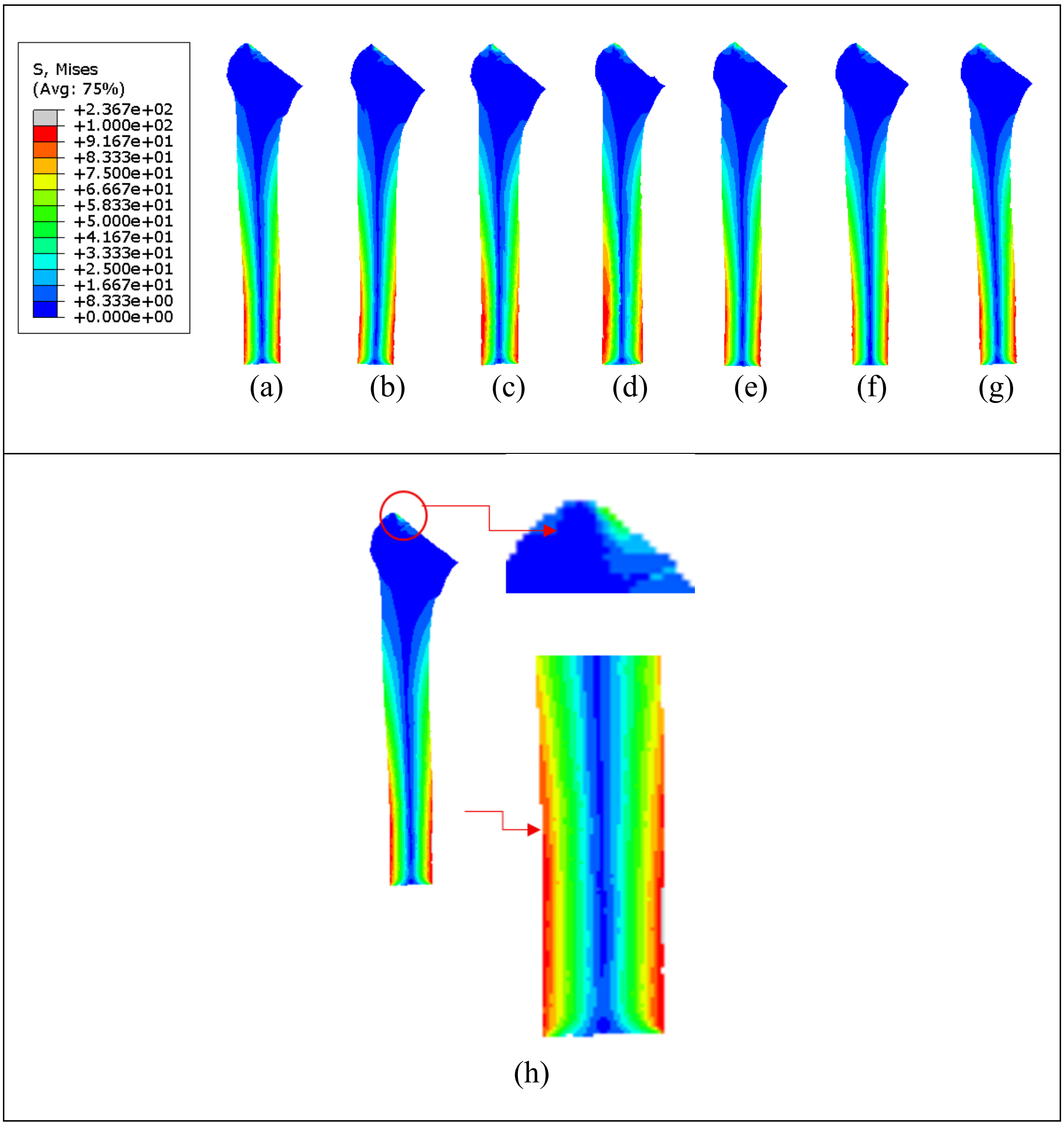

Figure 4.9 Stress Distribution Analysis for Femoral Bone at Different Sagittal Angles under Walking Loading Condition (a) -0.3°, (b) -0.2°, (c) -0.1°, (d) 0°, (e) 0.1°, (f) 0.2° and (g) 0.3° (h) Close up View

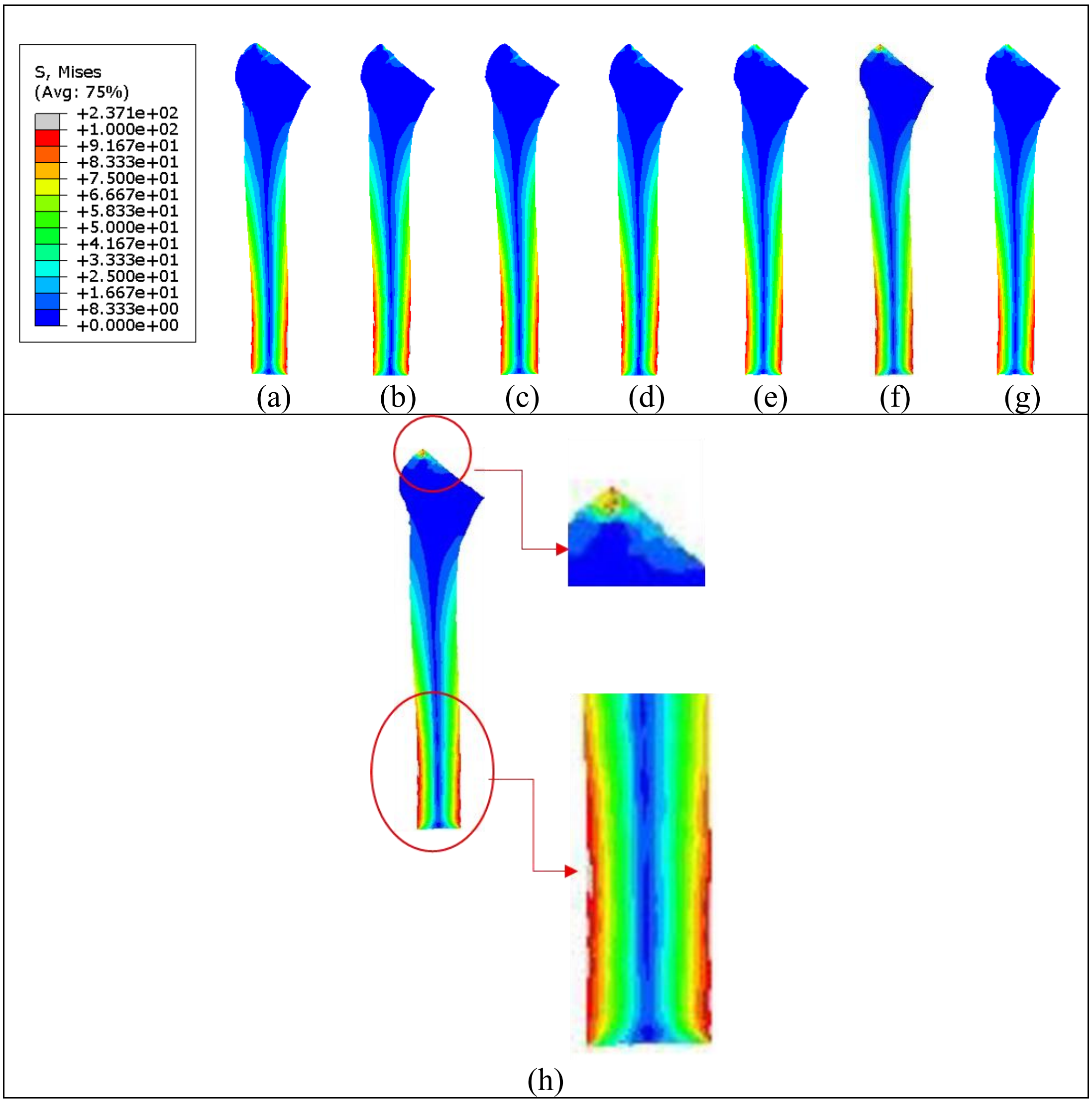

Figure 4.10 Stress Distribution Analysis for Femoral Bone at Different Sagittal Angles under Stair Climbing Loading Condition (a) -0.3°, (b) -0.2°, (c) -0.1°, (d) 0°, (e) 0.1°, (f) 0.2° and (g) 0.3° (h) Close-up View

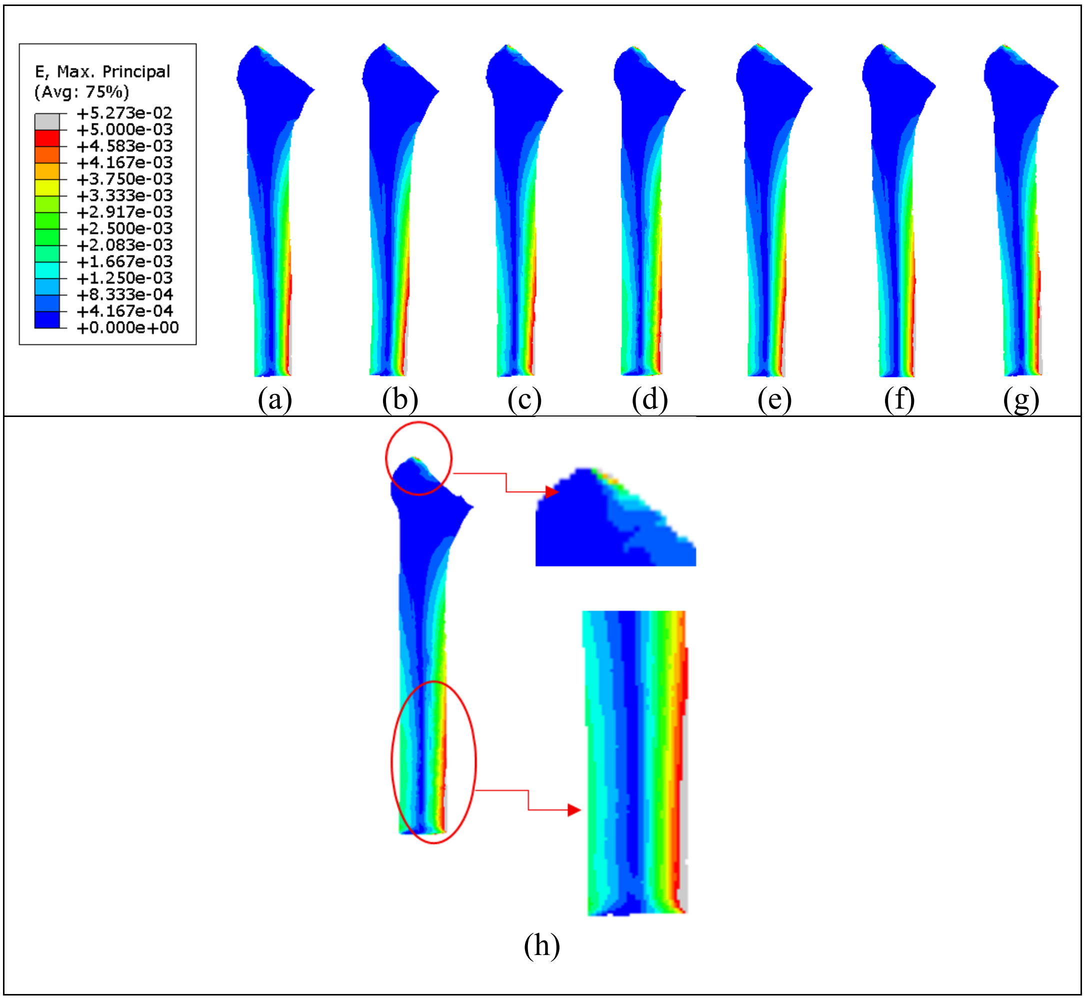

Figure 4.11 Strain Distribution Analysis for Femoral Bone at Different Sagittal Angles under Walking Loading Condition (a) -0.3°, (b) -0.2°, (c) -0.1°, (d) 0°, (e) 0.1°, (f) 0.2° and (g) 0.3° (h) Close-up View

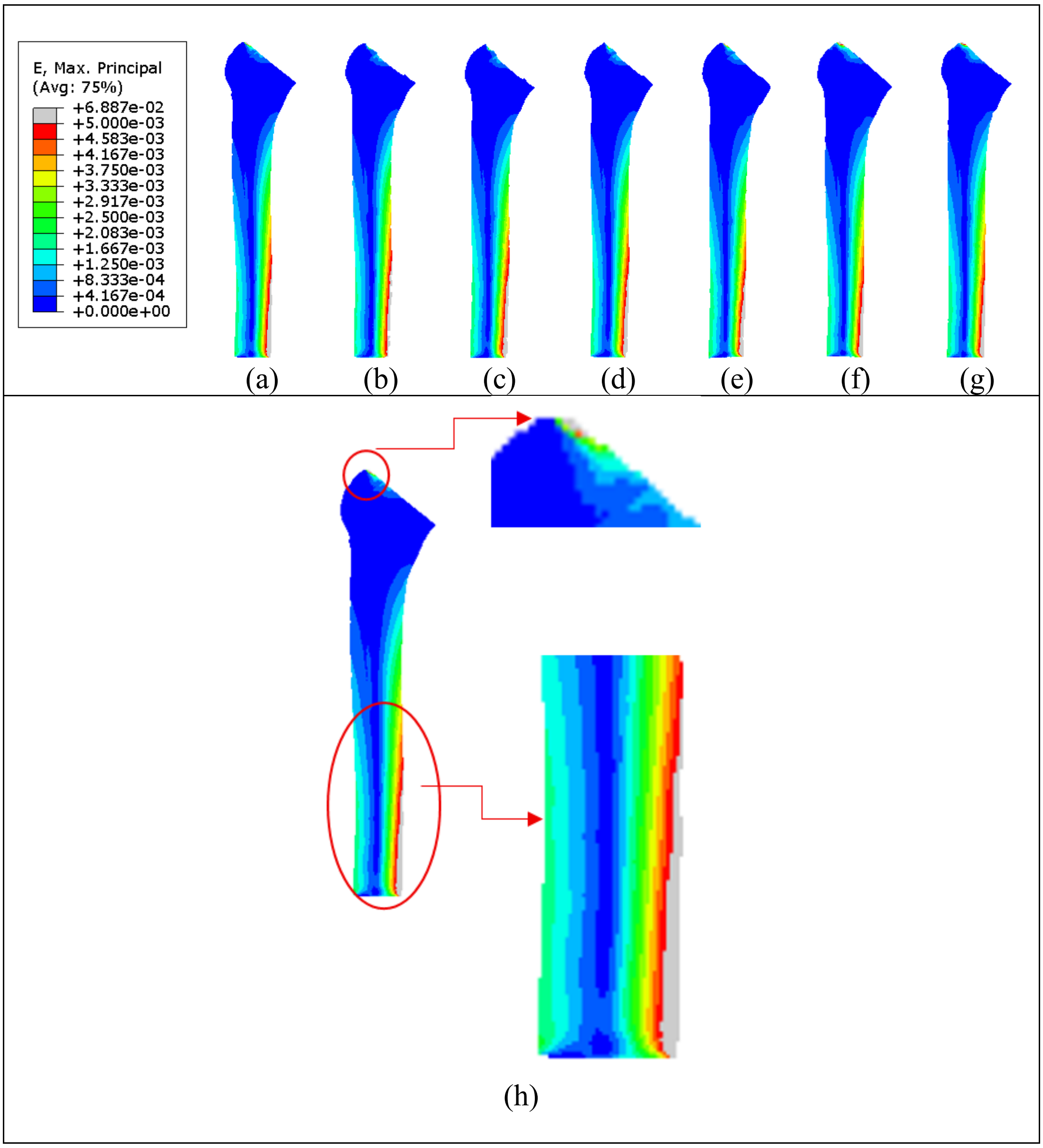

Figure 4.12 Strain Distribution Analysis for Femoral Bone at Different Sagittal Angles under Stair Climbing Loading Condition (a) -0.3°, (b) -0.2°, (c) -0.1°, (d) 0°, (e) 0.1°, (f) 0.2° and (g) 0.3° (h) Close-up View

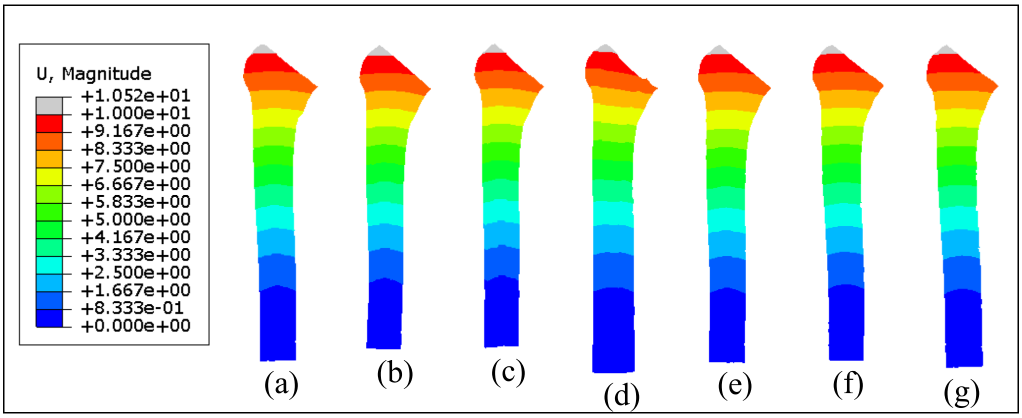

Figure 4.13 Total Deformation Analysis for Femoral Bone at Different Sagittal Angles under Walking Loading Condition (a) -0.3°, (b) -0.2°, (c) -0.1°, (d) 0°, (e) 0.1°, (f) 0.2° and (g) 0.3°

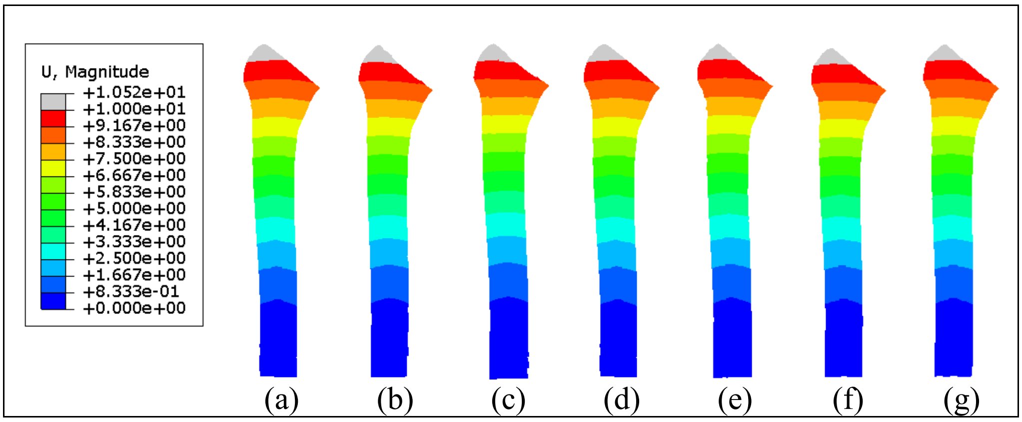

Figure 4.14 Total Deformation Analysis for Femoral Bone at Different Sagittal Angles under Stair Climbing Loading Condition (a) -0.3°, (b) -0.2°, (c) -0.1°, (d) 0°, (e) 0.1°, (f) 0.2° and (g) 0.3°

As shown in Figure 4.15, the highest stress value for the walking loading condition is 236.7 MPa which occurred between -0.1° to 0.3°. Angles -0.3° and -0.2° have a stress value of 236.6 MPa which indicates minimal difference in the maximum von Mises stress across the different angles. However, the deformation values remain consistent across all angles. This suggests that while there is a slight variation in the stress experienced by the bone at more negative angles, this does not result in a change in deformation, highlighting the resilience of the bone-implant system to these stress variations. As shown in Figure 4.16, The magnitude of deformation slightly decreases as the sagittal angle shifts from negative to positive. However, this change is minimal, indicating that the deformation of the femoral bone remains largely unaffected by the variations in the angles studied.

Meanwhile, Figure 4.17 reveals that the angles -0.3°, -0.2°, and 0.3° exhibit the highest strain, whereas the angles 0.1° and 0.2° display the lowest strain. Angles 0° and -0.1° lie between the highest and lowest strain values. The strain observed at the extreme angles which are -0.3° and 0.3°, may indicate potentially adverse biomechanical conditions, which could lead to increased wear or an elevated risk of bone remodelling over time. Figure 4.18 further illustrates that the maximum strain in the femoral bone remains remarkably consistent across different sagittal alignment angles. The maximum strain values range from 0.06886 to 0.06888, with only small fluctuations observed between the angles. These results suggest that there is no significant variation in the maximum strain as the sagittal alignment angle changes, indicating that the bone's response to mechanical loading stays relatively stable across the tested angles. Compared to walking activity, the strain distribution during stair climbing is higher. Research suggests that descending stairs induces higher femoral neck strains compared to ascending, potentially increasing the risk of hip pain and stress fractures, particularly in older individuals (Deng et al., 2021).

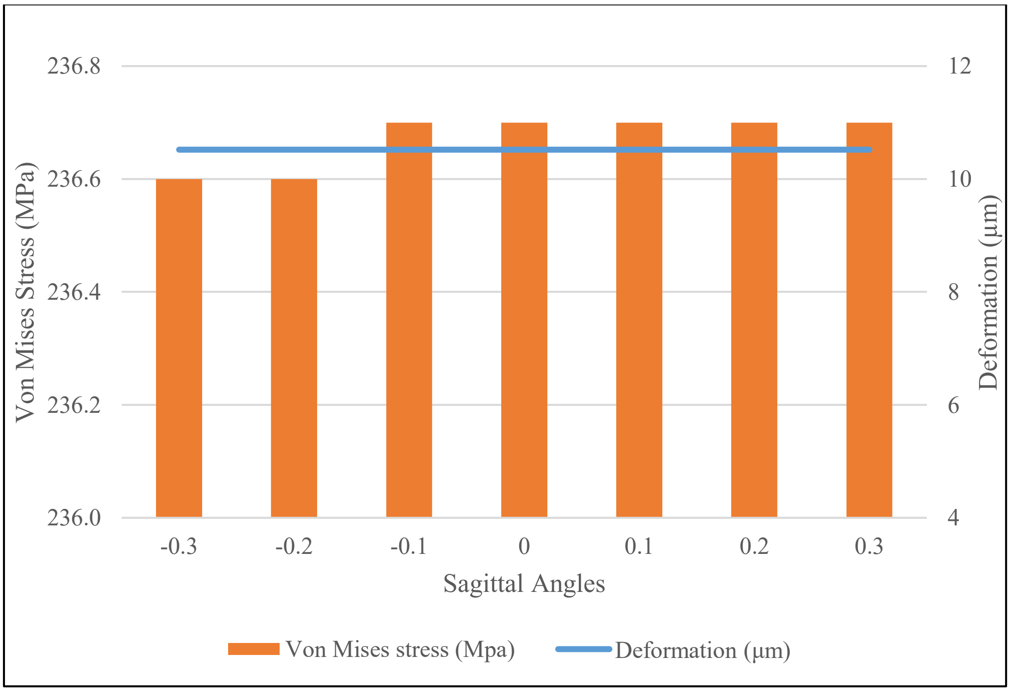

Figure 4.15 Comparison of Maximum Von Mises Stress and Displacement for Femoral Bone at Different Sagittal Angles under Walking Loading Condition

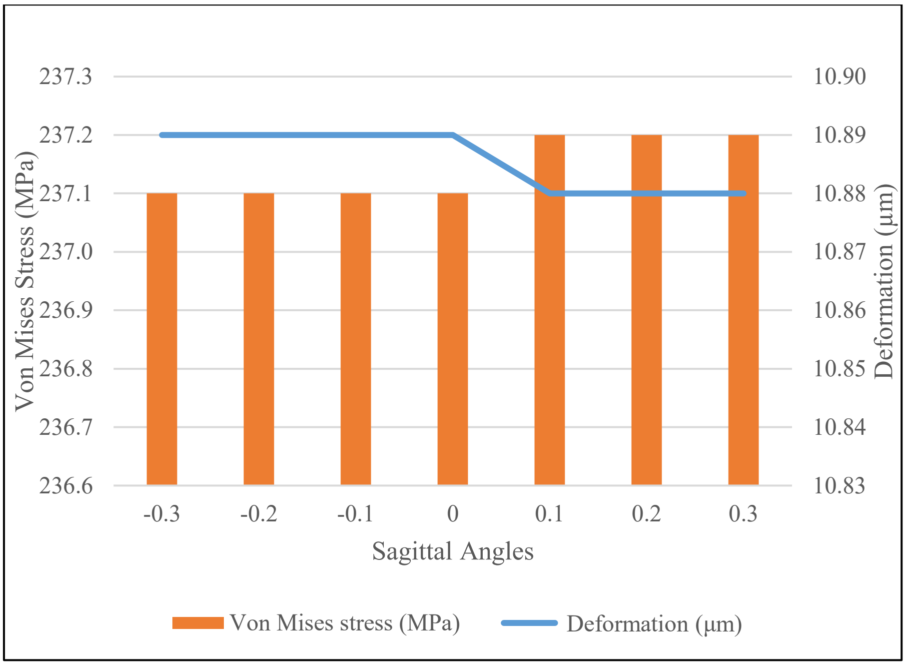

Figure 4.16 Comparison of Maximum Von Mises Stress And Displacement for Femur at Different Sagittal Angles under Stair Climbing Loading Condition

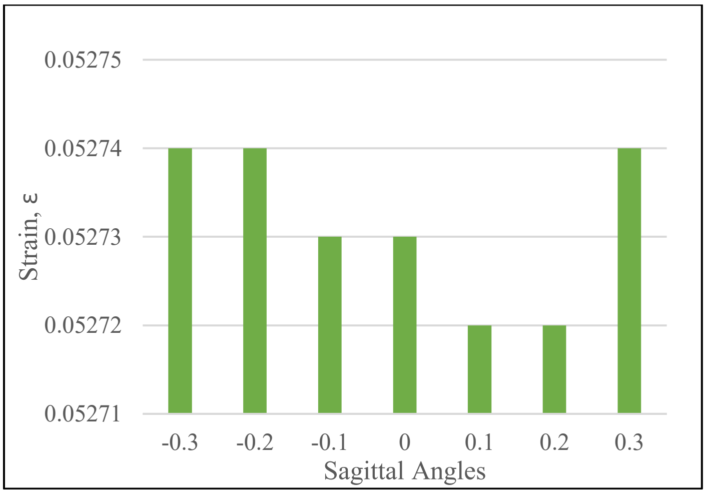

Figure 4.17 Strain of Femoral Bone Against Different Sagittal Angles under Walking Loading Condition

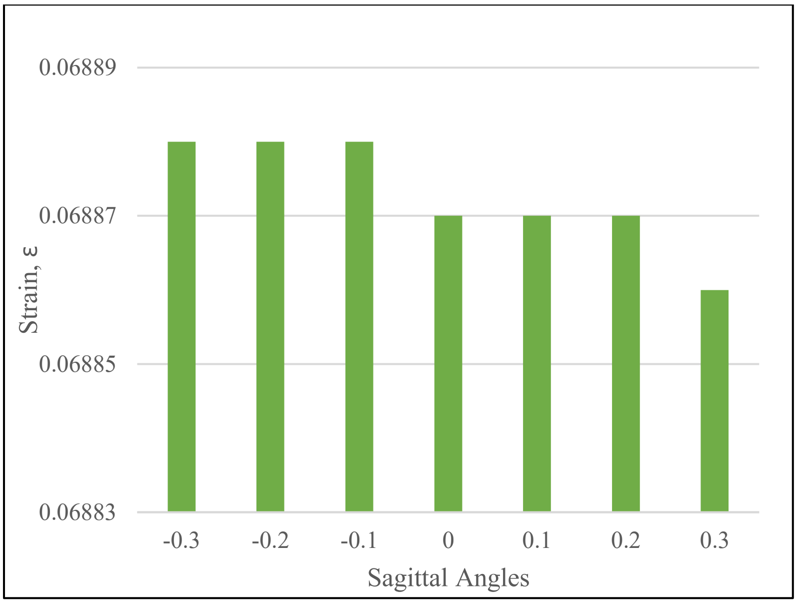

Figure 4.18 Strain of Femoral Bone Against Different Sagittal Angles under Stair Climbing Loading Condition

4.3.1.3 Cement mantle

Figure 4.19 and Figure 4.20 shows the relatively uniform pattern of stress distribution across various angles, suggesting that the sagittal alignment angle has minimal influence on the stress exerted on the cement mantle under walking and stair climbing loading conditions, respectively. The stress concentration localized near the proximal region of the cement mantle. It helps to prevent the prosthetic stem from migrating further into the femoral canal (Aznan et al., 2020). Similarly, higher stress concentrations are localized near the proximal region of the cement mantle due to the bending of the femoral stem, particularly with materials like titanium alloy (Ti6Al4V), which leads to increased interfacial stresses and micro movements (Singh & Harsha, 2016). A previous study from Kimura et al. found that the fixation of the cement mantle is frequently stronger distally, resulting in unsupported proximal areas that endure considerable bending moments during load application, which may lead to localized stress concentrations and the possibility of fractures (Kimura et al., 2018). 0° displays a relatively uniform stress distribution which indicates the optimal stress management in the cement at these alignments. In positive angles, the stress concentration is less severe than the negative angles but slightly higher than the neutral alignment. The stress zones appear more localized and contained near the medial region. High stress is primarily concentrated in the medical and proximal regions of the cement mantle for all tested angles. The distal area experiences significantly lower stress indicated by the predominantly blue colour.

Strain is concentrated in regions similar to the stress distribution as shown in Figure 4.21 and Figure 4.22 . Higher strain is located at the proximal medial and lateral ends of the cement mantle. This suggests that these areas experience concentrated mechanical stress regardless of sagittal alignment changes. Strain represents an adaptive reaction to applied stress and serves as an indication of the extent to which the material is undergoing deformation in response to the exerted load. The consistency observed in strain distribution pattern across various angles suggests that the response of the cement mantle to loading conditions remains stable, regardless of the slight changes in alignment. Variation in strain intensity at different angles indicates discrepancies in load transmission and possible failure regions. Furthermore, the optimal thickness of the cement mantle holds significant importance; a thickness exceeding 2mm may diminish stress-strain levels and alleviate stress shielding, thereby improving the mechanical performance of the cement (Levadnyi et al., 2017).

Figure 4.22 shows the grey region appears more intensive at 0.3° indicating increased strain in the cement mantle compared to the neutral position. At the neutral position, the strain distribution appears to be most uniform with minimal red regions suggesting that this position optimizes the stress distribution within the cement.

The total deformation of the cement mantle remains consistent across all angles both loading conditions as shown in Figure 4.23 and Figure 4.24 . This implies that changes in sagittal alignment have minimal impact on cement mantle deformation. The pattern of the deformation same as the previous study where the higher deformation is exhibited at the upper part of the cement mantle (Aznan et al., 2020). The displacement of the cement mantle under load remains relatively consistent despite variations in sagittal alignment, indicating that the cement mantle exhibits a uniform material response. This stability suggests that the cement mantle can accommodate the range of tested sagittal angles without compromising its structural integrity. The cement mantle demonstrates a consistent material behaviour in total hip arthroplasty attributable to its viscoelastic characteristics, which facilitate the even distribution of loads, thereby reducing stress concentrations and improving stability at the interfaces of cement-bone and cement-prosthesis (Hernigou et al., 2009). Figure 4.24 shows that the deformation, which is 10.29 µm, is constant at all angles.

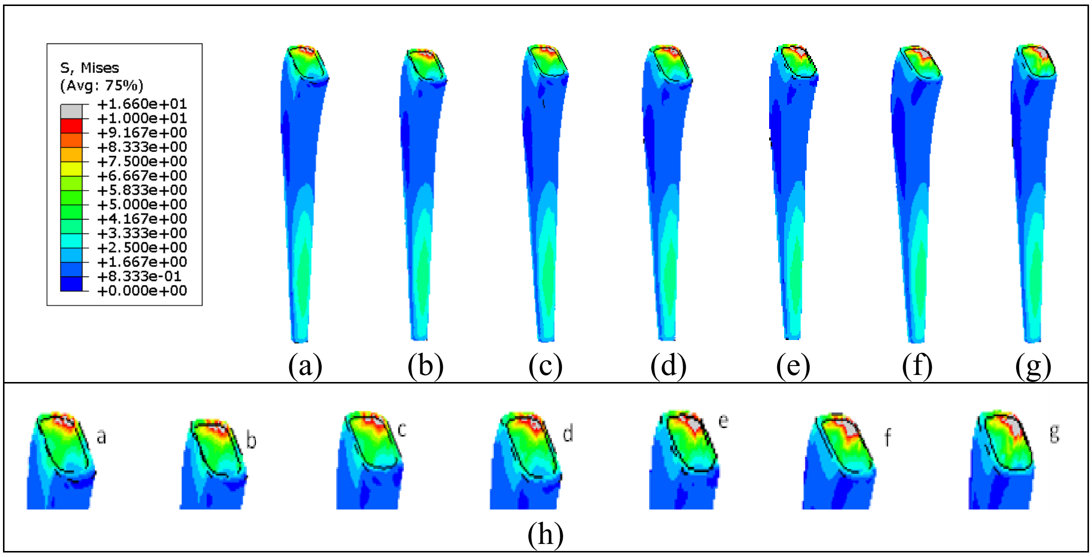

Figure 4.19 Stress Distribution Analysis for Cement Mantle at Different Sagittal Angles under Walking Loading Condition (a) -0.3°, (b) -0.2°, (c) -0.1°, (d) 0°, (e) 0.1°, (f) 0.2° and (g) 0.3° (h) Close-up View of Proximal Cement Mantle

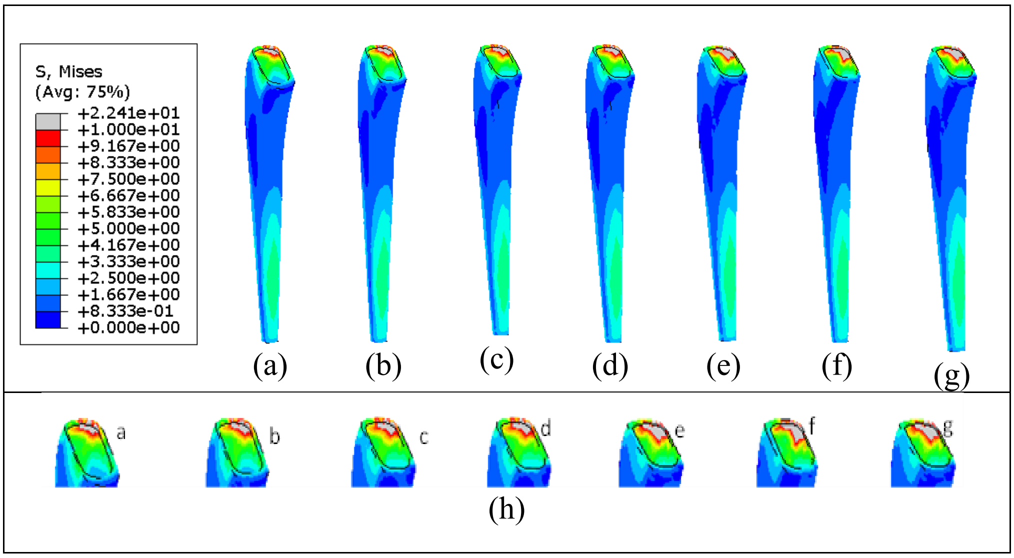

Figure 4.20 Stress Distribution Analysis for Cement Mantle at Different Sagittal Angles under Stair Climbing Loading Condition (a) -0.3°, (b) -0.2°, (c) -0.1°, (d) 0°, (e) 0.1°, (f) 0.2° and (g) 0.3° (h) Close-up View of Proximal Cement Mantle

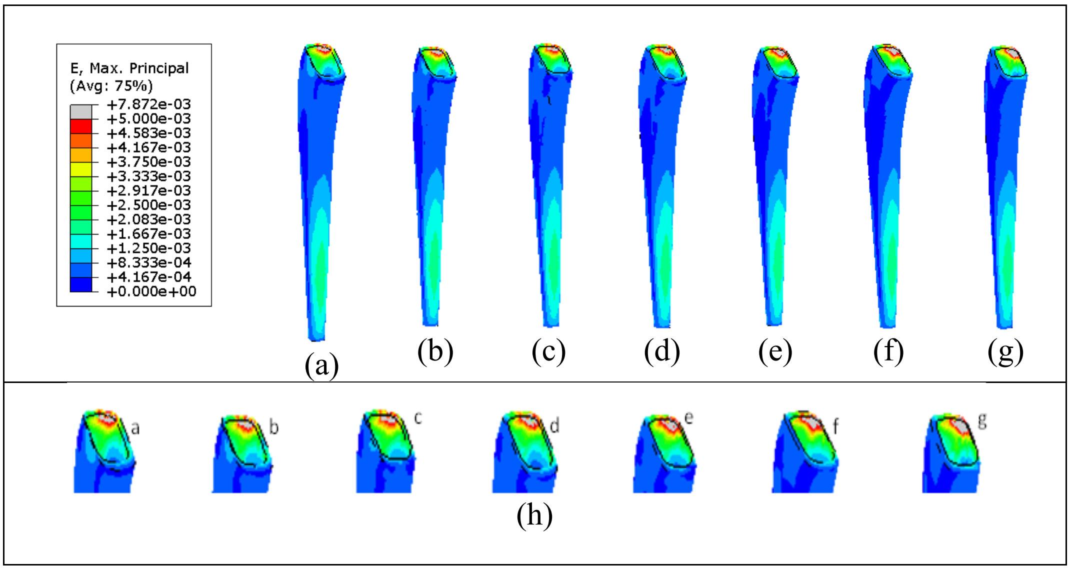

Figure 4.21 Strain Distribution Analysis for Cement Mantle at Different Sagittal Angles under Walking Loading Condition (a) -0.3°, (b) -0.2°, (c) -0.1°, (d) 0°, (e) 0.1°, (f) 0.2° and (g) 0.3° (h) Close-up View of Proximal Cement Mantle

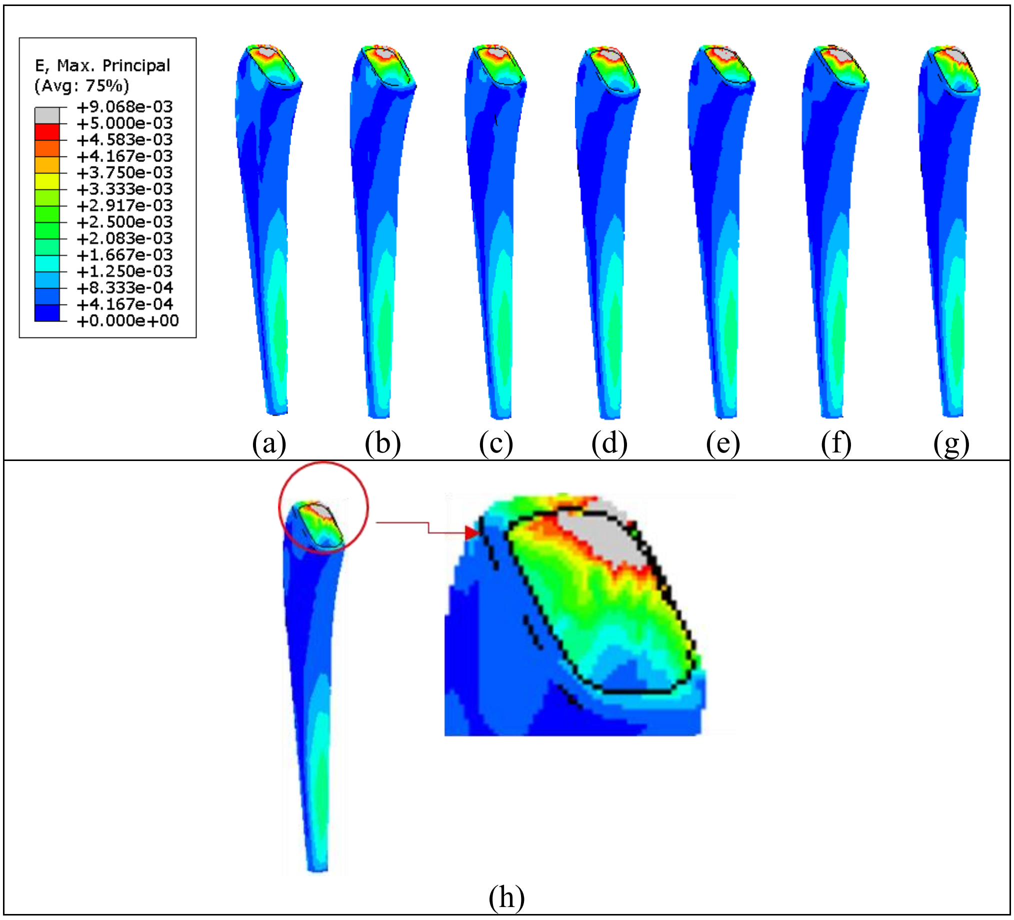

Figure 4.22 Strain Distribution Analysis for Cement Mantle at Different Sagittal Angles under Stair Climbing Loading Condition (a) -0.3°, (b) -0.2°, (c) -0.1°, (d) 0°, (e) 0.1°, (f) 0.2° and (g) 0.3° (h) Close-up View of Proximal Cement Mantle at 0.3°

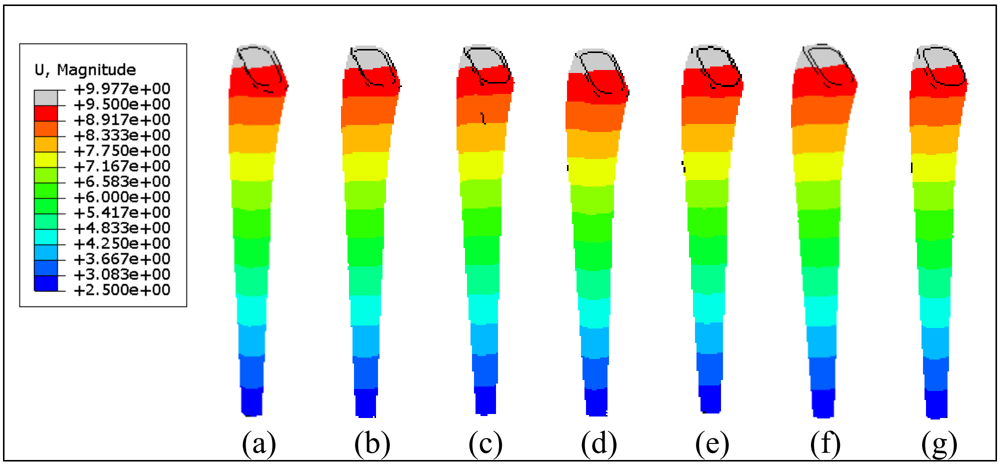

Figure 4.23 Total Deformation Analysis for Cement Mantle at Different Sagittal Angles under Walking Loading Condition (a) -0.3°, (b) -0.2°, (c) -0.1°, (d) 0°, (e) 0.1°, (f) 0.2° and (g) 0.3°

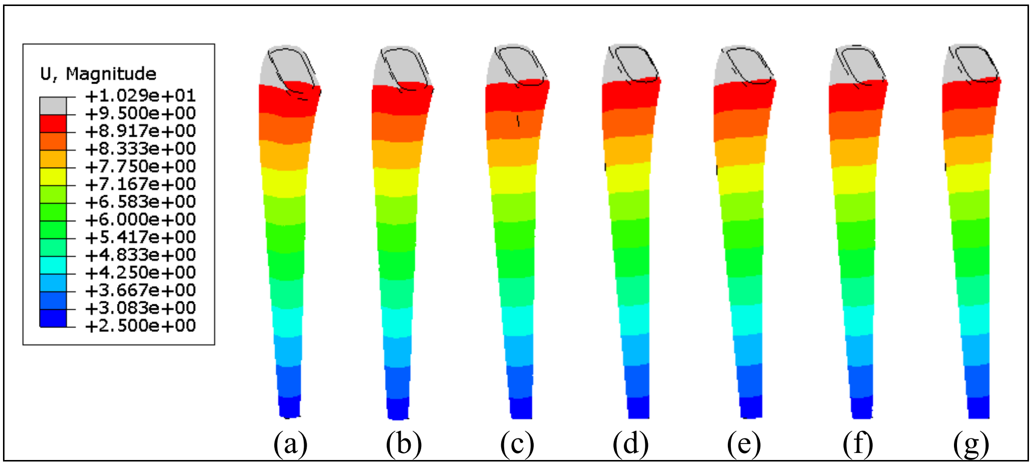

Figure 4.24 Total Deformation Analysis for Cement Mantle at Different Sagittal Angles under Stair Climbing Loading Condition (a) -0.3°, (b) -0.2°, (c) -0.1°, (d) 0°, (e) 0.1°, (f) 0.2° and (g) 0.3°

As shown in Figure 4.25, 0.3° exhibits the highest value of stress which is 21.36 MPa meanwhile 0.2° exhibits the lowest stress value which is 14.85 MPa. Both values are below the value of PMMA yield strength which is 29 MPa. The highest deformation is 9.974 µm at 0.3° while the lowest deformation is 9.974 µm at -0.3°, showing only a slight difference. Figure 4.26 indicates a trend in which Von Mises stress increases with positive sagittal angles. This suggests that as the sagittal angle shifts forward, the stress within the cement mantle progressively rises. Additionally, the stress values exhibit fluctuations within a specific range, with notable peaks observed at 0.2° and 0.3°. The deformation values, portrayed by the blue line, show a rather steady disposition through all sagittal angles, implying that there are no significant changes in the overall displacement should changes in implant orientation be made throughout the indicated range. This suggests that while stress within the cement mantle is sensitive to sagittal angle variation, the structural integrity and macroscopic deformation of the cement layer remain relatively unchanged.

Furthermore, Figure 4.27 demonstrates that the strain values vary from a maximum of 0.0095 at 0.3° to a minimum of 0.0075 at -0.2°. While the differences are minimal, they may still hold significance when considering long-term mechanical performance. Figure 4.28 illustrates the strain distribution within the cement mantle across different sagittal angles. The results indicate a relatively stable strain pattern for angles ranging from -0.3° to 0.1°, with a slight increase observed at 0.2° and 0.3°. An angle of 0.3° exhibit the highest value of strain which is 0.011 and -0.2° exhibits 0.009.

This implies that while strain remains consistent across most of the analysed angles, a forward tilt beyond 0.1° may contribute to higher strain levels within the cement mantle.

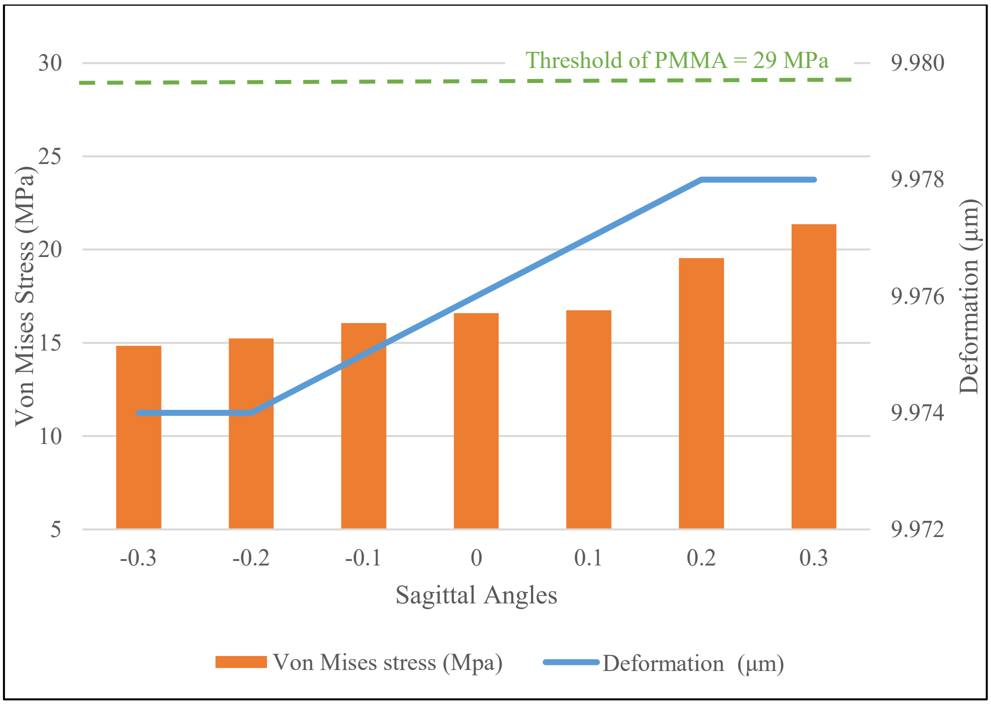

Figure 4.25 Comparison of Maximum Von Mises Stress and Deformation for Cement Mantle at Different Sagittal Angles under Walking Loading Condition

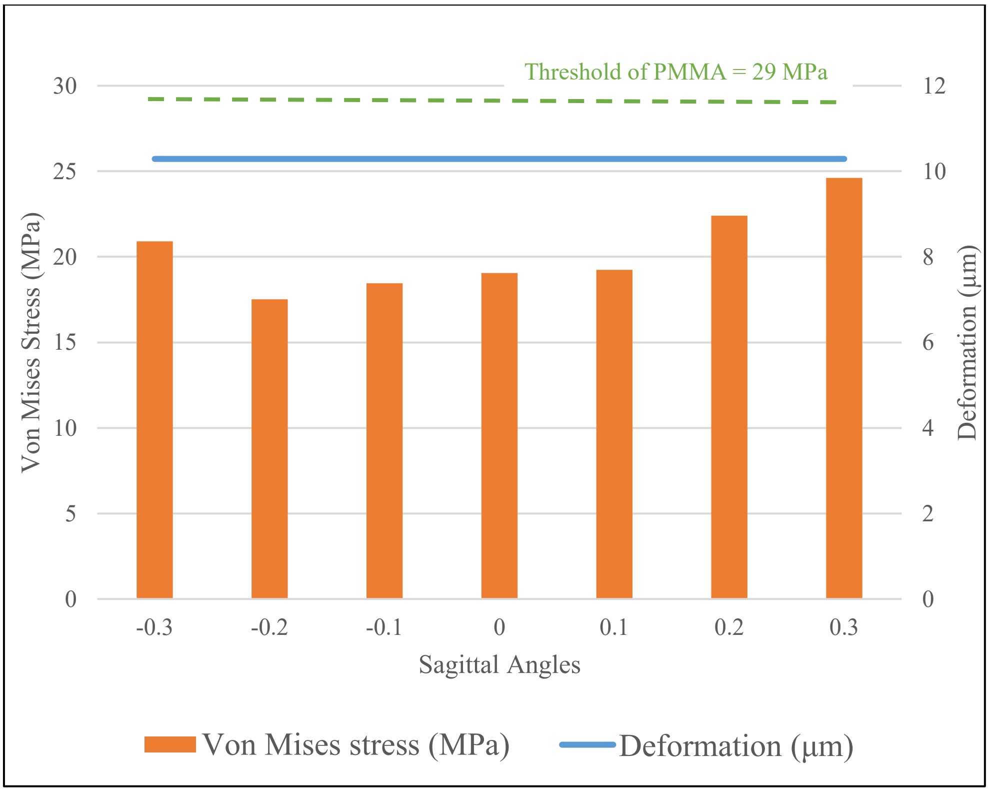

Figure 4.26 Comparison of Maximum Von Mises Stress and Deformation for Cement Mantle at Different Sagittal Angles under Stair Climbing Loading Condition

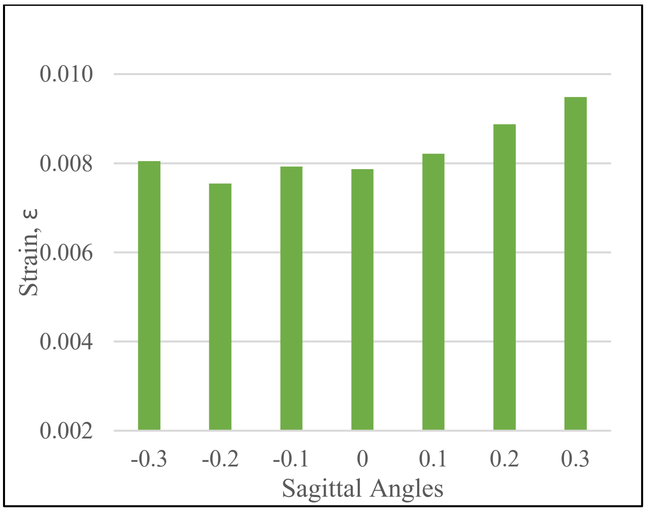

Figure 4.27 Strain of Cement Mantle Against Different Sagittal Angles under Walking Loading Condition

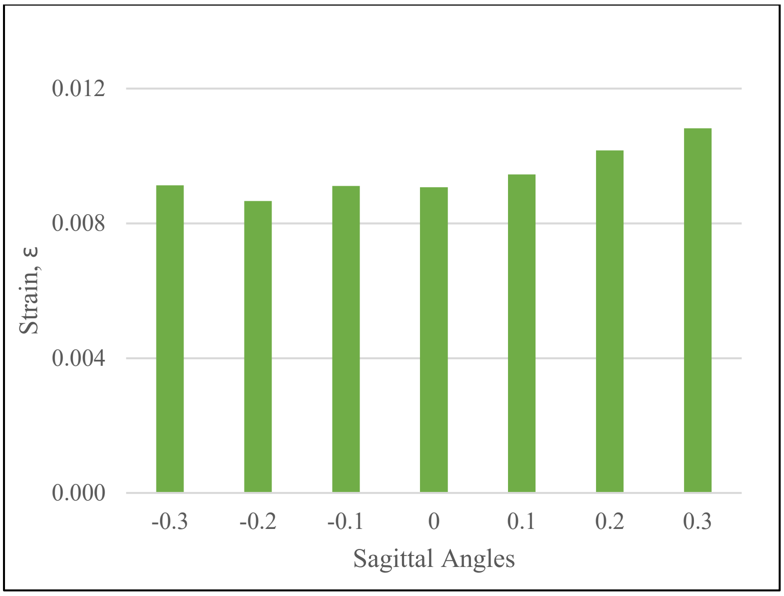

Figure 4.28 Strain of Cement Mantle Against Different Sagittal Angles under Stair Climbing Loading Condition

4.3.1.4 Hip Implant

The stress distribution is greater at the proximal and distal ends of the implant as shown in Figure 4.29. The upper part experiences elevated stress because it is the direct point of load application. Additionally, the lower part is a high-stress area as it is where the implant transfers load to the bone, leading to stress concentration at the interface which indicates areas experiencing greater mechanical loading, which eventually lead to material failure, implant loosening, or bone resorption (Firdaus et al., 2024). The pattern of stress distribution is uniform across all angles. Under stair climbing loading condition, the pattern of stress distribution is uniform within the implant as shown in Figure 4.30. Generally, the pattern of stress distribution is similar to the walking loading condition. However, during stair climbing activity, the neck region experiences greater stress too. The neck of the implant, being narrower due to its geometric design, concentrates stress at the lower part, the taper of the implant leads to a smaller contact area, concentrating the load in a smaller region, which increases the stress. The midsection consistently shows lower stress values, indicating it is less affected by sagittal positioning for both loading conditions.

According to the Figure 4.31 and Figure 4.32, the strain magnitude is higher at the proximal and distal of the implant as the strain distribution closely follows the stress distribution. The consistency observed across all angles indicates that the implant's material properties and geometry are well-suited to managing stress without significant changes in deformation, which is advantageous for the implant's long-term durability. The strain distribution is similar to the stress distribution, in which the lower part of the implant experienced the higher strain. Regions of high strain are generally observed in areas where the implant undergoes the greatest mechanical loading or at points of cross-sectional transitions, which can result in localized stress concentrations

The pattern of deformation across all tested angles is consistent for walking and stair climbing loading conditions as shown in Figure 4.33 and Figure 4.34. respectively. There is no significant changes in the shape or distribution of the deformation areas under both loading conditions This indicates that small variations in the sagittal angle have minimal effect on the implant's deformation where the implant can be positioned without substantially impacting its biomechanical performance in terms of stress and deformation. Such findings suggest the potential for a degree of flexibility in surgical implantation, without compromising the implant's structural integrity, patient safety, or comfort. The debonding of the hip implant will result in the formation of a void between the implant and the femur. This phenomenon is induced by the subsidence of the hip implant within the cement mantle. The loosening of the hip implant may predispose the individual to fractures and dislocation of the femur (Aznan et al., 2020).

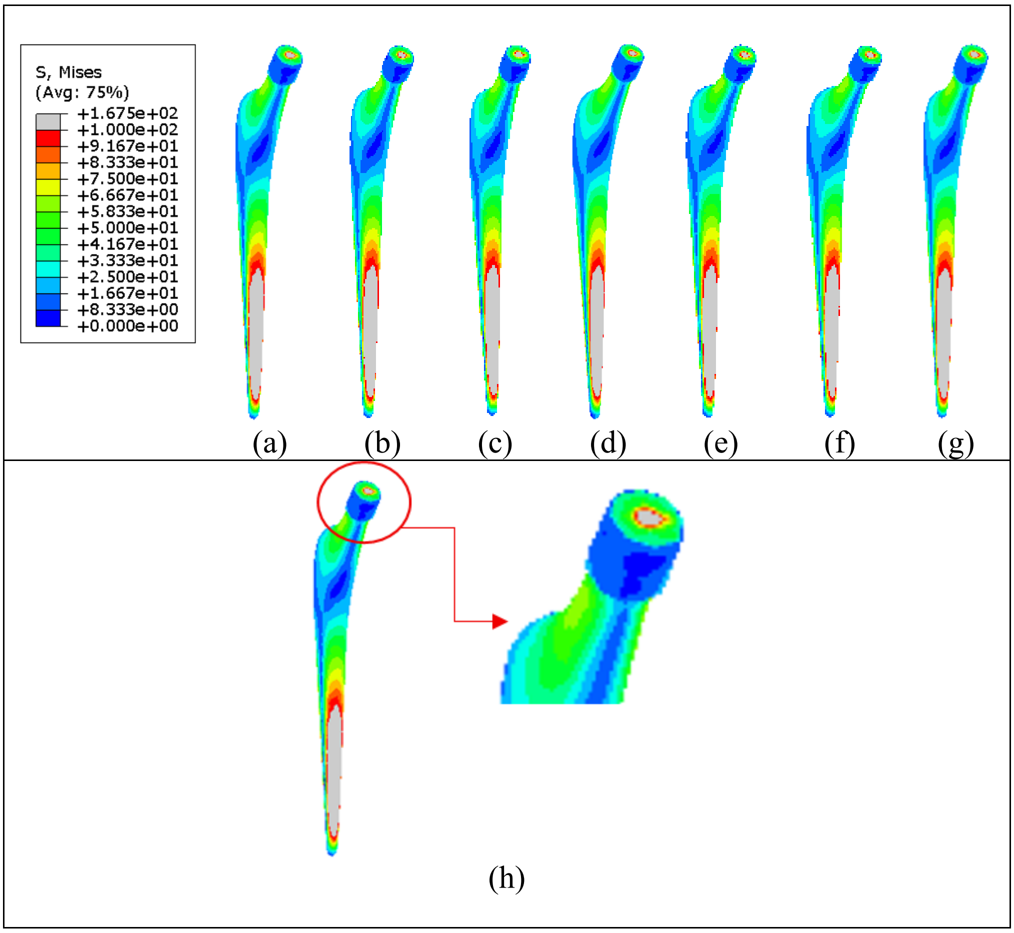

Figure 4.29 Stress Distribution Analysis for Implant at Different Sagittal Angles under Walking Loading Condition (a) -0.3°, (b) -0.2°, (c) -0.1°, (d) 0°, (e) 0.1°, (f) 0.2° and (g) 0.3° (h) Close-up view of upper part of hip implant

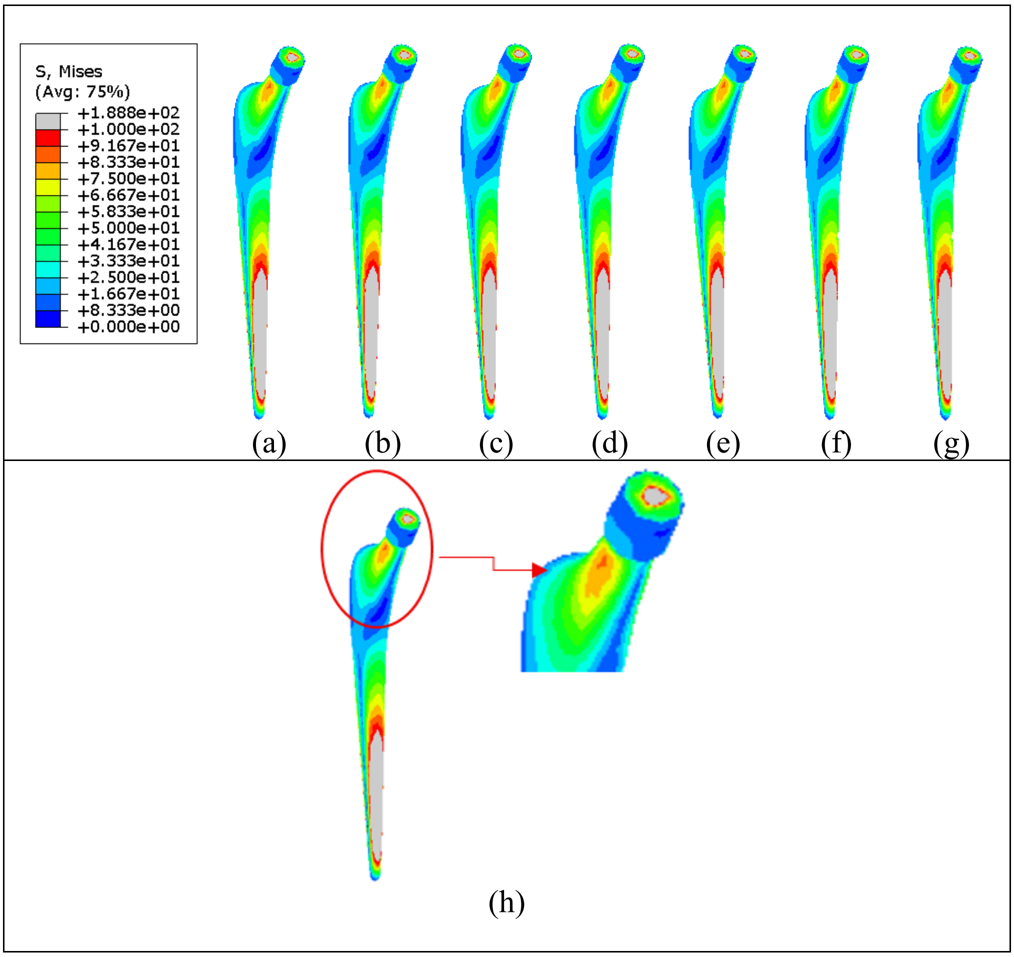

Figure 4.30 Stress Distribution Analysis for Implant at Different Sagittal Angles under Stair Climbing Loading Condition (a) -0.3°, (b) -0.2°, (c) -0.1°, (d) 0°, (e) 0.1°, (f) 0.2° and (g) 0.3° (h) Close-up View of Upper Part of Hip Implant

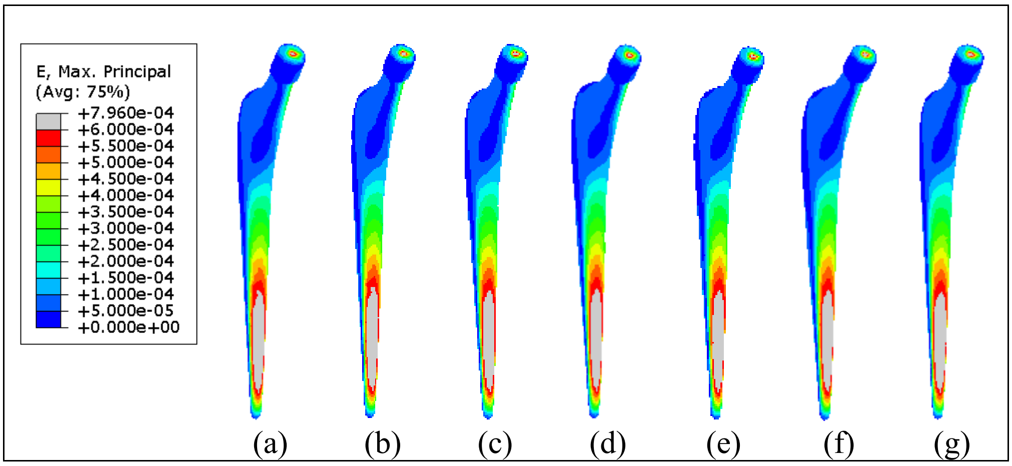

Figure 4.31 Strain Distribution Analysis for Implant at Different Sagittal Angles under Walking Loading Condition (a) -0.3°, (b) -0.2°, (c) -0.1°, (d) 0°, (e) 0.1°, (f) 0.2° and (g) 0.3°

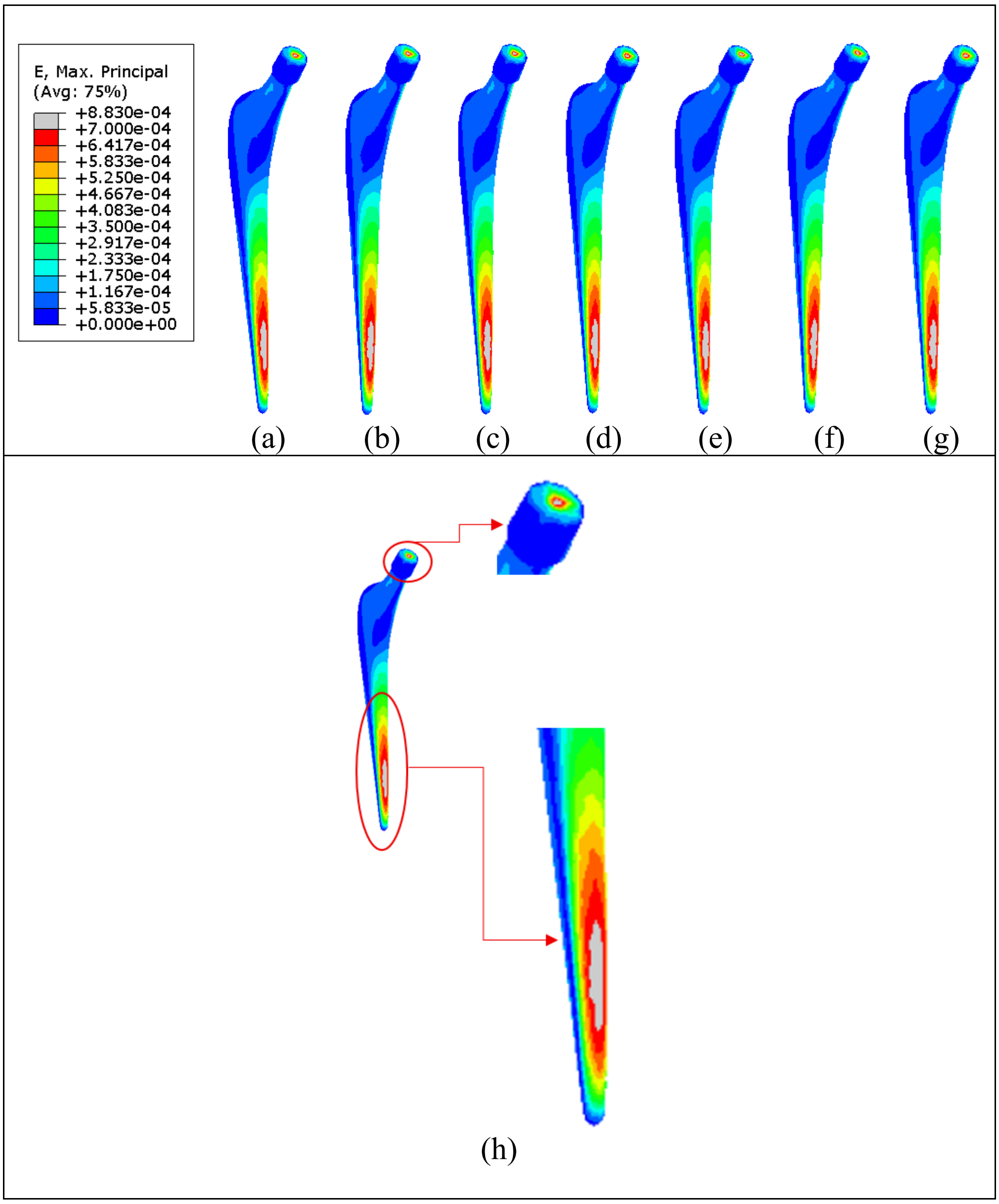

Figure 4.32 Strain Distribution Analysis for Implant at Different Sagittal Angles under Stair Climbing Loading Condition (a) -0.3°, (b) -0.2°, (c) -0.1°, (d) 0°, (e) 0.1°, (f) 0.2° and (g) 0.3° (h) Close up view

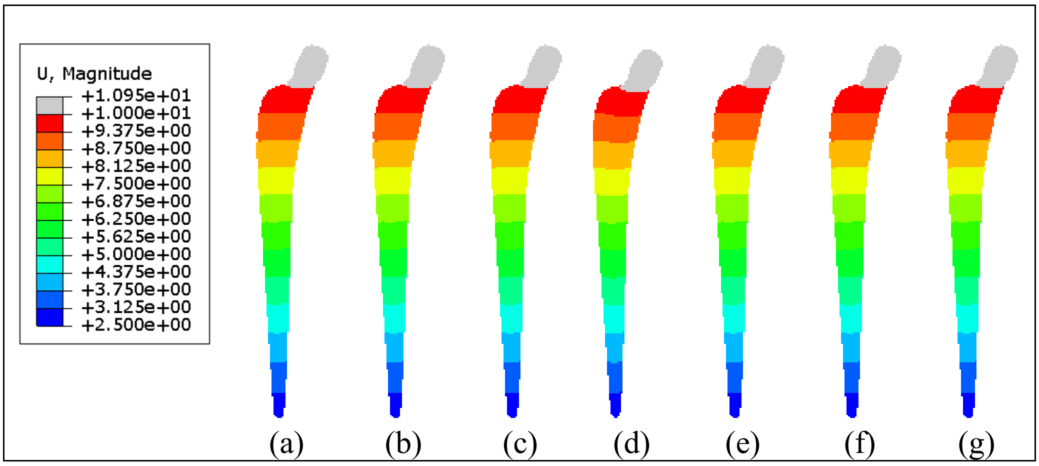

Figure 4.33 Total Deformation Analysis for Implant at Different Sagittal Angles under Walking Loading Condition (a) -0.3°, (b) -0.2°, (c) -0.1°, (d) 0°, (e) 0.1°, (f) 0.2° and (g) 0.3°

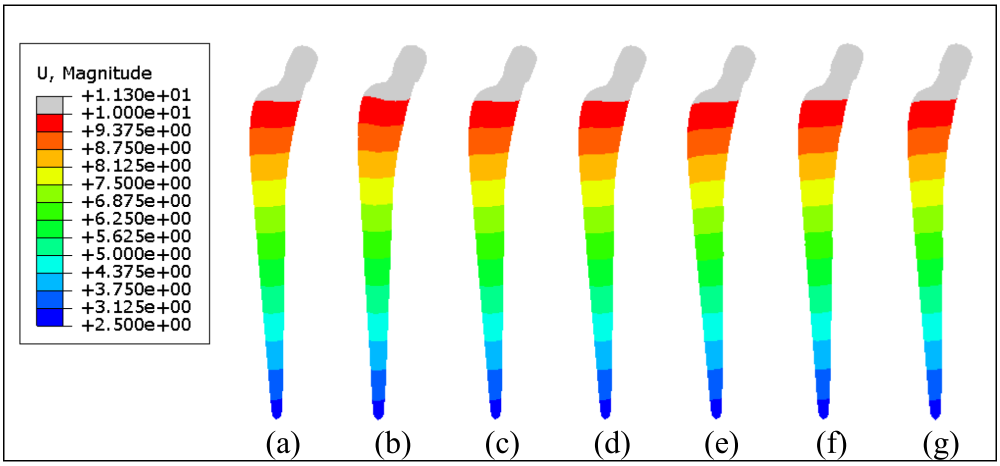

Figure 4.34 Total Deformation Analysis for Implant at Different Sagittal Angles under Stair Climbing Loading Condition (a) -0.3°, (b) -0.2°, (c) -0.1°, (d) 0°, (e) 0.1°, (f) 0.2° and (g) 0.3°

Figure 4.35 illustrates that the neutral 0° angle experiences a significantly higher stress, measuring 173.7 MPa, compared to other angles, which range from 164.7 MPa to 167.4 MPa. Despite these variations in stress, the deformation remains consistent across all angles at 10.95 µm, indicating that the implant's deformation is unaffected by changes in sagittal alignment. In other words, the deformation does not vary with sagittal angles. Figure 4.36 illustrates that the magnitude of deformation remains constant at 11.3 µm across all implantation angles from -0.3° to 0.3°. This consistency indicates that the deformation experienced by the implant does not vary significantly within the studied angular range. It suggests that the implant material, polymethyl methacrylate (PMMA), and its structure can effectively withstand physiological loads encountered during stair-climbing activities without notable deformation changes.

Furthermore, Figure 4.36 reveals that the lowest Von Mises stress occurs at -0.3°, while the highest is observed at 0.3° with the value of 188.4 MPa and 188.8 MPa, respectively. However, this increase is minimal, demonstrating that variations in the implant angle within the sagittal plane have a negligible impact on the stress distribution under the simulated physiological loads. Compare to the previous study, the circular-shaped implant has the stress values 218.78MPa and deformation of 0.16mm (Chethan et al., 2019). This different may be attributed to the behaviour of the implant design and the magnitude of applied loading conditions.

Figure 4.37 shows a slight increase in strain across the angles, with the highest strain at 0.3° and the lowest at -0.3°, with a difference of 0.7µ between the highest and lowest values. This trend could be attributed to the biomechanical responses of the implant to changes in sagittal alignment. As the sagittal angle shifts, it may alter the distribution of mechanical forces and moments acting on the implant, which in turn affects the strain patterns within the implant structure. The bar graph in Figure 4.38 demonstrates the uniformity of strain values across the range of tested angles, indicating that the implant design is optimized to achieve consistent strain distribution despite minor angular variations within the investigated range. While the differences in strain values are subtle, the highest strain is observed at an angle of 0.3°, suggesting a relative increase in deformation at this specific angle. This phenomenon may be attributed to factors such as changes in contact pressure or variations in load distribution on the implant with increasing angle.

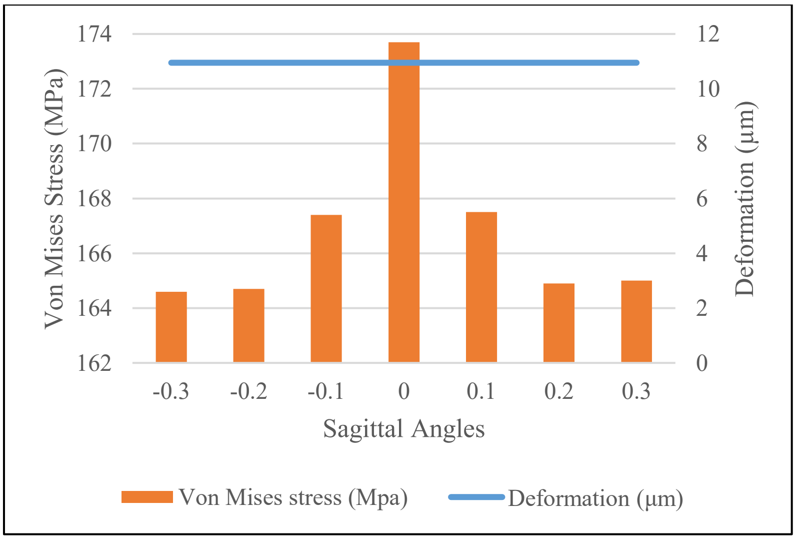

Figure 4.35 Comparison of Maximum Von Mises Stress And Displacement for Implant at Different Sagittal Angles under Walking Loading Condition

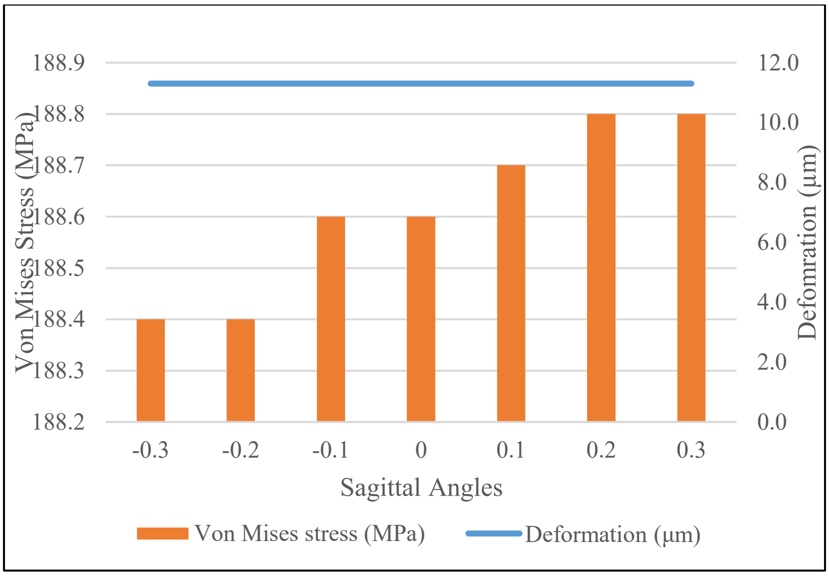

Figure 4.36 Comparison of Maximum Von Mises Stress and Displacement for Implant at Different Sagittal Angles under Stair Climbing Loading Condition

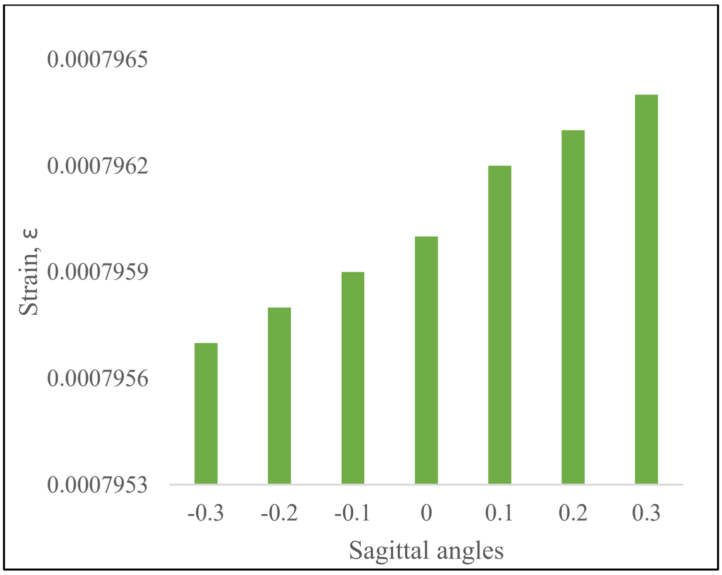

Figure 4.37 Strain of Cement Implant Different Sagittal Angles under Walking Loading Condition

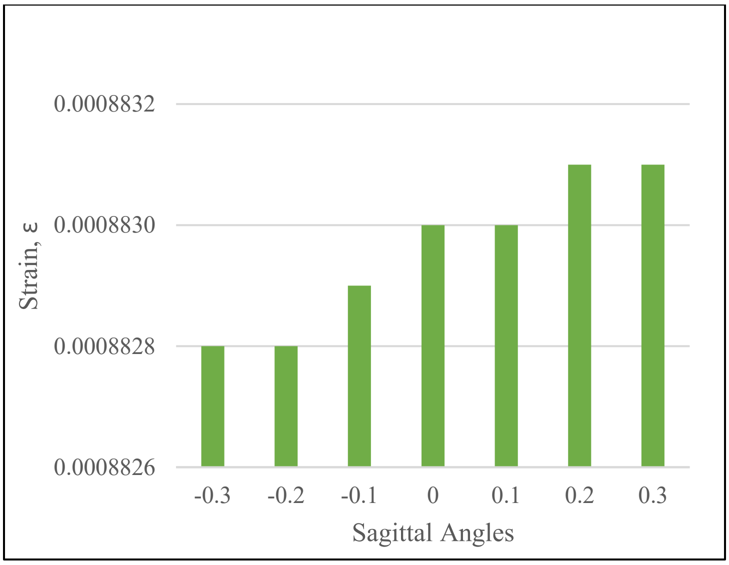

Figure 4.38 Strain of Implant Against Different Sagittal Angles under Stair Climbing Loading Condition

4.3.2 Variation in Small Angles at Varus Positioning

Varus alignment during walking and stair climbing activity was assessed by examining six angles which are 0.75°, -0.5°, -0.25°, 0.25°, 0.5° and 0.75°, with 0° designated as the reference angle.

4.3.2.1 Total Hip Arthroplasty

Figure 4.39 and Figure 4.40 shows barely any variation in the distribution of stress across all varus angles ranging from -0.75° to 0.75°, with more pronounced concentration of stress along the medial and lateral aspects of the bone and implant which possibly indicates an uneven distribution of load due to the misalignment. These localized increases in stress are likely due to the abrupt transition in stiffness between the implant and the surrounding bone tissue. It is anticipated that elevated stress could result from the significant reaction force at the lower cement mantle, as the force is exerted at the hip joint contact (Aznan et al., 2020). This pattern seems to be consistent with other research, which found the maximum von Mises stress distribution was observed at the distal region of the hip prosthesis, while the peak von Mises stress at the inner femoral bone was located at the medial side (Ismail et al., 2023). However, Ismail et al focusing on the cementless hip arthroplasty. High von Mises stress in the implant indicates that it is experiencing a significant load, which could exacerbate stress shielding in the surrounding bone. In particular, the existence of a hip implant can instigate the development of denser osseous tissue in regions subjected to mechanical stresses exceeding physiological levels, while simultaneously leading to atrophic bone formation in areas of the femur that are no longer subjected to physiological loading (commonly referred to as the stress-protected or stress-shielded zone). This phenomenon occurs due to the introduction of a prosthetic device into the skeletal structure, which substantially modifies the load distribution, thereby altering the mechanisms of bone remodelling (Savio & Bagno, 2022).

Additionally, Figure 4.41 and Figure 4.42 demonstrates that the medial region of the femoral bone consistently experiences high strain across all tested angles under walking and stair climbing loading conditions, respectively. This region is subjected to bending and compressive forces as the load is transferred through the implant, leading to elevated strain levels with an increased likelihood of mechanical failure based on the placement of the implant. In cemented THA, load transfer transpires when the cement promptly secures the implant to the bone, facilitating efficient load distribution from the implant to the adjacent bone, hence improving initial stability and long-term fixation (Enoksen et al., 2017). The uniform strain distribution across different varus angles suggests that these angles do not influence the overall strain pattern. Previous study found that the strain measurements observed in the cemented stem exhibited higher concentration on the medial aspect of the femur in contrast to those recorded for the uncemented stem (Enoksen et al., 2017).

Similarly, Figure 4.43 and Figure 4.44 reveals a consistent deformation pattern across all varus angles, indicating a uniform response of the implant system to applied loads. The red and grey regions highlight the highest deformation levels, primarily in the upper portion of the implant. Notably, the grey area appears more extensive under stair climbing loading condition as shown in Figure 4.44. This observation aligns with expectations, as the upper part of the THA model experiences the most deformation due to its greater distance from the fixed support at the base of the femoral bone. This finding similar to the previous study where the highest deformation was found at the femoral head . According to Ammarullah et al., the upper region of the THA model undergoes the greatest deformation due to the elevated vertical loads associated with higher body mass index (BMI) categories, leading to increased displacement in the negative y-direction under normal walking conditions (Ammarullah et al., 2022).

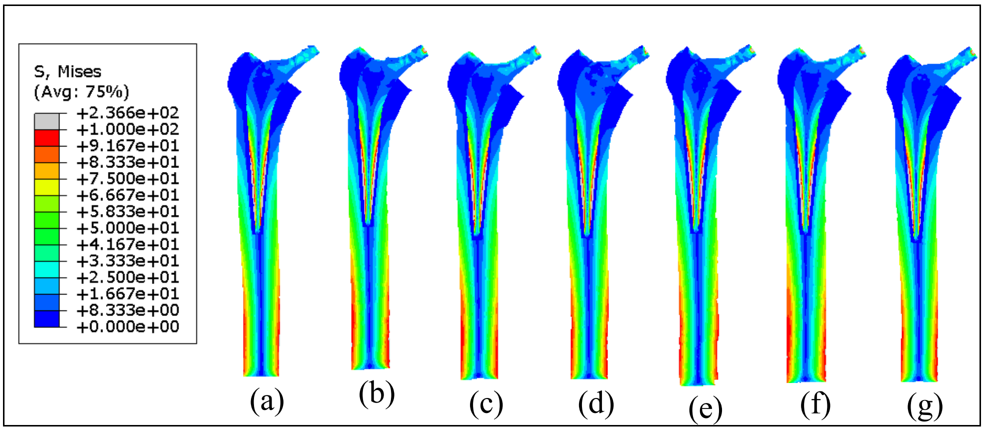

Figure 4.39 Stress Distribution Analysis for All Components at Different Varus Angles under Walking Loading Condition (a) -0.75°, (b) -0.5°, (c) -0.25°, (d) 0°, (e) 0.25°, (f) 0.5° and (g) 0.75°

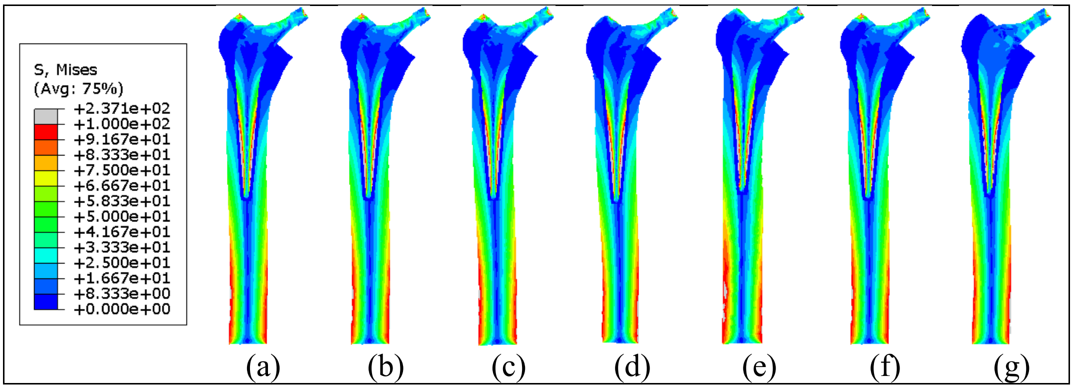

Figure 4.40 Stress Distribution Analysis for All Components at Different Varus Angles under Stair Climbing Loading Condition (a) -0.75°, (b) -0.5°, (c) -0.25°, (d) 0°, (e) 0.25°, (f) 0.5° and (g) 0.75°

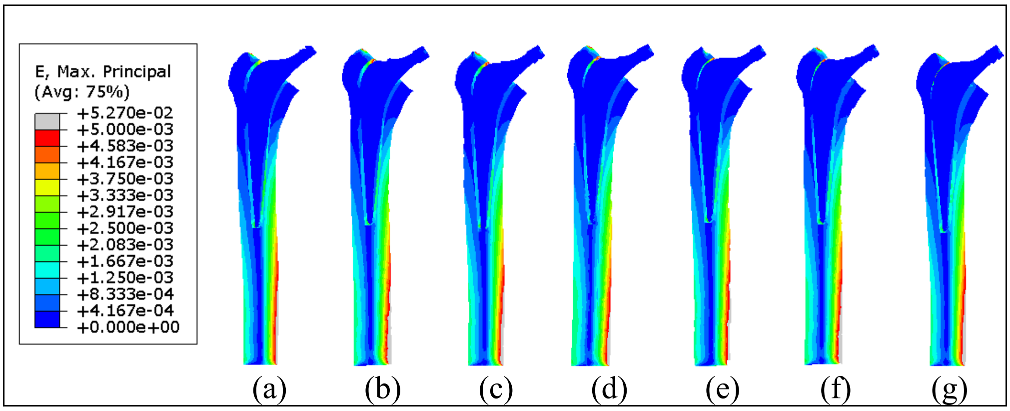

Figure 4.41 Strain Distribution Analysis for All Components at Different Varus Angles under Walking Loading Condition (a) -0.75°, (b) -0.5°, (c) -0.25°, (d) 0°, (e) 0.25°, (f) 0.5° and (g) 0.75°

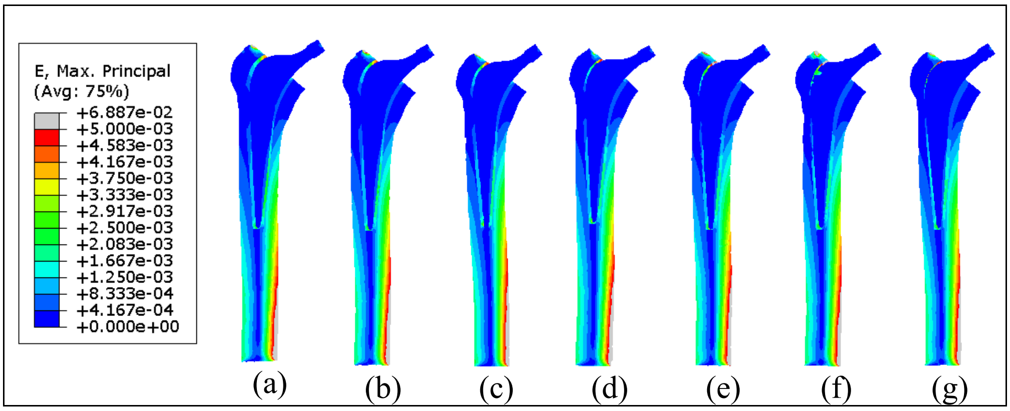

Figure 4.42 Strain Distribution Analysis for All Components at Different Varus Angles under Stair Climbing Loading Condition (a) -0.75°, (b) -0.5°, (c) -0.25°, (d) 0°, (e) 0.25°, (f) 0.5° and (g) 0.75°

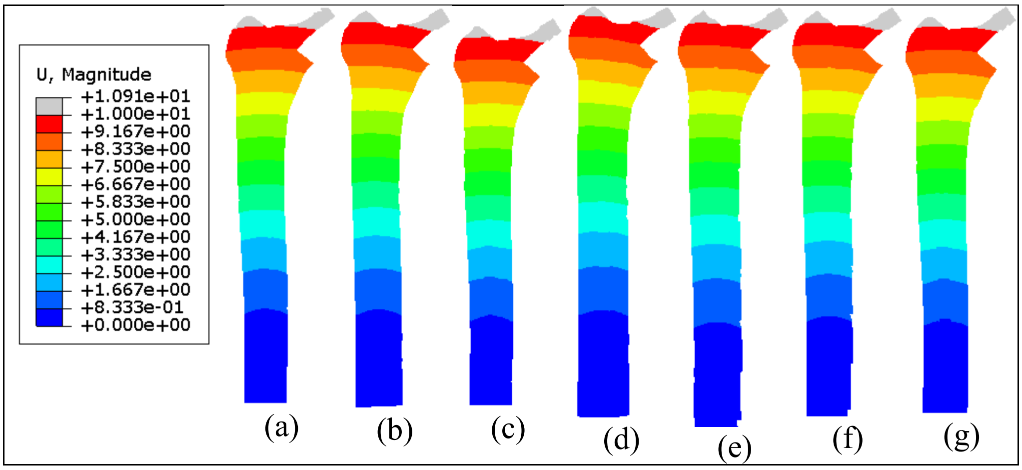

Figure 4.43 Total Deformation Analysis for All Components at Different Varus Angles under Walking Loading Condition (a) -0.75°, (b) -0.5°, (c) -0.25°, (d) 0°, (e) 0.25°, (f) 0.5° and (g) 0.75°

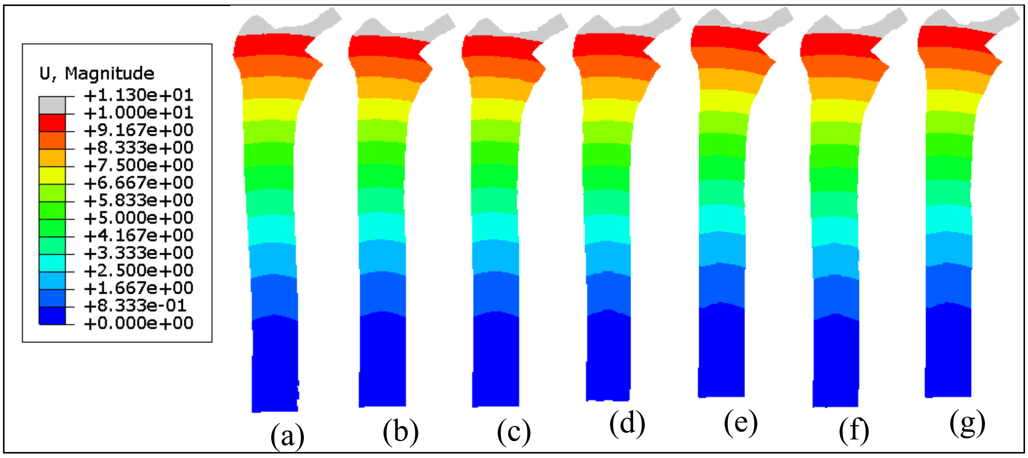

Figure 4.44 Total Deformation Analysis for All Components at Different Varus Angles under Stair Climbing Loading Condition (a) -0.75°, (b) -0.5°, (c) -0.25°, (d) 0°, (e) 0.25°, (f) 0.5° and (g) 0.75°

4.3.2.2 Half Femur

Figure 4.45 and Figure 4.46 demonstrate the constant pattern of stress distribution in the femur bone at various varus angles under walking and stair climbing loading conditions, respectively. This demonstrates that the stress distribution is not impacted by the various varus angles. The maximum stress is concentrated mostly in the distal and medial areas of the femur. This stress distribution pattern is similar to the previous research that found the stress level progressively increased from the proximal to the distal region, peaking in the middle and lower parts of the femur which likely associated with the bending moment effect of the femur (Luo et al., 2020). At the neutral position, the stress appears symmetrically distributed. As has been previously reported in the literature, the stress distribution followed a predictable pattern. This was observed under neutral loading cases, meaning the forces applied were balanced. Since the stress pattern was regular, it suggests that the femur was mainly experiencing pure bending which means the bone is mainly bending in one direction without additional twisting or compression (Belaïd et al., 2022). Meanwhile Figure 4.46 shows slight variations in colours across different varus angles indicating a change in the stress distribution pattern of the femur bone under stair climbing loading condition. At -0.75°, -0.5°, and -0.25°, there is a slightly higher stress at the proximal femur which possibly indicates an uneven distribution of load due to the misalignment. However, the overall stress distribution shows minimal variation. The distribution might be affected by how the bone normally transmits load, notably because the varus positioning alters biomechanics.

Figure 4.47 and Figure 4.48 illustrates the strain distribution across the femur under varus alignment under walking and stair climbing loading conditions, respectively. The higher strain are primarily concentrated in the medial regions of the femur, consistent with the strain distribution observed in the sagittal plane under stair climbing loading conditions. This pattern is likely influenced by the directional forces acting on the bone due to the implant's alignment. Despite variations in varus angles, the strain distribution remains consistent, suggesting that the femur's biomechanical adaptation to the implant does not significantly vary within the tested range. Previous studies suggested that areas of elevated strain are predominantly localized in the medial and distal femur, resulting from altered load distribution and stress shielding effects induced by the implant. These factors contribute to modifications in tensile and compressive stresses within these areas (Todo & Fukuoka, 2020). Higher strain values raise the risk of hip pain, falls, and stress fractures (Deng et al., 2018).

Similarly, Figure 4.49 and Figure 4.50 highlights a uniform deformation pattern across different angles in the magnitude deformation analysis under walking and stair climbing loading conditions, respectively. As shown in Figure 4.50, the proximal femur experiences greater deformation under stair climbing loading conditions compared to walking. This indicates that implant placement within the tested range has minimal impact on bone deformation under simulated physiological loads. The results suggest that the femur maintains its structural integrity despite changes in alignment, which is crucial for the implant-bone complex's durability and stability. However, identifying the optimal implant positioning remains a challenge, emphasizing the need for further research to refine alignment strategies for improved biomechanical outcomes.

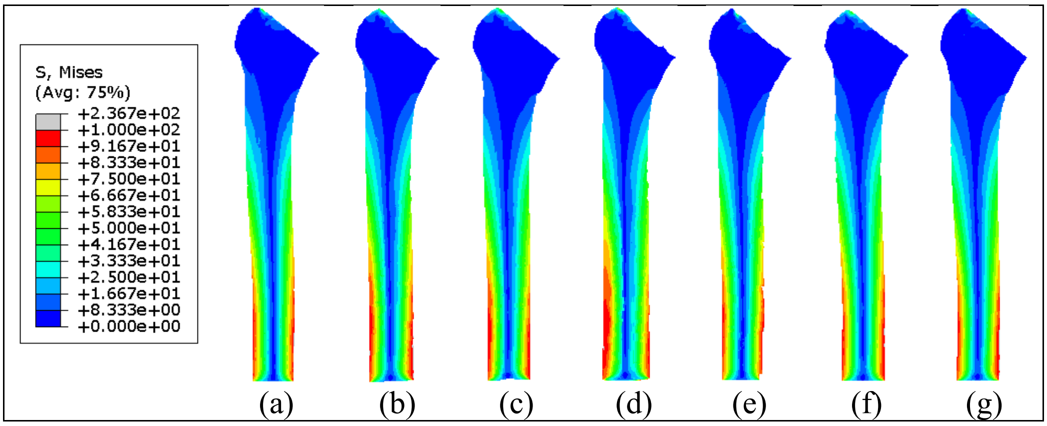

Figure 4.45 Stress Distribution Analysis for Femur Bone at Different Varus Angles under Walking Loading Condition (a) -0.75°, (b) -0.5°, (c) -0.25°, (d) 0°, (e) 0.25°, (f) 0.5° and (g) 0.75°

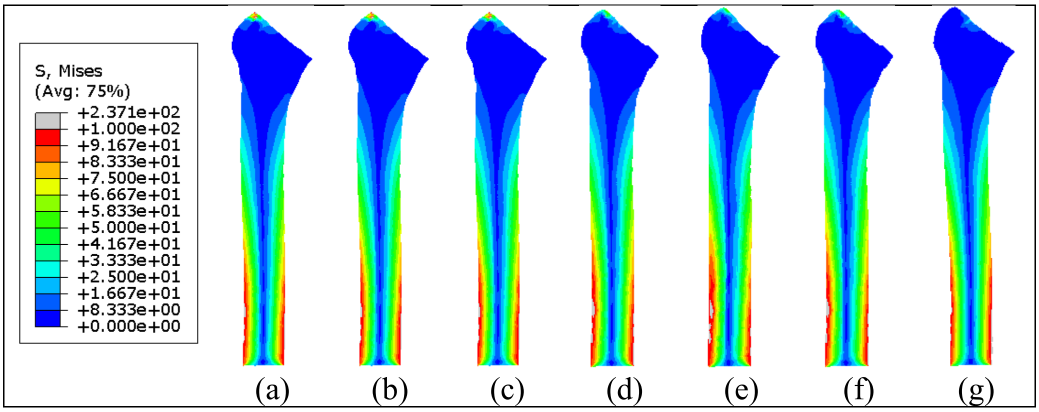

Figure 4.46 Stress Distribution Analysis for Femoral Bone at Different Varus Angles under Stair Climbing Loading Condition (a) -0.75°, (b) -0.5°, (c) -0.25°, (d) 0°, (e) 0.25°, (f) 0.5° and (g) 0.75°

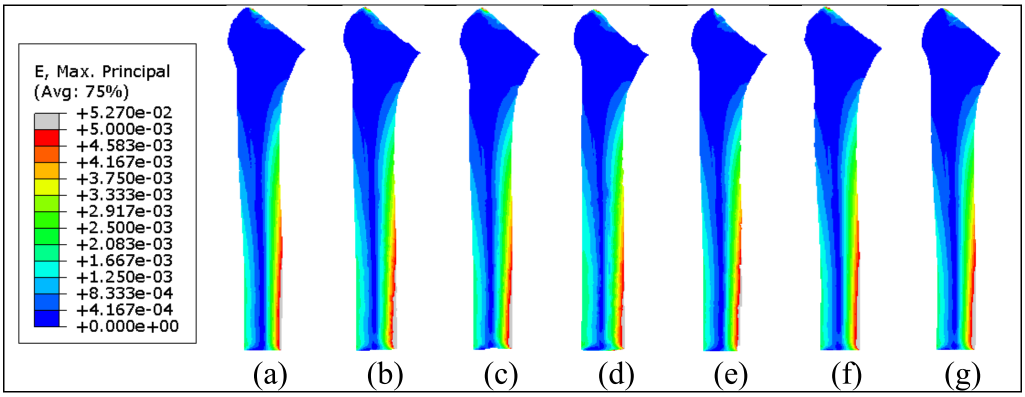

Figure 4.47 Strain Distribution Analysis for Femur Bone at Different Varus Angles under Walking Loading Condition (a) -0.75°, (b) -0.5°, (c) -0.25°, (d) 0°, (e) 0.25°, (f) 0.5° and (g) 0.75°

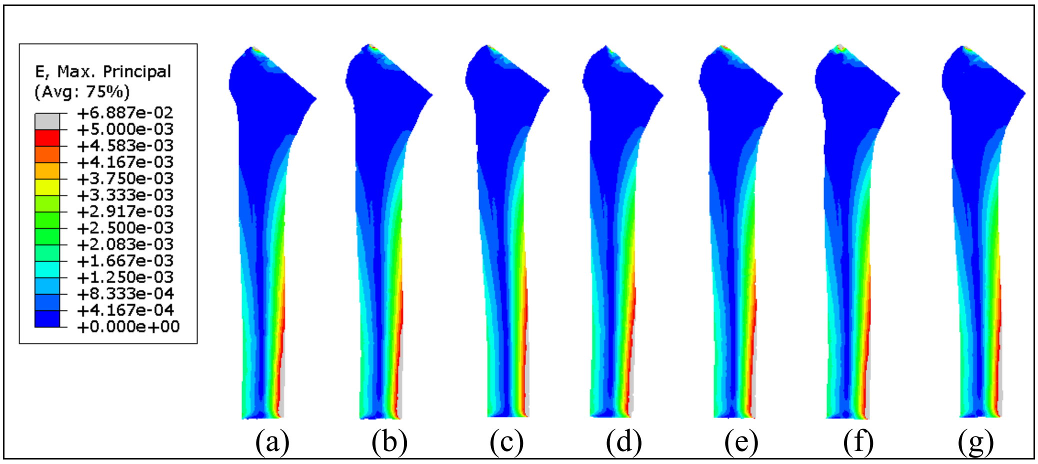

Figure 4.48 Strain Distribution Analysis for Femoral Bone at Different Varus Angles under Stair Climbing Loading Condition (a) -0.3°, (b) -0.2°, (c) -0.1°, (d) 0°, (e) 0.1°, (f) 0.2° and (g) 0.3°

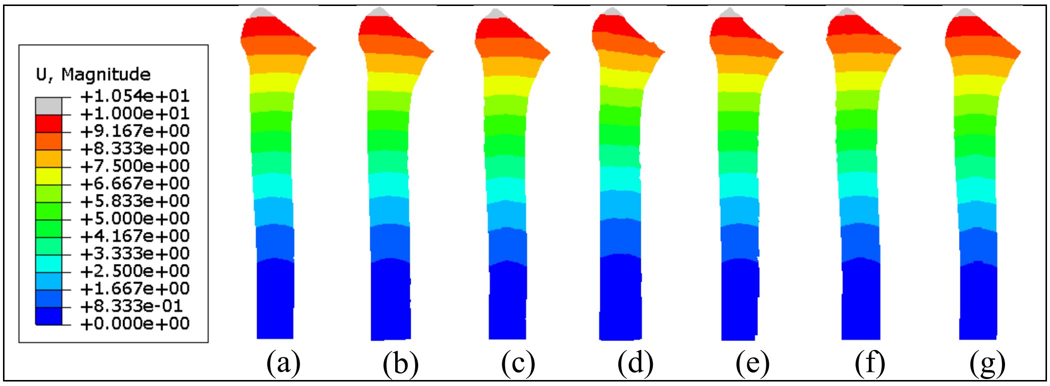

Figure 4.49 Total Deformation Analysis for Femur Bone at Different Varus Angles under Walking Loading Condition (a) -0.75°, (b) -0.5°, (c) -0.25°, (d) 0°, (e) 0.25°, (f) 0.5° and (g) 0.75°

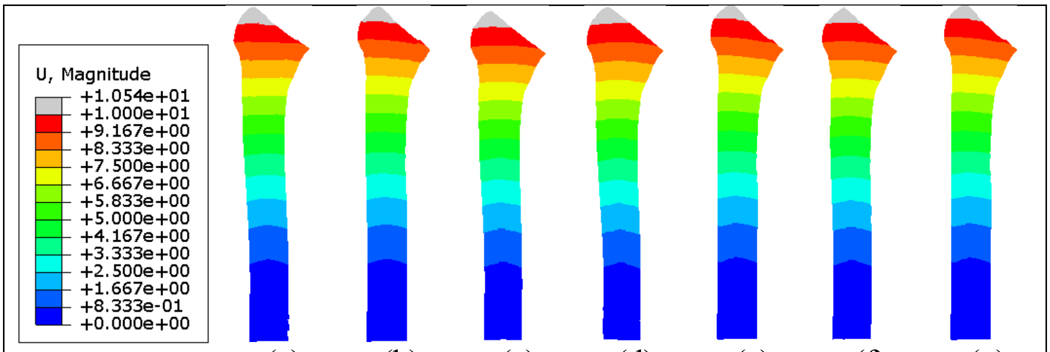

Figure 4.50 Total Deformation Analysis for Femoral Bone at Different Varus Angles under Stair Climbing Loading Condition (a) -0.75°, (b) -0.5°, (c) -0.25°, (d) 0°, (e) 0.25°, (f) 0.5° and (g) 0.75°

Figure 4.51 demonstrates that Von Mises stress values are marginally higher at more negative varus angles, with a peak stress value of 236.8 MPa observed at -0.75°. The stress slightly decreases as the angles become less negative, stabilizing at approximately 236.6 MPa for angles ranging from 0.25° to 0.75°. Conversely, deformation exhibits an inverse relationship with the varus angle, with higher angles corresponding to slightly lower deformation values. This suggests that the bone-implant system may exhibit increased rigidity as the varus angle increases. Figure 4.52 demonstrates that as the angle of the varus increases from -0.75° to 0.75°, there is a slight decrease in Von Mises stress. This might suggest that as the implant angle approaches the neutral which is at 0°, the stress on the femur decreases. However, the change in stress is very minimal, indicating that within the range of angles assessed, the stress distribution does not vary significantly. Besides, as the varus angle increases from -0.75° to 0.75°, the magnitude of deformation reduces from 10.92 μm to 10.85 μm, implying that the femoral bone experiences less deformation as the implant angle moves towards the positive side. The trend is relatively linear, suggesting a predictable and proportional relationship between the varus angle and the deformation magnitude within the tested range. This information could be indicative of how the bone would behave under a load in real-world scenarios, where a slight variance in the angle of implantation could potentially affect the deformation experienced by the bone.

Similarly, Figure 4.53 highlights a slight but noticeable variation in strain across the angles, with the highest strain occurring at -0.75° and the lowest at 0.75°. The graph in Figure 4.53 reveals a linear decrease in strain values as the varus angle increases. The elevated strain at more negative angles may indicate that these angles impose slightly greater mechanical demands on the femoral bone. However, the minimal differences observed suggest that the bone-implant system's strain response remains highly consistent across the analyzed range of varus angles. Figure 4.54 shows the strain distributions against the varus angles under stair climbing loading condition. The strain magnitude remains consistent across all the tested angles, with only a slight increase observed at -0.75° with the value of 0.069.

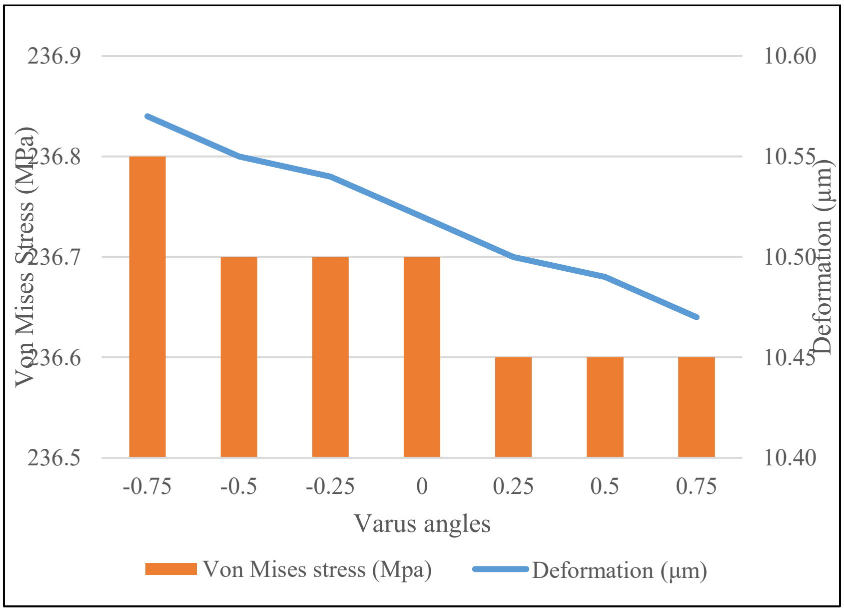

Figure 4.51 Comparison of Maximum Von Mises Stress And Deformation for Femur Bone at Different Varus Angles under Walking Loading Condition

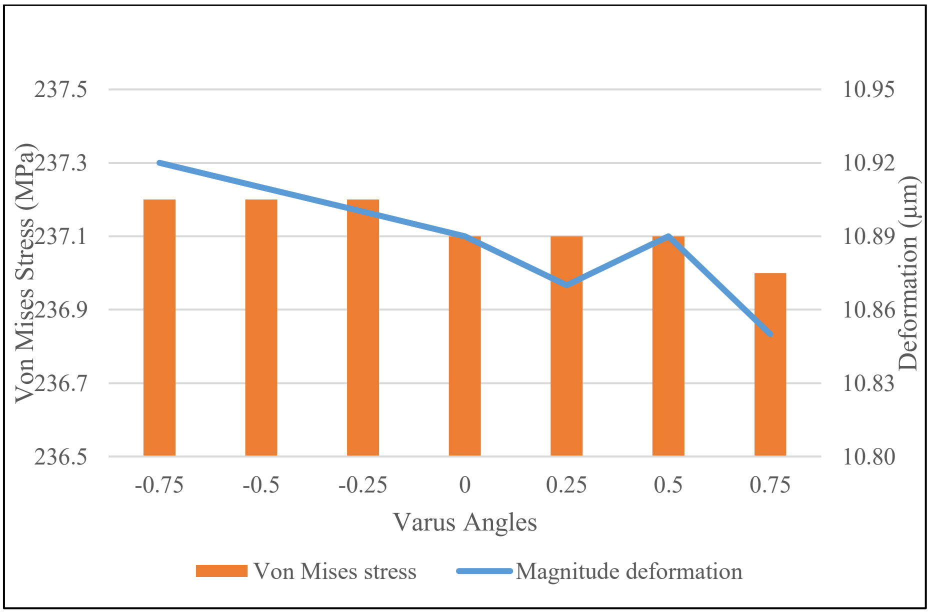

Figure 4.52 Comparison of Maximum Von Mises Stress And Deformation for Femur at Different Varus Angles under Stair Climbing Loading Condition

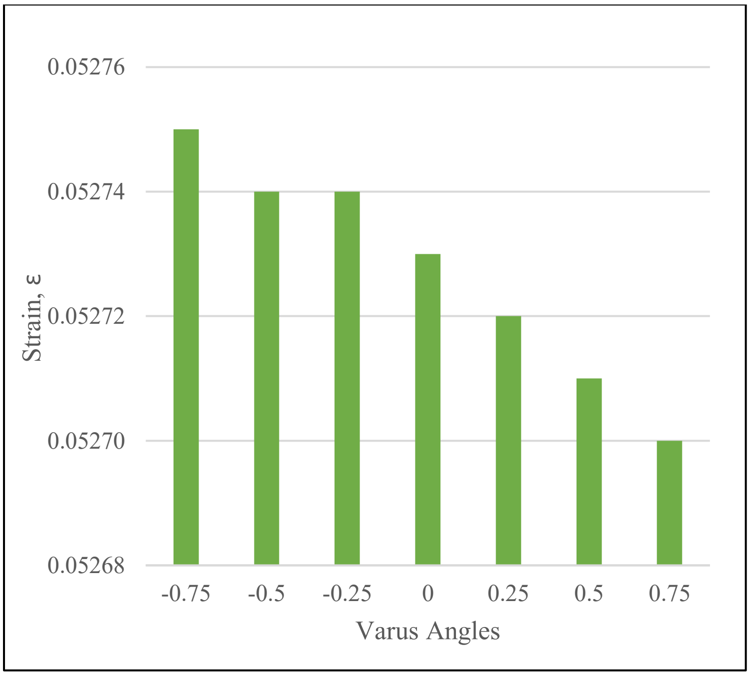

Figure 4.53 Strain of Femur Bone Against Different Varus Angles under Walking Loading Condition

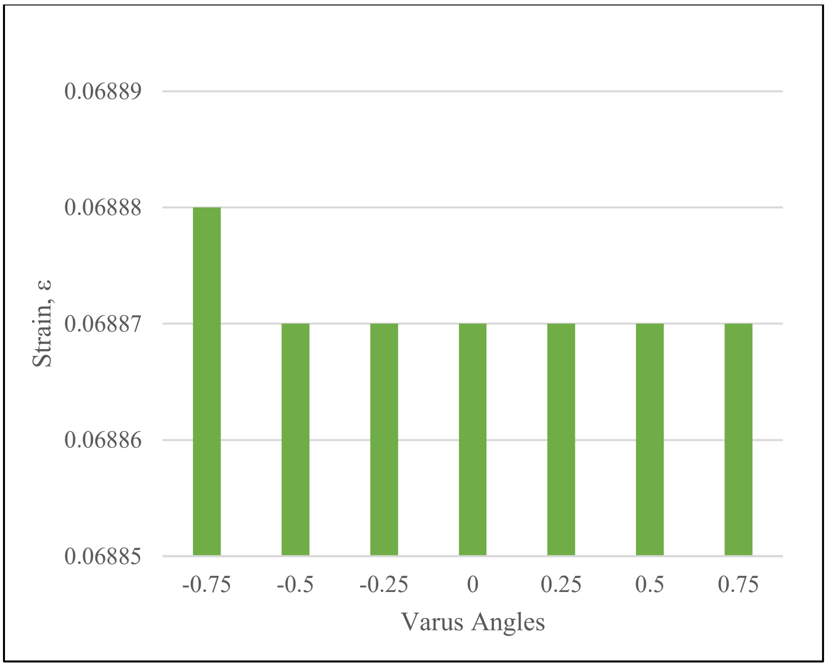

Figure 4.54 Strain of Femur Against Different Varus Angles under Stair Climbing Loading Condition

4.3.2.3 Cement mantle

Figure 4.55 and Figure 4.56 shows the pattern of stress distribution for the cement mantle remains consistent across all angles due to the von Mises stress values exhibiting minimal differences. The majority of the model exhibits a pronounced gradient of the blue colour, signifying lower values of von Mises stress. However, the upper part of the cement mantle, near the load application point, exhibits a noticeable concentration of high stress. This finding similar with the previous study by Aznan et al that concluded this phenomenon occured due to its critical role in transferring load from the prosthesis to the bone. This particular site is either in proximity to the external loading points or linked with geometric stress concentrators resulting from abrupt alterations in the cross-sectional area of the prosthesis (Aznan et al., 2020). Previous studies suggested that the stiffness difference between the rigid femoral stem and the adjacent bone results in stress shielding, particularly in the proximal femur where load is concentrated during activities like walking and stair climbing (Shuib et al., 2023; Xiao et al., 2023).

Besides, Figure 4.57 and Figure 4.58 show the strain distribution for cement mantle across different varus angles under walking and stair climbing loading conditions, respectively. Both figures highlight greater strain in the upper regions of the cement mantle, aligning with areas of elevated stress under physiological loading conditions. The strain distribution across various angles suggests that the cement mantle effectively absorbs and dissipates the mechanical forces exerted by the implant, irrespective of the varus angle. This demonstrates the material's ability to deform in response to stress. Additionally, the high stiffness of materials, such as ceramics with a large Young's modulus, can intensify stress shielding effects, resulting in an uneven strain distribution and an increased strain energy density in the upper regions (Saadoon et al., 2021). The pattern of the strain distribution under both loading conditions is similar to the sagittal positioning which corresponds to the pattern of stress distribution.

Additionally, Figure 4.59 and Figure 4.60 reveals that deformation is highest in the upper regions of the cement mantle, corresponding to areas of high stress and strain similar to the previous study (Aznan et al., 2020). The analysis further shows that the overall deformation distribution remains consistent across all angles, confirming that total deformation is unaffected by the varus angles tested.

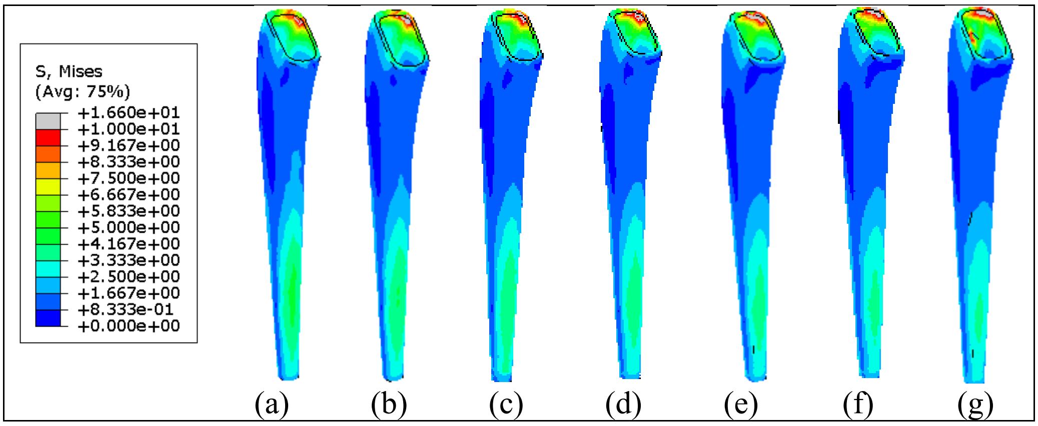

Figure 4.55 Stress Distribution Analysis for Cement Mantle at Different Varus Angles under Walking Loading Condition (a) -0.75°, (b) -0.5°, (c) -0.25°, (d) 0°, (e) 0.25°, (f) 0.5° and (g) 0.75°

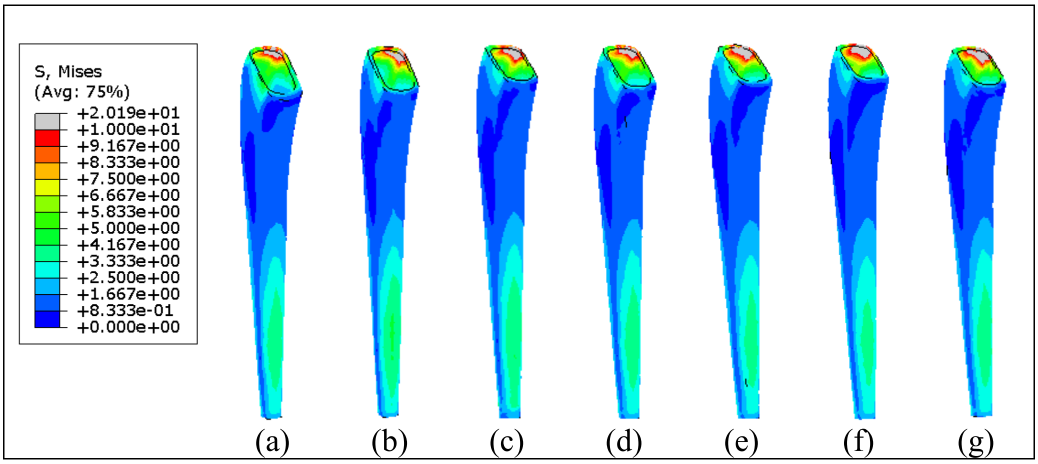

Figure 4.56 Stress Distribution Analysis for Cement Mantle at Different Varus Angles under Stair Climbing Loading Condition (a) -0.75°, (b) -0.5°, (c) -0.25°, (d) 0°, (e) 0.25°, (f) 0.5° and (g) 0.75°

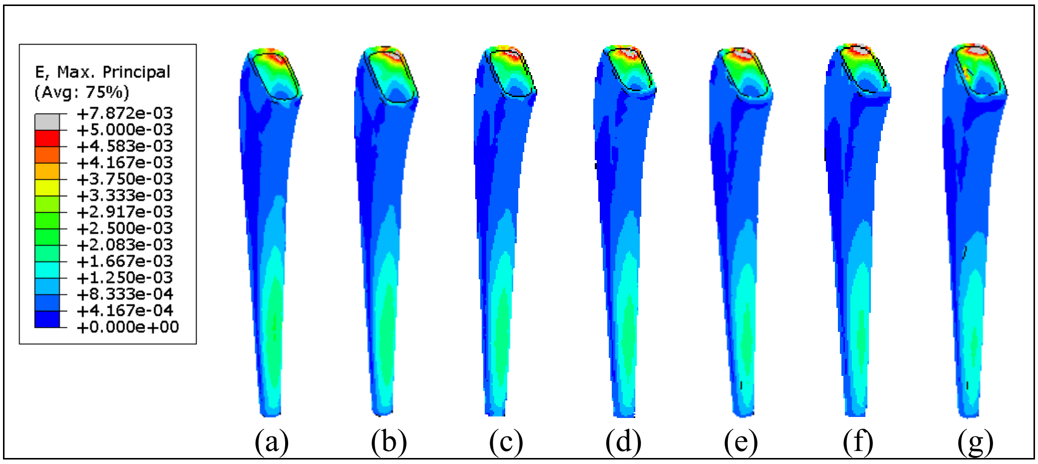

Figure 4.57 Strain Distribution Analysis for Cement Mantle at Different Varus Angles under Walking Loading Condition (a) -0.75°, (b) -0.5°, (c) -0.25°, (d) 0°, (e) 0.25°, (f) 0.5° and (g) 0.75°

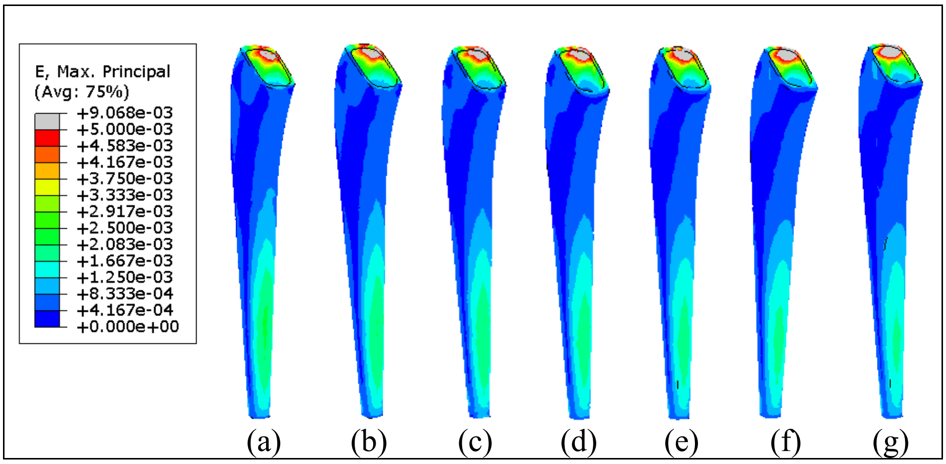

Figure 4.58 Strain Distribution Analysis for Cement Mantle at Different Varus Angles under Stair Climbing Loading Condition (a) -0.75°, (b) -0.5°, (c) -0.25°, (d) 0°, (e) 0.25°, (f) 0.5° and (g) 0.75°

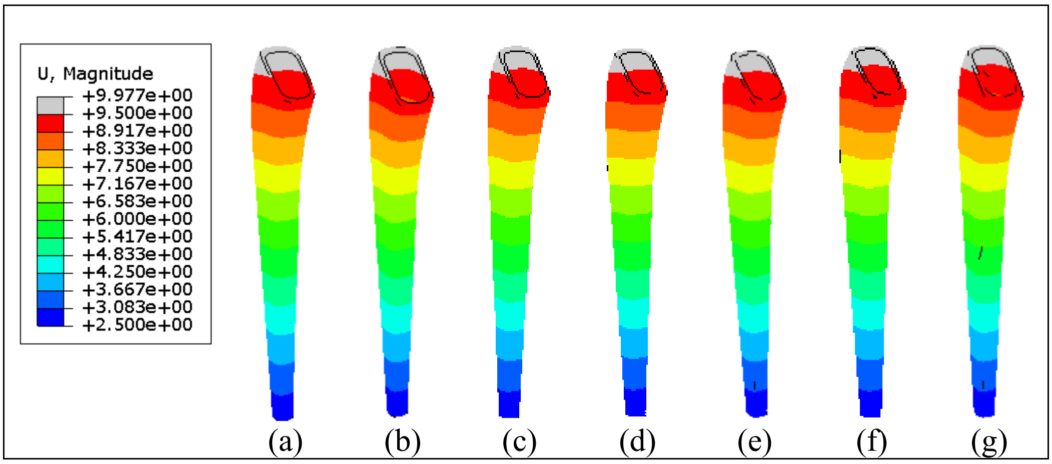

Figure 4.59 Total Deformation Analysis for Cement Mantle at Different Varus Angles under Walking Loading Condition (a) -0.75°, (b) -0.5°, (c) -0.25°, (d) 0°, (e) 0.25°, (f) 0.5° and (g) 0.75°

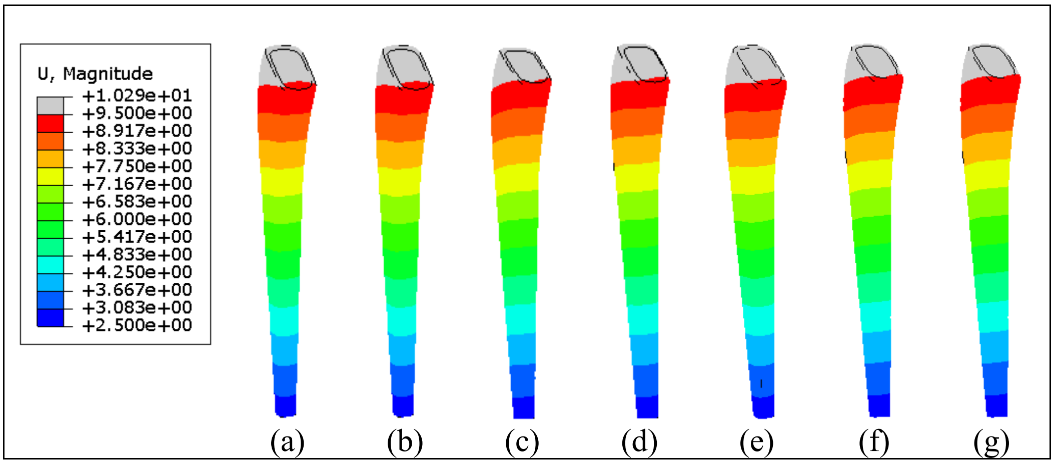

Figure 4.60 Total Deformation Analysis for Cement Mantle at Different Varus Angles under Stair Climbing Loading Condition (a) -0.75°, (b) -0.5°, (c) -0.25°, (d) 0°, (e) 0.25°, (f) 0.5° and (g) 0.75°

According to Figure 4.61, the stress values vary across different angles, with the highest stress of 17.61 MPa occurring at -0.25° and the lowest stress of 12.33 MPa observed at -0.75°. In contrast, deformation follows an inverse pattern where the greatest deformation, 10.02 µm, is recorded at -0.75°, while the smallest deformation, 9.9285 µm, is observed at 0.75°. This inverse relationship suggests that as varus angles become more extreme, the cement mantle may undergo slightly greater deformation. This could indicate a more compliant material response or a more flexible interaction between the cement mantle and the implant.

Furthermore, Figure 4.62 illustrates that the von Mises stress values fluctuate as the varus angle changes under stair climbing condition. Notably, there is a peak at -0.25° and -0.5°, suggesting these positions experience higher stress. There is a noticeable reduction in stress as the angle shifts from -0.25° to 0.25°, followed by a slight increase towards 0.75°. This pattern could suggest that certain angles are more prone to induce stress within the cement mantle, which could affect the longevity and stability of the implant. This may result from PMMA being softer facilitating the adaptation of implants and femurs to mitigate the strain transmitted from the implants to the femurs through deformation akin to a dashpot (Yavuz Solmaz et al., 2018). The magnitude of deformation gently decreases as the angle moves from -0.75° to 0.75° as shown in Figure 4.62. The changes are small but consistent. The highest deformation occurred at -0.75° with the value of 10.33µm. The smallest deformation is observed at 0.75° with the value of 10.26µm, indicating this may be a more stable configuration under the simulated conditions.

The strain graph in Figure 4.61 illustrates minimal variance, with the highest strain observed at -0.75° and the lowest at 0.25°. These small differences in strain values indicate that the cement mantle's deformation capacity under load remains consistent across the studied range of varus angles. However, even minor variations could hold clinical importance, implying that slight changes in the varus angle might influence how the cement mantle responds to strain during loading.

Figure 4.63 shows the strain of the cement mantle against different varus angles. The greatest strain is observed at the most negative varus angle (-0.75) with the value of 0.0097 and typically diminishes as the varus angle nears zero. After that, it experiences a slight increase once more at positive varus angles. The lowest strain is found at 0.25 varus angle with the value of 0.0069, indicating that this position may offer enhanced stability or reduced stress to the cement mantle.

According to Figure 4.64, as the varus angles moves toward the positive angles, the strain value generally decrease. The highest value of strain is 0.0111 at -0.75° and the lowest strain is 0.0079 occurred at 0.25°, which means the neutral position does not exhibit the lowest strain.

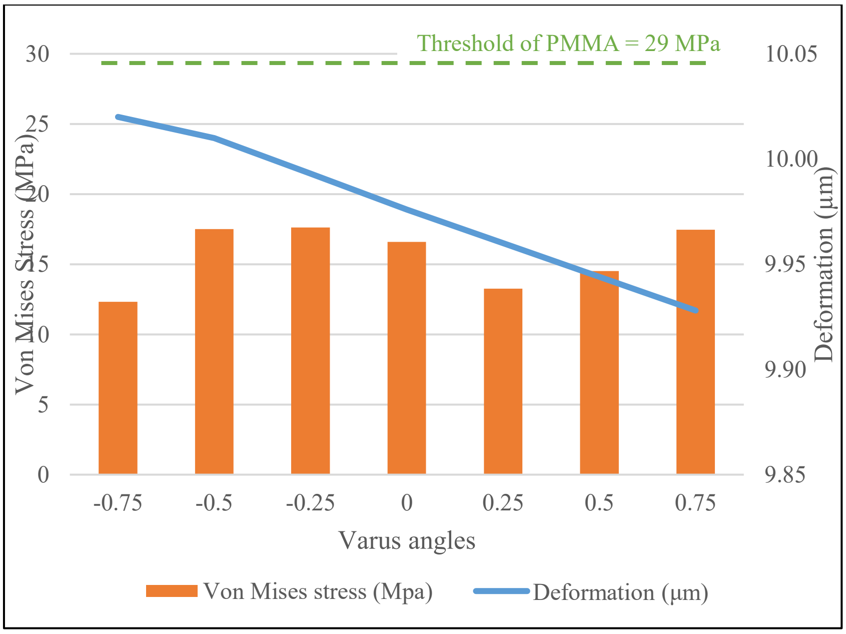

Figure 4.61 Comparison of Maximum Von Mises Stress And Displacement for Cement Mantle at Different Varus Angles under Walking Loading Condition

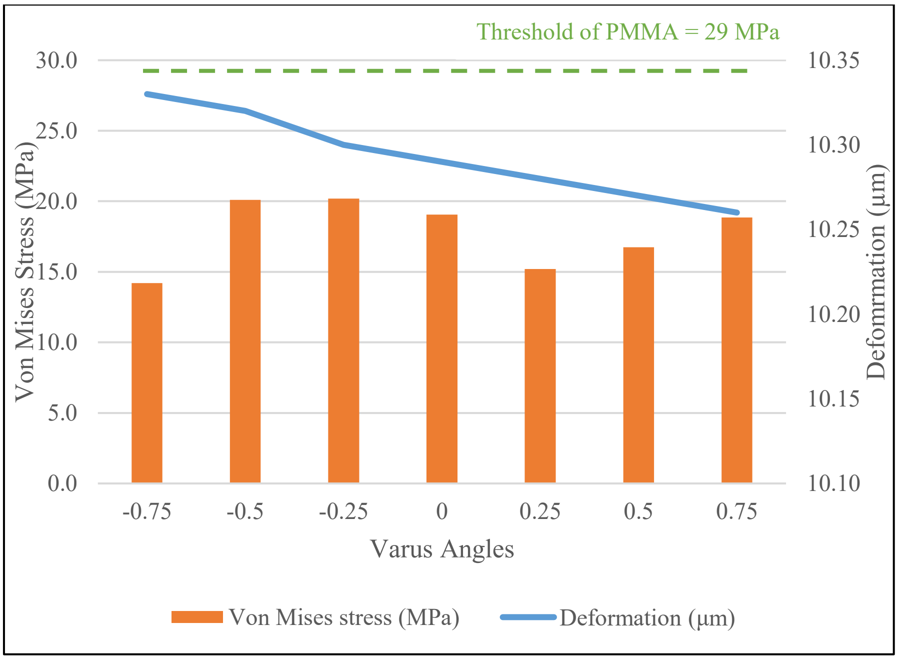

Figure 4.62 Comparison of Maximum Von Mises Stress And Displacement for Cement Mantle at Different Varus Angles under Stair Climbing Loading Condition

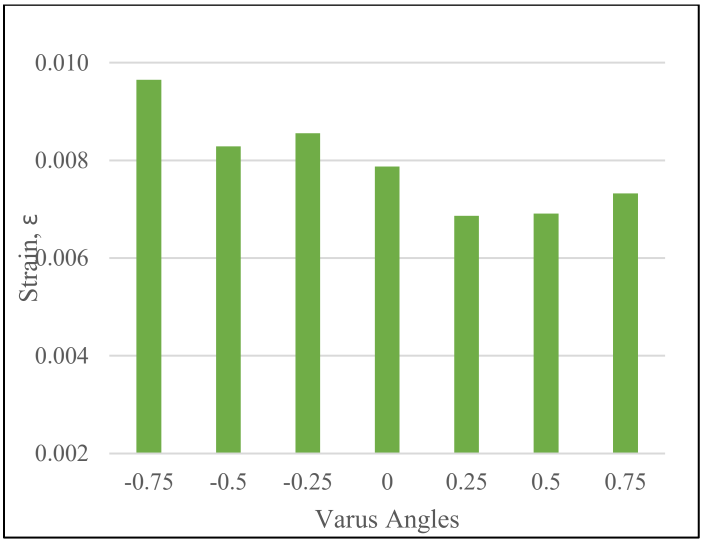

Figure 4.63 Strain of Cement Mantle Against Different Varus Angles under Walking Loading Condition

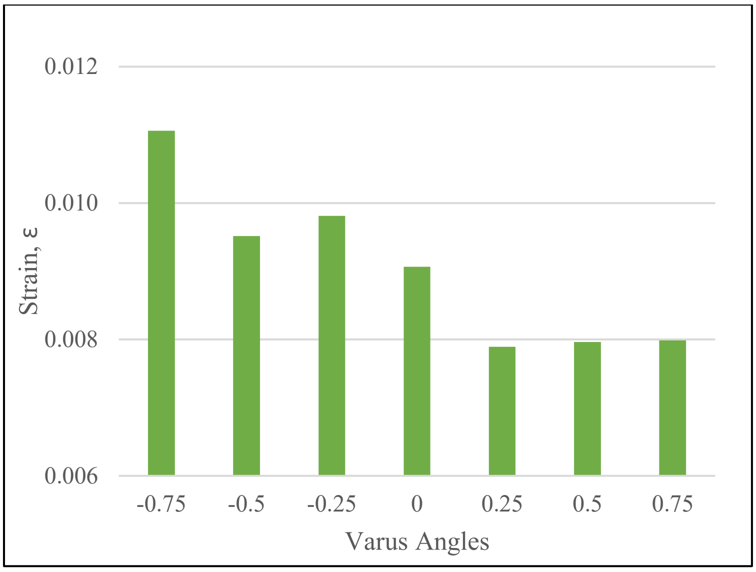

Figure 4.64 Strain of Cement Mantle Against Different Varus Angles under Stair Climbing Loading Condition

4.3.2.4 Hip Implant

Figure 4.65 and Figure 4.66 illustrate implant models with a colour gradient representing Von Mises stress distribution at different alignment varus angles under walking and stair climbing loading conditions, respectively. Under walking loading conditions, regions of higher stress are observed at the head and distal part of the implant. This distribution aligns with fundamental mechanical principles, as these areas are subjected to the greatest forces during walking activity. Meanwhile, under stair climbing conditions, not only the head and distal part, but also the neck of the implant. As the findings from both computational and experimental analyses are consistent, Patra et al concludes that the maximum stress occurs at the neck of the hip prosthesis. The stress concentration gradually decreases along the shaft of the prosthesis. This stress distribution plays a critical role in the loosening or failure of the prosthesis (Patra et al., 2020). The stress distribution pattern remains consistent across all tested angles, suggesting that slight variations in implant positioning have minimal impact on the overall stress distribution within the implant. These subtleties might not lead to immediate clinical issues but could have long-term implications for the integrity of the implant. Besides, a previous study found that varus and valgus deflections have a minor effect in the coronal plane, particularly under varying loading condition which are standing and walking (Kaku et al., 2022). In contrast, previous studies indicate that an increase in the varus angle correlates with higher maximum von Mises stress values, suggesting an elevated fracture risk associated with varying degrees of varus positioning (Belaïd et al., 2022).

Besides, Figure 4.67 and Figure 4.68 present the strain distribution analysis for an implant under different varus angles under walking and stair climbing loading conditions, respectively. The regions of maximum strain are consistently localized near the distal end of the implant, indicating that this area experiences the highest mechanical loading (Firdaus et al., 2024). According to Vogel et al, increased strain distribution in the lower region of the hip implant arises from differences in stiffness between the implant materials and the surrounding bone, resulting in stress shielding effects, especially when using stiffer materials (Vogel et al., 2021). The minimal variations in the magnitude and pattern of strain across the angles suggest that the implant maintains mechanical stability despite slight varus positioning. The stable strain pattern indicates effective load transfer between the implant and the bone, reducing the risk of stress shielding, which can lead to bone resorption and implant loosening. Since slight varus positioning does not significantly impact the strain distribution, this suggests some flexibility in surgical alignment during implantation.

Figure 4.69 and Figure 4.70 show the total deformation analysis of the implant at various varus angles under walking and stair climbing loading conditions. Across all varus angles, the deformation pattern remains largely consistent, with maximum deformation localized near the proximal end of the implant and minimum deformation occurring near the distal end of the implant. This pattern suggests that the mechanical behaviour is dominated by the loading conditions associated with the femoral head during walking and stair climbing activities. The pattern of deformation also similar to the previous study in which the greater deformation occurred at the upper part of the various type of the hip implant (K.N. et al., 2019).While slight variations in deformation magnitude are observed across the tested angles, these changes are minimal. The magnitude of deformation appears to be stable within a narrow range, indicating that the implant is resilient to minor varus misalignments. The consistent deformation behaviour highlights the implant's ability to maintain structural integrity and functionality across a range of small angular deviations. This is essential for preventing excessive stress or strain that could lead to implant failure or damage to surrounding bone tissue.

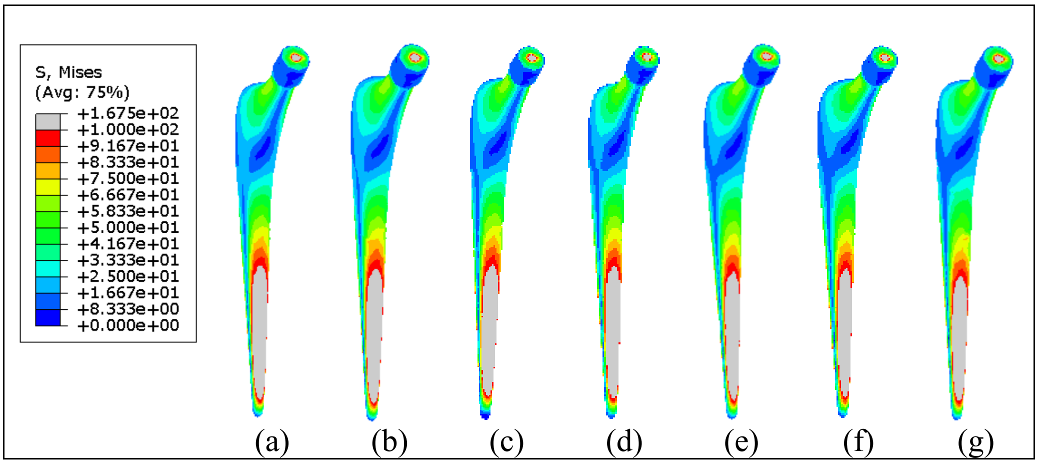

Figure 4.65 Stress Distribution Analysis for Implant at Different Varus Angles under Walking Loading Condition (a) -0.75°, (b) -0.5°, (c) -0.25°, (d) 0°, (e) 0.25°, (f) 0.5° and (g) 0.75°

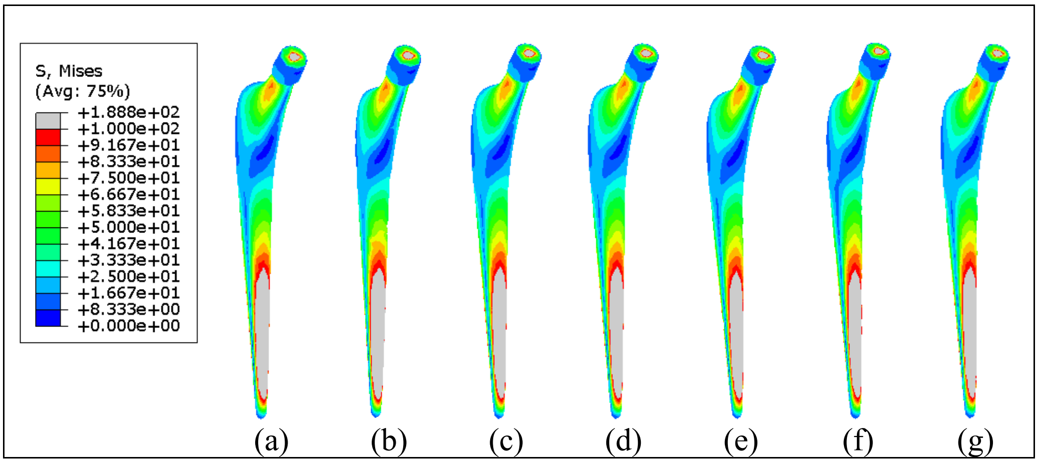

Figure 4.66 Stress Distribution Analysis for Implant at Different Varus Angles under Stair Climbing Loading Condition (a) -0.75°, (b) -0.5°, (c) -0.25°, (d) 0°, (e) 0.25°, (f) 0.5° and (g) 0.75°

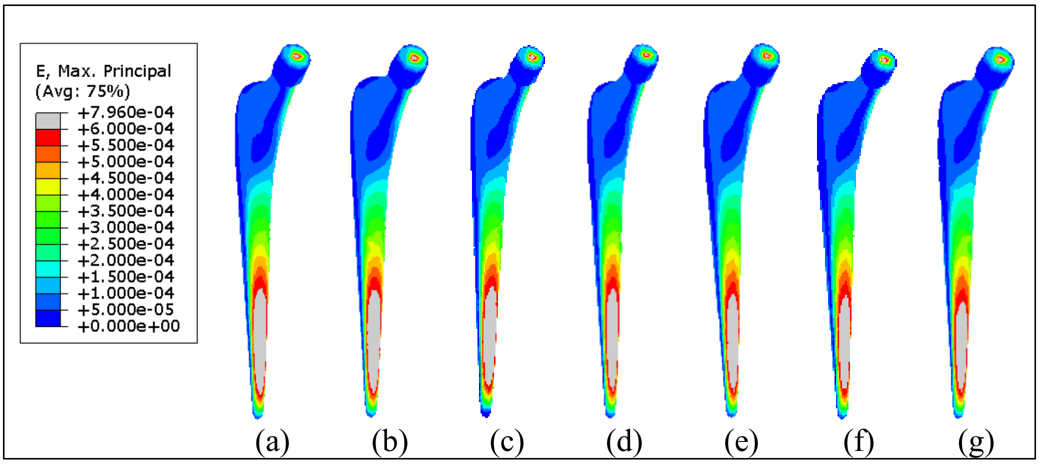

Figure 4.67 Strain Distribution Analysis for Implant at Different Varus Angles under Walking Loading Condition (a) -0.75°, (b) -0.5°, (c) -0.25°, (d) 0°, (e) 0.25°, (f) 0.5° and (g) 0.75°

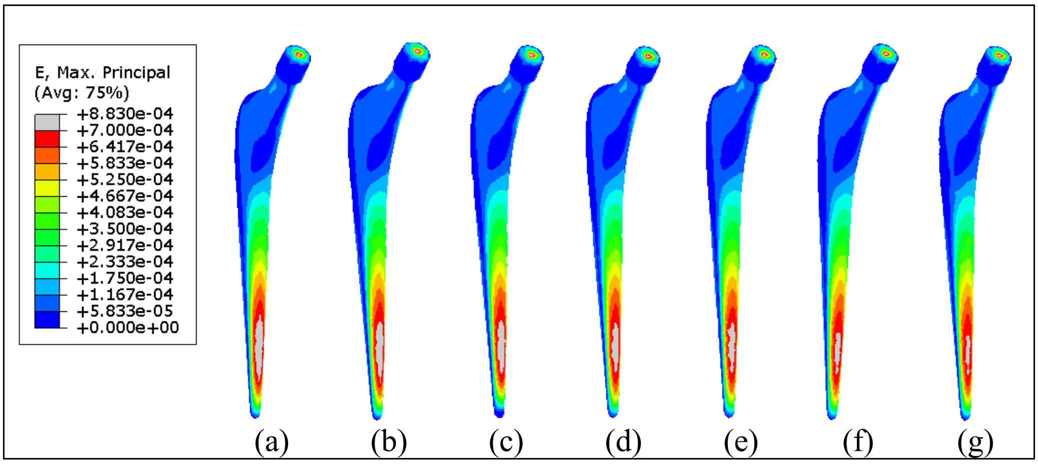

Figure 4.68 Strain Distribution Analysis for Implant at Different Varus Angles under Stair Climbing Loading Condition (a) -0.75°, (b) -0.5°, (c) -0.25°, (d) 0°, (e) 0.25°, (f) 0.5° and (g) 0.75°

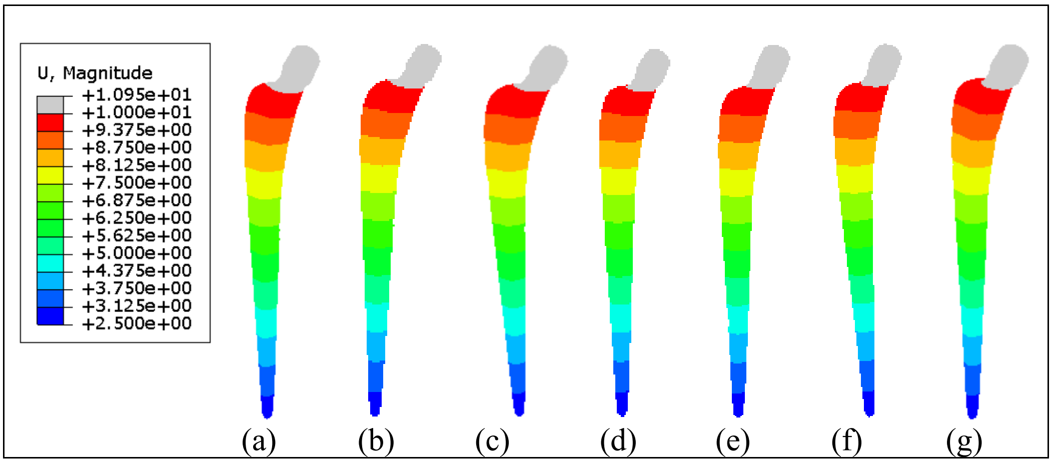

Figure 4.69 Total Deformation Analysis for Implant at Different Varus Angles under Walking Loading Condition (a) -0.75°, (b) -0.5°, (c) -0.25°, (d) 0°, (e) 0.25°, (f) 0.5° and (g) 0.75°

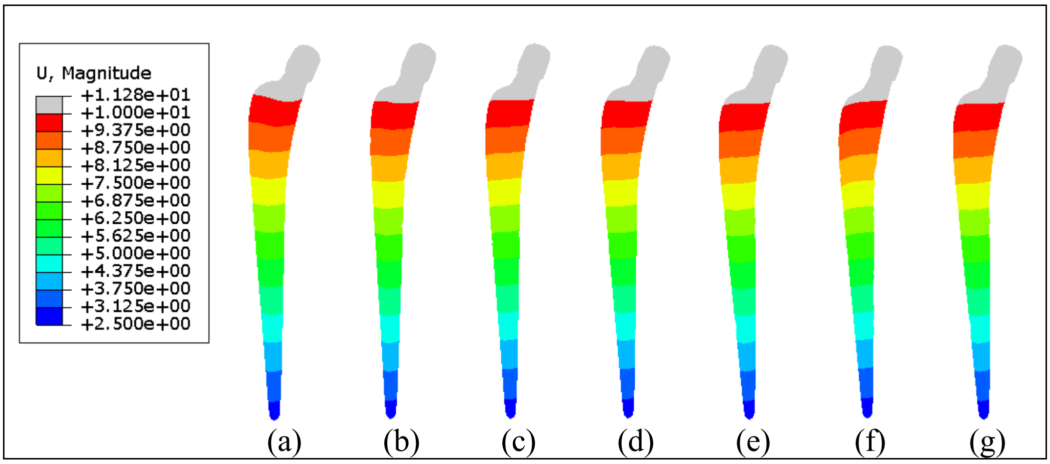

Figure 4.70 Total Deformation Analysis for Implant at Different Varus Angles under Stair Climbing Loading Condition (a) -0.75°, (b) -0.5°, (c) -0.25°, (d) 0°, (e) 0.25°, (f) 0.5° and (g) 0.75°

Additionally, Figure 4.71 shows the neutral implant position experienced the highest stress, and stress decreased with small deviations from the neutral position whether in the negative or positive direction. This implies that small varus angles from the neutral position would decrease peak stress, possibly affecting the longevity of the implant and durability of the cement. The trend of deformation, represented by the blue line, decreases from -0.75° to 0.75° indicating that the greater the varus angle from neutral, the deformation is slightly lower. The deformation is highest at -0.75°, with a value of 10.99µm, and lowest at 0.75 °, with a value of 10.91µm, The small range of deformation variation suggests that stress is sensitive to varus positioning, whereas the displacement does not change throughout this analysis. Then, Figure 4.72 shows a slight but consistent increase as the angle moves from negative to positive. The stress increases from 188.3 MPa at -0.75° to 188.9 MPa at 0.75°. This trend suggests that the prosthesis experiences progressively higher stress as the angle deviates from the baseline position. The higher value of Von Mises stress leads to the stress shielding phenomenon, which might result in aseptic loosening and instability of the implant (Yusof et al., 2021) . Besides, it also shows that the magnitude of deformation decreases slightly as the angle increases, from 11.33 µm at -0.75° to 11.27 µm at 0.75°. Even though the changes are minimal, there is a consistent trend where the deformation decreases as the angle becomes more positive.

The strain values are relatively small but show a distinct increasing trend as the varus angle moves from -0.75° to 0.75° as shown in Figure 4.73. The strain at the negative varus angles is low and approximately constant. Then, at 0° varus, there is a slight increase in strain. With increasing varus angles, the strain gradually increases. Strain is greatest at the 0.75° varus angle. Figure 4.74 indicates that the strain values at the implant show a slight yet consistent increase as the varus alignment angle shifts from negative to positive. However, the overall variation remains minimal, with a difference of only 0.4µ between the highest and lowest strain values.

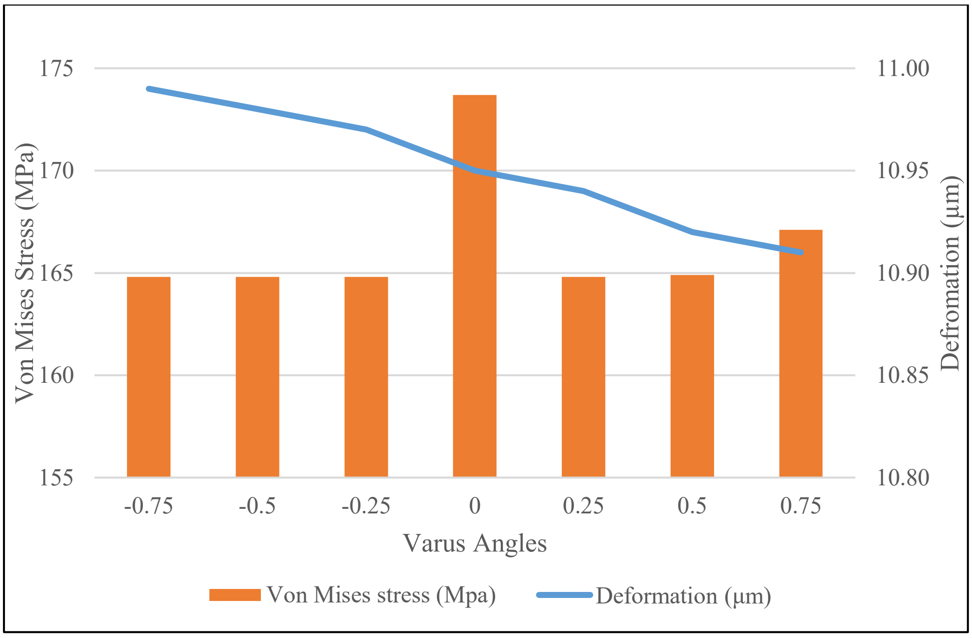

Figure 4.71 Comparison of Maximum Von Mises Stress and Displacement for Implant at Different Varus Angles under Walking Loading Condition

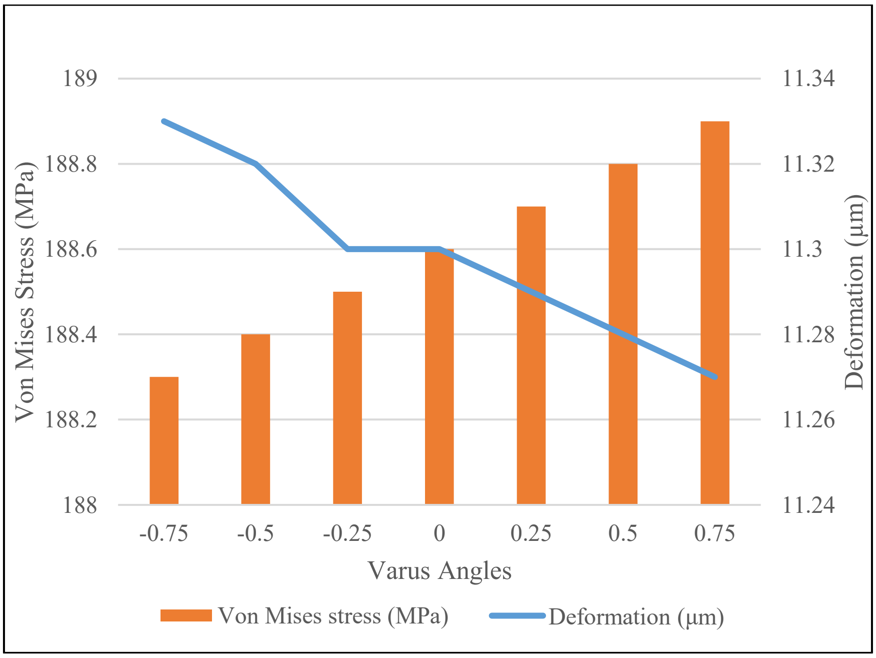

Figure 4.72 Comparison of Maximum Von Mises Stress And Displacement for Implant at Different Varus Angles under Stair Climbing Loading Condition

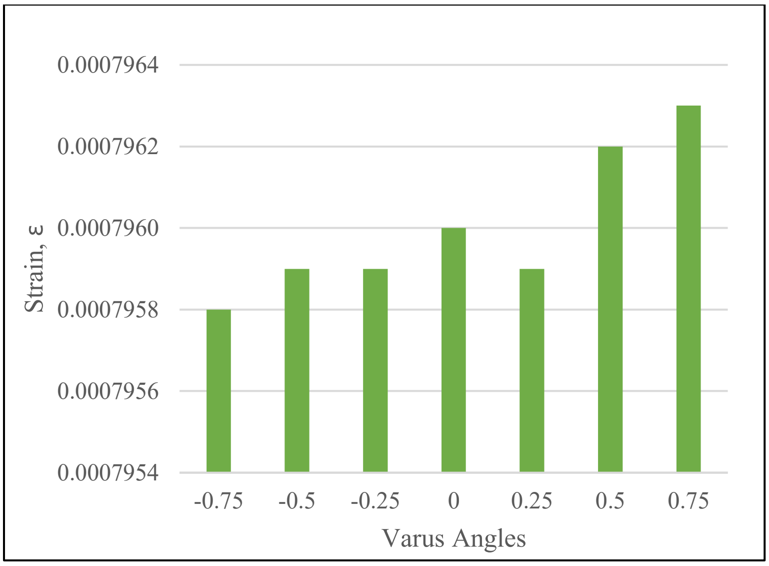

Figure 4.73 Strain of Implant Against Different Varus Angles under Walking Loading Condition

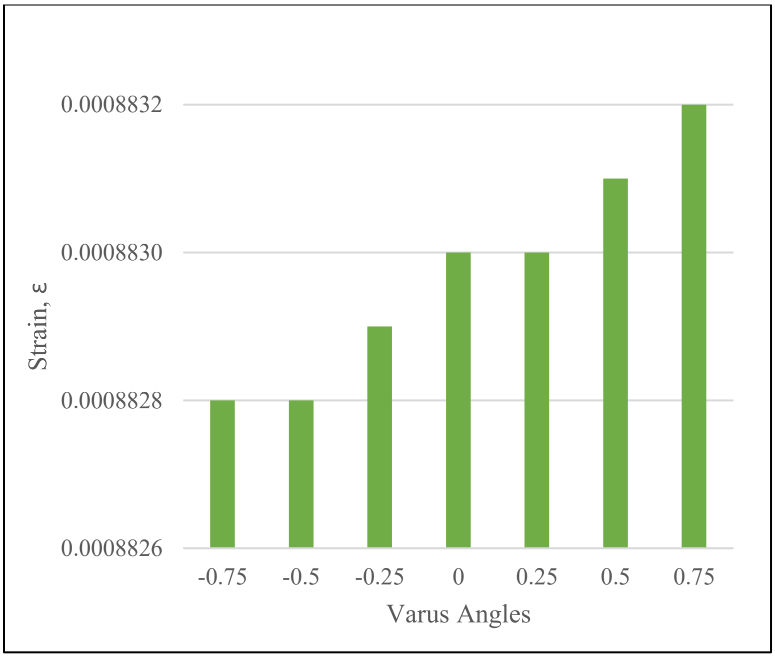

Figure 4.74 Strain of Implant Against Different Varus Angles under Stair Climbing Loading Condition

4.3.3 Comparison of Highest Stress Distribution, Strain Distribution and Deformation between Sagittal and Varus Position.

4.3.3.1 Stress Distribution in Total Hip Arthroplasty, Femur, Cement Mantle and Hip Implant

The graphs indicate that stress distribution represented by Von Mises Stress (VMS), strain distribution, and deformation values are higher during stair climbing compared to walking. While differences are observed between these activities, the VMS value remains unchanged in stair climbing for both sagittal and varus positions in Figure 4.75. However, sagittal angles exhibit more VMS compared to varus angles. Figure 4.76 demonstrates that varus positioning at -0.75° results in higher stress in the femur compared to sagittal (-0.1°, 0°, 0.1°, 0.2° and 0.3°) during walking activity. Figure 4.77 shows no significant difference between sagittal and varus during the two activities. For sagittal orientation, during walking activity the highest VMS occurred at 0.3° while the highest VMS occurred at 0.2° and 0.3° during stair climbing activity. Figure 4.78 highlights that VMS in the cement mantle is higher in sagittal orientation (0.3°) than in varus for both loading conditions.

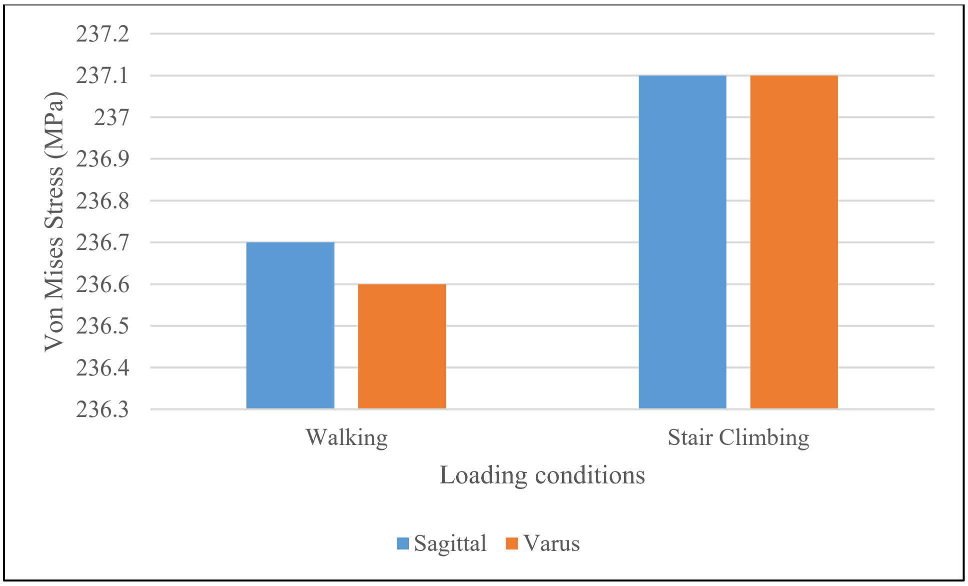

Figure 4.75 Comparison of Von Mises Stress in Total Hip Arthroplasty for Sagittal and Varus Positioning under Two Different Loading Conditions

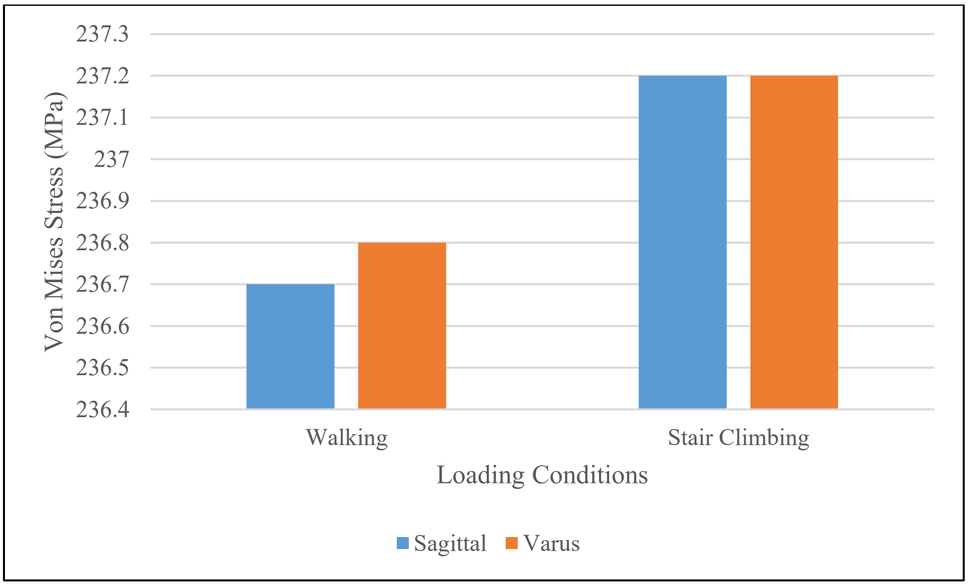

Figure 4.76 Comparison of Von Mises Stress in the Femur for Sagittal and Varus Positioning under Two Different Loading Conditions.

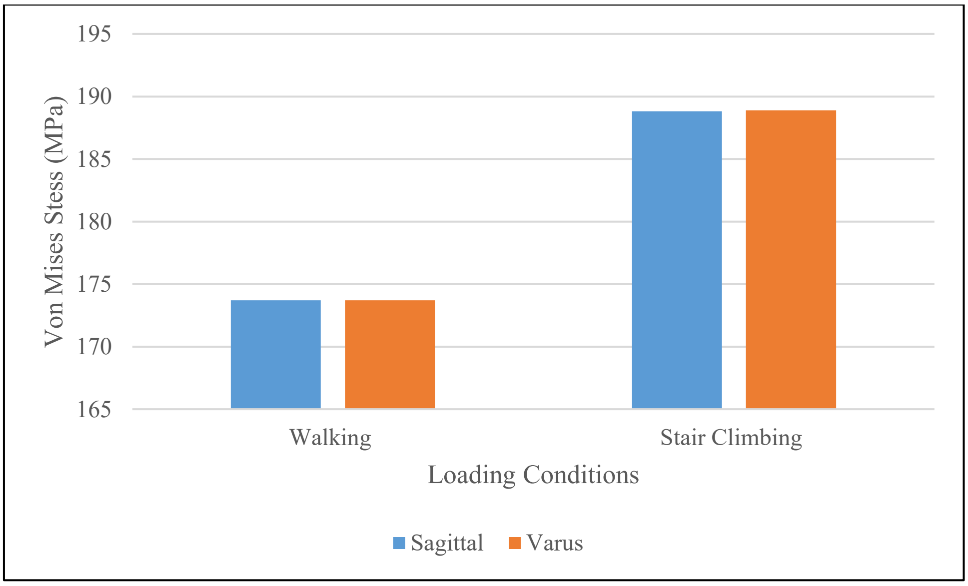

Figure 4.77 Comparison of Von Mises Stress in the Implant for Sagittal and Varus Positioning under Two Different Loading Conditions.

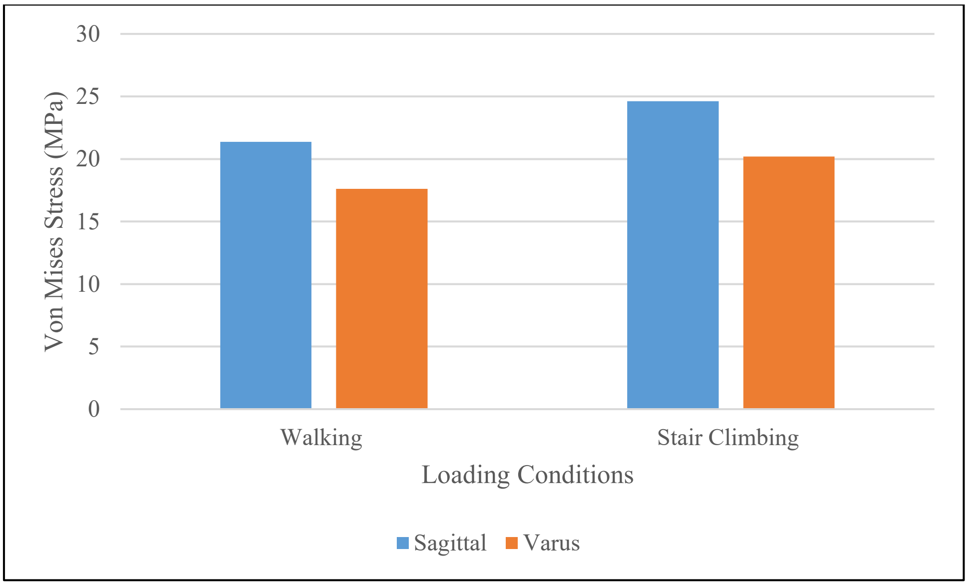

Figure 4.78 Comparison of Von Mises Stress in the Cement Mantle for Sagittal and Varus Positioning under Two Different Loading Conditions.

4.3.3.2 Strain Distribution in Total Hip Arthroplasty, Femur, Cement mantle and Hip Implant

Figure 4.79 shows that strain distribution in THA is slightly higher in sagittal positioning than in varus during walking. Figure 4.80 indicates that strain distribution in the femur is similar for both varus and sagittal orientation. Under walking loading conditions, the highest strain exhibited at -0.3°, -0.2° and 0.3° at sagittal orientation while -0.75° exhibited the highest strain at varus orientation. According to Figure 4.81, strain in the cement mantle is higher during both walking and stair climbing activities at 0.75° varus orientation. Meanwhile, Figure 4.82 demonstrates that strain distribution is similar for both loading conditions in the hip implant. Under sagittal orientation, the highest strain exhibited at 0° and 0.2°, 0.3° under walking and stair climbing loading conditions, respectively.

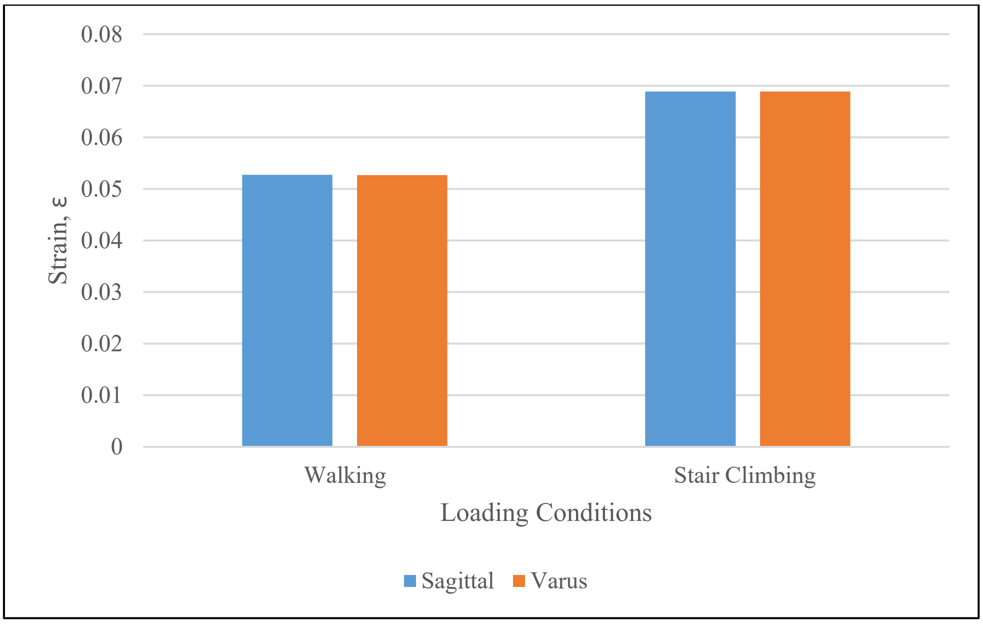

Figure 4.79 Comparison of Strain Distribution in Total Hip Arthroplasty for Sagittal and Varus Positioning under Two Different Loading Conditions.

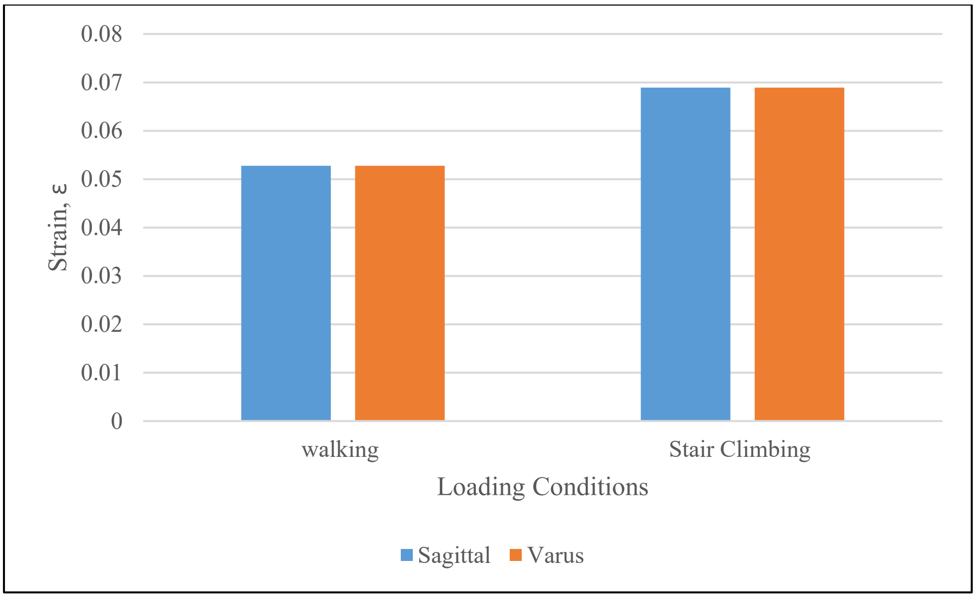

Figure 4.80 Comparison of Strain Distribution in Femur for Sagittal and Varus Positioning under Two Different Loading Conditions.

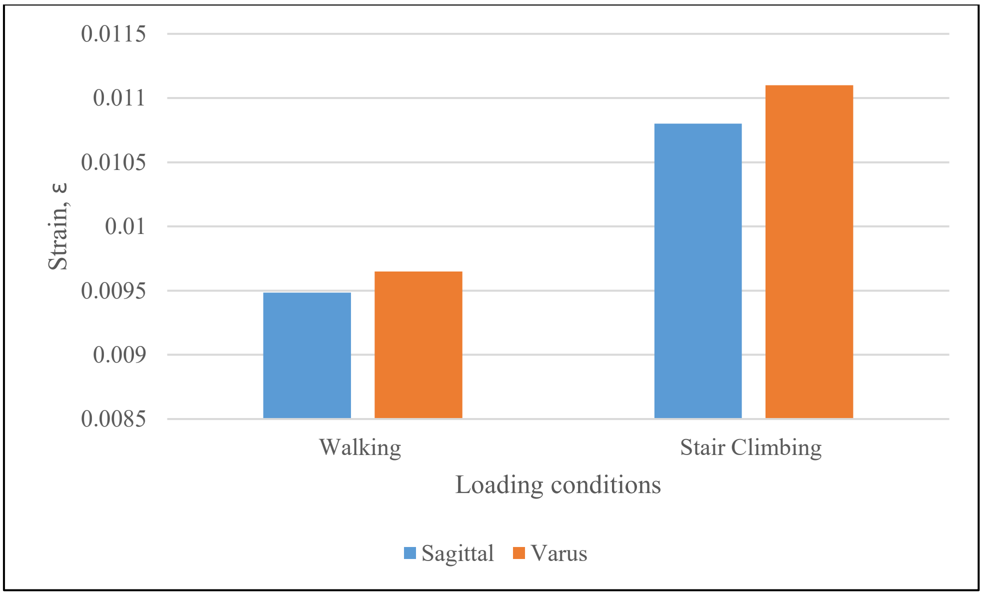

Figure 4.81 Comparison of Strain Distribution in Cement Mantle for Sagittal and Varus Positioning under Two Different Loading Conditions.

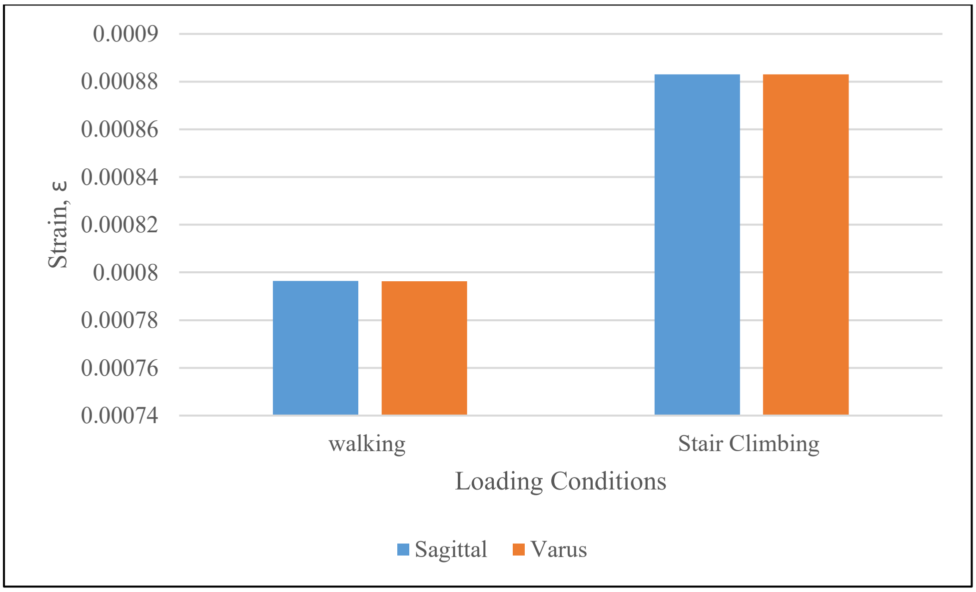

Figure 4.82 Comparison of Strain Distribution in Implant for Sagittal and Varus Positioning under Two Different Loading Conditions.

4.3.3.3 Deformation in Total Hip Arthroplasty, Femur, Cement mantle and Hip Implant

Figure 4.83 illustrates that when walking, the sagittal position experiences more deformation than the varus position. For both walking and stair climbing, Figure 4.84 shows that the femur deforms more in the varus position than in the sagittal position with the highest deformation occurred at -0.75°. At sagittal position, femur experienced the highest deformation at -0.3°, 0.2°, 0.1° and 0° under stair climbing loading conditions meanwhile the deformation is consistent under walking conditions. Likewise, Figure 4.85 shows that for both activities, the cement mantle deforms more in the varus position. In sagittal orientation, cement mantles experienced the highest deformation at 0.3° during walking activity while deformation is consistent during stair climbing activity at the various angles. Similarly, Figure 4.86 shows that during walking and stair climbing, the hip implant deforms more in the varus position than in the sagittal position. In varus orientation, the highest deformation occurred at -0.75° for walking and stair climbing. In sagittal orientation, both loading conditions experienced a consistent deformation across all the angles.

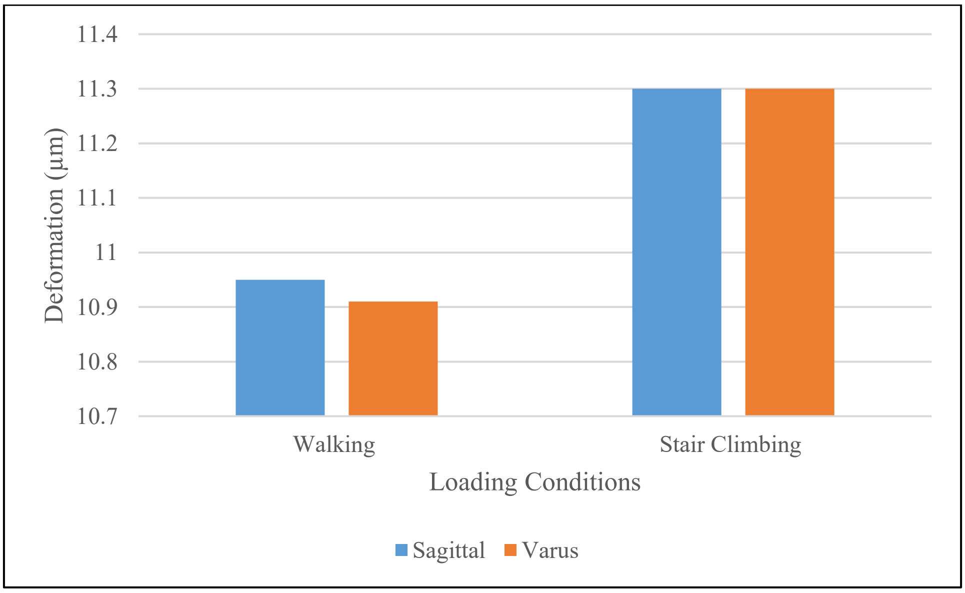

Figure 4.83 Comparison of Deformation in Total Hip Arthroplasty for Sagittal and Varus Positioning under Two Different Loading Conditions

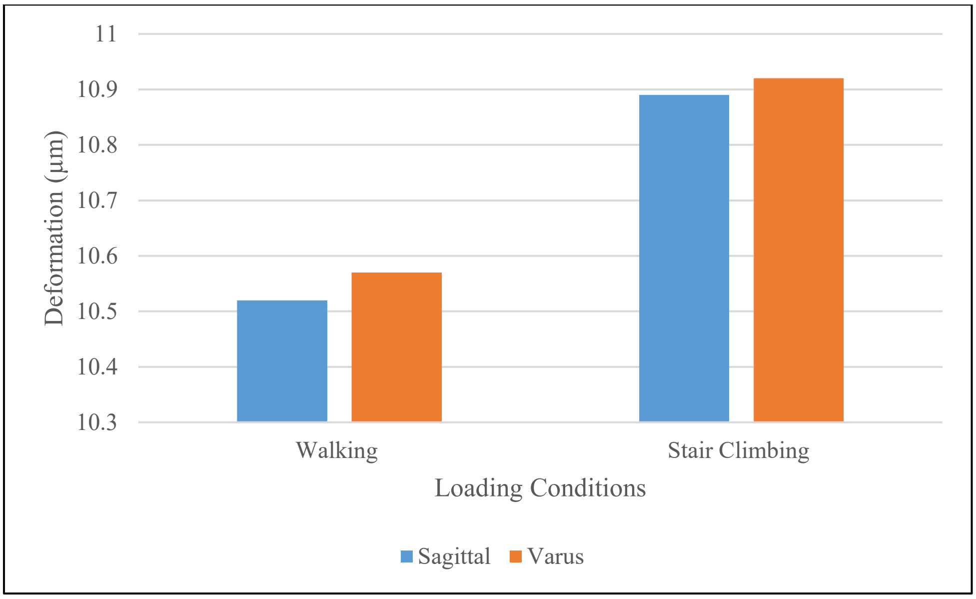

Figure 4.84 Comparison of Deformation in Femur for Sagittal and Varus Positioning under Two Different Loading Conditions.

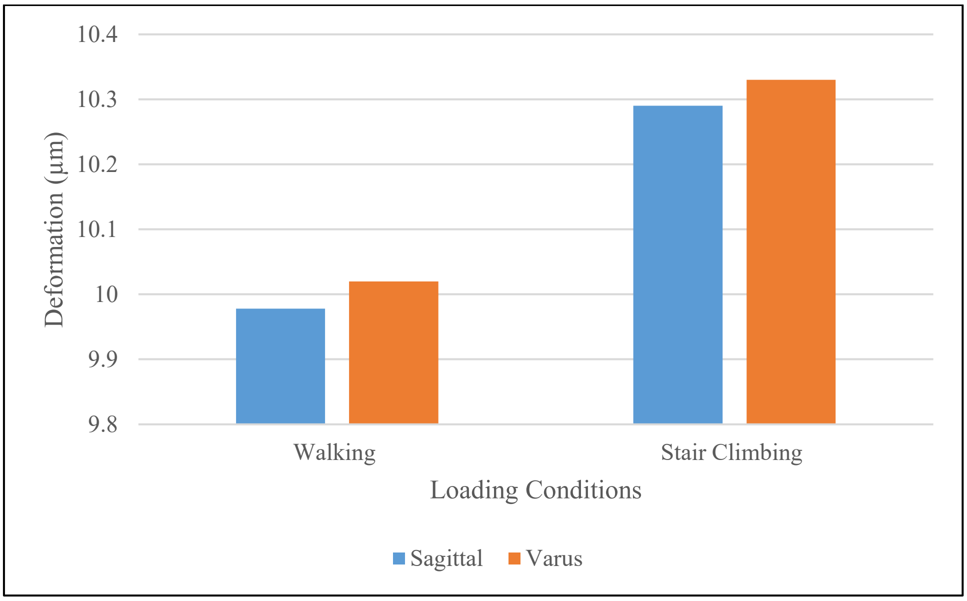

Figure 4.85 Comparison of Deformation in Cement Mantle for Sagittal and Varus Positioning under Two Different Loading Conditions.

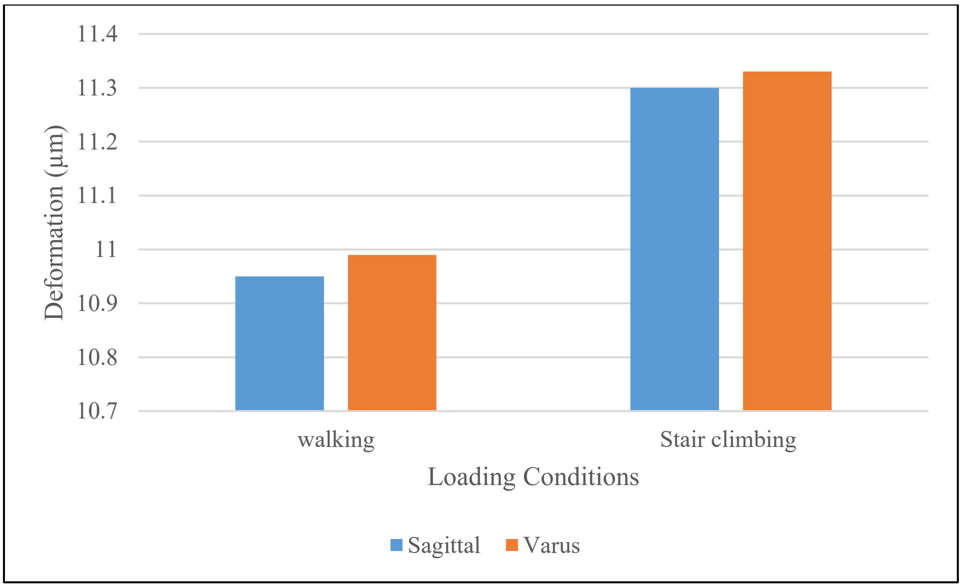

Figure 4.86 Comparison of Deformation in Implant for Sagittal and Varus Positioning under Two Different Loading Conditions.

CHAPTER 5
CONCLUSION

5.1 Conclusion

In the present study, a three-dimensional femoral model was created using the images of the CT scan, and the results were compared with previous research to validate the finite element model used. A cemented total hip arthroplasty model was created with a variable position of the implant to measure the biomechanical behavior of the cement mantle, which is an essential factor for the estimation of implant stability in cemented THA.

The results show that small deviations in the position of the implants significantly affect the stress distribution and deformation of the cement mantle. In the sagittal positioning, the maximum stress and deformation occurred at the 0.3° with the value of 24.62MPa and 10.29MPa respectively. The amount of deformation during stairs climbing is relatively independent of the sagittal position, and thus stress values are more significant for the position-dependent effects for the stairs loading condition. For varus positioning, under loading conditions of stair climbing, maximum stress occurred at -0.25° with the value of 20.19 MPa while the highest deformation occurred at the most negative angle with the value of 10.33µm. In sagittal orientation, Optimal positioning can be considered at -0.3° and -0.2° that exhibited lowest stress distribution and deformation under walking and stair climbing conditions, respectively. Meanwhile, in varus orientation, 0.75° can be considered as the optimal positioning. Although it exhibited relatively high stress with low deformation under both loading conditions, but the stress value did not exceed the threshold of the PMMA.

Since the cement mantle serves as the primary load transfer medium between the implant and bone in cemented THA, any data that is derived from cement mantle mechanics is a rational estimation of the stability of the implant. Although all orientations led to cement mantle stresses lower than the yield strength for PMMA which is 29 MPa, it is evident that, despite not leading to material failure, high levels in malpositioned implants may pose risks in fatigue-related damage, thus leading to implant instability.

In general, this study confirms that the mechanical behaviour of the cement mantle is a sensitive and reliable indicator for the assessment of implant stability in cemented THA. These results stress how important precise positioning of the implants is during surgery and support the use of cement mantle stress and deformation as predictive metrics for long-term performance.

5.2 Recommendations

For future work, below are the recommendations to enhance clinical relevance and simulation depth:

- The mechanical performance of the hip implant system is highly dependent on the properties of both the cement mantle and the implant orientation. Future research should explore the impact of using various bone cement types at different type of orientation.
- Simulating the imperfections of cement mantle such as voids and cracks to reveal significant stress concentrations and potential failure locations. Future models must incorporate the impacts of cement porosity and inadequate pressurization during implantation.
- Simulating more actual-life events to the finite element simulations, like sitting-to-standing transitions, seated postures, and fall impacts. By applying different load magnitudes and directions, these scenarios provide information about stress patterns and possible danger areas that might not be visible when walking or stair climbing.

REFERENCES

Abdullah, A. H., Nor, M. A. M., & Saman, A. M. (2009). Stress and strain distribution in cemented total hip arthroplasty for walking load case. *ICCTD 2009 - 2009 International Conference on Computer Technology and Development*, *2*, 260–263. https://doi.org/10.1109/ICCTD.2009.28

Aghayan, S., & Lee, W.-S. (2014). *Calculation and Visualization of Range of Motion of Hip Joint from MRI*. https://doi.org/10.1109/CBMS.2014.66

Ahmad, M. A., Zulkifli, N. N. M. E., Shuib, S., Sulaiman, S. H., & Abdullah, A. H. (2020). Finite Element Analysis of Proximal Cement Fixation in Total Hip Arthroplasty. *International Journal of Technology*, *11*(5), 1046–1055. https://doi.org/10.14716/ijtech.v11i5.4318

Alpkaya, A. T., Yılmaz, M., Şahin, A. M., & Mihçin, D. Ş. (2024). Investigation of stair ascending and descending activities on the lifespan of hip implants. *Medical Engineering and Physics*, *126*. https://doi.org/10.1016/j.medengphy.2024.104142

Altai, Z., Montefiori, E., van Veen, B., Paggiosi, M. A., McCloskey, E. V., Viceconti, M., Mazzà, C., & Li, X. (2021). Femoral neck strain prediction during level walking using a combined musculoskeletal and finite element model approach. *PLoS ONE*, *16*(2 February 2021). https://doi.org/10.1371/journal.pone.0245121

Alzaid, A., Lineham, B., Dogramadzi, S., Pandit, H., Frangi, A. F., & Xie, S. Q. (2024). Simultaneous Hip Implant Segmentation and Gruen Landmarks Detection. *IEEE Journal of Biomedical and Health Informatics*, *28*(1), 333–342. https://doi.org/10.1109/JBHI.2023.3323533

Ammarullah, M. I., Afif, I. Y., Maula, M. I., Winarni, T. I., Tauviqirrahman, M., Bayuseno, A. P., Basri, H., Syahrom, A., Md Saad, A. P., & Jamari. (2022). Deformation analysis of CoCrMo-on-CoCrMo hip implant based on body mass index using 2D finite element procedure. *Journal of Physics: Conference Series*, *2279*(1). https://doi.org/10.1088/1742-6596/2279/1/012004

Anil, U., Singh, V., & Schwarzkopf, R. (2022). Diagnosis and Detection of Subtle Aseptic Loosening in Total Hip Arthroplasty. *Journal of Arthroplasty*, *37*(8), 1494–1500. https://doi.org/10.1016/j.arth.2022.02.060

Aznan, N., Yusof, M. S., Abdullah, A. H., Sulaiman, S. H., & Todo, M. (2020). Effects of Retroversion and Anteversion Alignment in Cemented Hip Arthrosplasty. *Journal of Mechanical Engineering*, *9*(1), 25–41.

Belaid, D., & Bouchoucha, A. (2015). Modeling of the mechanical behavior of the human femur: Stress analysis and strain. *AIP Conference Proceedings*, *1702*. https://doi.org/10.1063/1.4938990

Belaïd, D., Germaneau, A., Vendeuvre, T., Ben Brahim, E., Aubert, K., & Severyns, M. (2022). Varus malalignment of the lower limb increases the risk of femoral neck fracture: A biomechanical study using a finite element method. *Injury*, *53*(6), 1805–1814. https://doi.org/10.1016/j.injury.2022.04.018

Belwanshi, M., Jayaswal, P., & Aherwar, A. (2022). A study on finite element analysis methodologies and approaches used for total hip arthroplasty. *Materials Today: Proceedings*, *56*, 2596–2604. https://doi.org/10.1016/j.matpr.2021.09.161

Blythe, R., O'Gorman, P. M., Crawford, R. W., Feenan, R., Hatton, A., Whitehouse, S. L., & Graves, N. (2020). Fixation Method for Hip Arthroplasty Stem Following Hip Fracture: A Population-Level Cost-Effectiveness Analysis. *Journal of Arthroplasty*, *35*(6), 1614–1621. https://doi.org/10.1016/j.arth.2020.02.001

Carey, J. J., Chih-Hsing Wu, P., & Bergin, D. (2022). Risk assessment tools for osteoporosis and fractures in 2022. In *Best Practice and Research: Clinical Rheumatology*. Bailliere Tindall Ltd. https://doi.org/10.1016/j.berh.2022.101775

Chang, M. W., Liu, H. T., Huang, C. Y., Chien, P. C., Hsieh, H. Y., & Hsieh, C. H. (2018). Location of femoral fractures in patients with different weight classes in fall and motorcycle accidents: A retrospective cross-sectional analysis. *International Journal of Environmental Research and Public Health*, *15*(6). https://doi.org/10.3390/ijerph15061082

Chen, A. G., Sogbein, O. A., McClure, J. A., Reid, J., Welk, B., Lanting, B. A., & Degen, R. M. (2023). Total Hip Arthroplasty in Patients Aged 40 to 60 Years Old: A Population-Based Study. *Journal of Arthroplasty*, *38*(7), S83-S88.e2. https://doi.org/10.1016/j.arth.2023.04.027

Chen, S.-H., Abbas, S., & Briant-Evans, T. (2023). Surgical approaches to the hip. *Surgery (Oxford)*. https://doi.org/10.1016/j.mpsur.2023.02.006

Chen, X. T., Christ, A. B., Chung, B. C., Ton, A., Ballatori, A. M., Shahrestani, S., Gettleman, B. S., & Heckmann, N. D. (2023). Cemented versus Cementless Femoral Fixation for Elective Primary Total Hip Arthroplasty: A Nationwide Analysis of Short-Term Complication and Readmission Rates. *Journal of Clinical Medicine*, *12*(12). https://doi.org/10.3390/jcm12123945

Chethan, K. N., Shyamasunder Bhat, N., Zuber, M., & Satish Shenoy, B. (2019). Finite element analysis of different hip implant designs along with femur under static loading conditions. *Journal of Biomedical Physics and Engineering*, *9*(5), 507–516. https://doi.org/10.31661/jbpe.v0i0.1210

Clynes, M. A., Harvey, N. C., Curtis, E. M., Fuggle, N. R., Dennison, E. M., & Cooper, C. (2020). The epidemiology of osteoporosis. In *British Medical Bulletin* (Vol. 133, Number 1, pp. 105–117). Oxford University Press. https://doi.org/10.1093/bmb/ldaa005

Cosman, F., de Beur, S. J., LeBoff, M. S., Lewiecki, E. M., Tanner, B., Randall, S., & Lindsay, R. (2014). Clinician's Guide to Prevention and Treatment of Osteoporosis. *Osteoporosis International*, *25*(10), 2359–2381. https://doi.org/10.1007/s00198-014-2794-2

Deng, C., Gillette, J. C., & Derrick, T. R. (2018). Femoral Neck Stress in Older Adults During Stair Ascent and Descent. *Journal of Applied Biomechanics*, *34*(3), 191–198. https://doi.org/https://doi.org/10.1123/jab.2017-0122

Deng, C., Gillette, J. C., & Derrick, T. R. (2021). Finite element analysis of femoral neck strains during stair ascent and descent. *Scientific Reports*, *11*(1). https://doi.org/10.1038/s41598-021-87936-y

Douglas, A., Jonathan, R., & Howell, R. (2021). *Cemented hip arthroplasty: techniques used in primary and revision surgery*.

Enoksen, C. H., Wik, T. S., Klaksvik, J., Arthursson, A. J., Husby, O. S., & Gjerdet, N. R. (2017). Load transfer in the proximal femur and primary stability of a cemented and uncemented femoral stem: An experimental study on cadaver femurs. *Proceedings of the Institution of Mechanical Engineers, Part H: Journal of Engineering in Medicine*, *231*(12), 1195–1203. https://doi.org/10.1177/0954411917737804

Firdaus, M., Ariffin, T., & Abdullah, H. (2024). Simulation of Hip Prosthesis based on Dynamic Loading using Finite Element Method. *Research Progress In Mechanical And Manufacturing Engineering*, *5*(2), 88–100. https://doi.org/10.30880/rpmme.2024.05.02.010

Fontalis, A., Epinette, J. A., Thaler, M., Zagra, L., Khanduja, V., & Haddad, F. S. (2021). Advances and innovations in total hip arthroplasty. In *SICOT-J* (Vol. 7). EDP Sciences. https://doi.org/10.1051/sicotj/2021025

Fowler, T. J., Sayers, A., & Whitehouse, M. R. (2019). Two-stage revision surgery for periprosthetic joint infection following total hip arthroplasty. *Annals of Translational Medicine*, *7*(S8), S261–S261. https://doi.org/10.21037/atm.2019.12.126

Gabriele, C., Mileti, I., Nalli, F., Palermo, E., & Cortese, L. (2022). Additive Manufacturing Structural Redesign of Hip Prostheses for Stress-shielding reduction and improved Functionality and Safety. *Mechanics of Materials*, *165*. https://doi.org/https://doi.org/10.1016/j.mechmat.2021.104173.

Galvain, T., Mantel, J., Kakade, O., & Board, T. N. (2022). Treatment patterns and clinical and economic burden of hip dislocation following primary total hip arthroplasty in England. *Bone Joint J*, *104*(7), 811–819. https://doi.org/10.1302/0301-620X.104B7

Gómez Alcaraz, J., Pardo García, J., Sevilla Fernández, J., Delgado Díaz, E., Moreno Beamud, J., & Sevilla, J. (2021). Primary total hip arthroplasty in elderly patients over 85 years old: Risks, complications and medium-long term results-NC-ND license (http:// creativecommons.org/licenses/by-nc-nd/4.0/). In *Revista Española de Cirugía Ortopédica y Traumatología* (Vol. 65).

Gupta, A., & Ming Tse, K. (2013). *Finite Element Analysis on Vibration Modes of Femur Bone*.

Hermansen, L. L., Viberg, B., & Overgaard, S. (2022). Patient-reported outcome after dislocation of primary total hip arthroplasties: a cross-sectional study derived from the Danish Hip Arthroplasty Register. *Acta Orthopaedica*, *93*, 29–36. https://doi.org/10.1080/17453674.2021.1983973

Hernigou, P., Daltro, G., Henri, C., Lachaniette, F., Roussignol, X., Mukasa, M. M., & Poignard, A. (2009). Fixation of the Cemented Stem: Clinical Relevance of the Porosity and Thickness of the Cement Mantle. In *The Open Orthopaedics Journal* (Vol. 3).

Hung, J. P., Bai, Y. W., Hung, C. Q., & Lee, T. E. (2019). Biomechanical performance of the cemented hip stem with different surface finish. *Applied Sciences (Switzerland)*, *9*(19). https://doi.org/10.3390/app9194082

Hwang, D., Kim, C. H., Lee, Y., & Kim, J. W. (2022). Association of atypical femoral fracture location and lower limb mechanical axis: a computed tomography-based finite element analysis. *Osteoporosis International*, *33*(6), 1285–1293. https://doi.org/10.1007/s00198-021-06173-1

Ismail, N. F., Shuib, S., & Manap, M. F. A. (2023). Study of Stress Distribution at the

Inner Surface of Uncemented Total Hip Replacement (THR). *2023 IEEE 14th Control and System Graduate Research Colloquium, ICSGRC 2023 - Conference Proceeding*, 149–152. https://doi.org/10.1109/ICSGRC57744.2023.10215416

Kaku, N., Pramudita, J. A., Yamamoto, K., Hosoyama, T., & Tsumura, H. (2022). Stress distributions of the short stem and the tapered wedge stem at different alignments: a finite element analysis study. *Journal of Orthopaedic Surgery and Research*, *17*(1). https://doi.org/10.1186/s13018-022-03425-6

Kanaizumi, A., Suzuki, D., Nagoya, S., Teramoto, A., & Yamashita, T. (2022). Patient-specific three-dimensional evaluation of interface micromotion in two different short stem designs in cementless total hip arthroplasty: a finite element analysis. *Journal of Orthopaedic Surgery and Research*, *17*(1). https://doi.org/10.1186/s13018-022-03329-5

Kimura, M., Ando, K., & Yamada, H. (2018). A mechanical review of postoperative stem fractures of cemented total hip arthroplasty implants without femoral fracture. *Fujita Medical Journ*, *4*(4), 83–87. https://doi.org/https://doi.org/10.20407/fmj.4.4_83

K.N., C., Zuber, M., Bhat N., S., Shenoy B., S., & R. Kini, C. (2019). Static structural analysis of different stem designs used in total hip arthroplasty using finite element method. *Heliyon*, *5*(6). https://doi.org/10.1016/j.heliyon.2019.e01767

Kobayashi, N., & Yukizawa, Y. (2023). Causes of failure after total hip arthroplasty: A narrative review of literatures. *Journal of Joint Surgery and Research*, *1*(1), 56–61. https://doi.org/10.1016/j.jjoisr.2023.01.006

Lamvohee, J., Ingle, P., Cheah, K., Dowell, J., & Mootanah, R. (2014). Total Hip Replacement: Tensile Stress in Bone Cement is influenced by Cement Mantle Thickness, Acetabular Size, Bone Quality, and Body Mass Index. *Journal of Computer Science & Systems Biology*, *7*(3). https://doi.org/10.4172/jcsb.1000140

Lespasio, M. J., Sultan, A. A., Piuzzi, N. S., Khlopas, A., Husni, M. E., Muschler, G. F., & Mont, M. A. (2018). Hip Osteoarthritis: A Primer. In *The Permanente journal* (Vol. 22). https://doi.org/10.7812/TPP/17-084

Levadnyi, I., Awrejcewicz, J., Loskutov, A., & Szymanowska, O. (2017). On the choice of thickness of the cement mantle in cemented hip arthroplasty. *Journal of Theoretical and Applied Mechanics (Poland)*, *55*(4), 1235–1244. https://doi.org/10.15632/jtam-pl.55.4.1235

Luo, C., Wu, X. D., Wan, Y., Liao, J., Cheng, Q., Tian, M., Bai, Z., & Huang, W.

(2020). Femoral Stress Changes after Total Hip Arthroplasty with the Ribbed Prosthesis: A Finite Element Analysis. *BioMed Research International*, *2020*. https://doi.org/10.1155/2020/6783936

Maggs, J., & Wilson, M. (2017). The relative merits of cemented and uncemented prostheses in total hip arthroplasty. *Indian Journal of Orthopaedics*, *51*(4), 377–385. https://doi.org/10.4103/ortho.IJOrtho_405_16

Marwan, S. H., Tardan, G., Syafiq, M., Zainal, B., & Abdullah, A. H. (2017). Effects of Stem Mal-alignment in The Primary Stability of Total Hip Arthroplasty. *Journal of Mechanical Engineering*, *4*(4), 229–241.

Meißner, N., Halder, A. M., & Schrednitzki, D. (2023). Cemented and hybrid total hip arthroplasty lead to lower blood loss in primary total hip arthroplasty: a retrospective study. *Archives of Orthopaedic and Trauma Surgery*, *143*(10), 6447–6451. https://doi.org/10.1007/s00402-023-04851-9

Mendonça, C. J. A., Guimarães, R. M. da R., Pontim, C. E., Gasoto, S. C., Setti, J. A. P., Soni, J. F., & Schneider, B. (2023). An Overview of 3D Anatomical Model Printing in Orthopedic Trauma Surgery. *Journal of Multidisciplinary Healthcare*, *16*, 875–887. https://doi.org/10.2147/JMDH.S386406

Meneghini, R. M. (2018). Investigation of the Unstable Total Hip Arthroplasty. *Journal of Arthroplasty*, *33*(5), 1325–1327. https://doi.org/10.1016/j.arth.2018.01.052

Moarrefzadeh, A., Sarveazad, A., Mohammadpour, M., Zareinejad, M., Bahardoust, M., Pisoudeh, K., Asgarian, S., Shamseddin, J., & Semiromi, H. toghraei. (2022). Evaluation of health-related quality of life before and after total hip arthroplasty in the elderly in Iran: a prospective cohort study. *BMC Psychology*, *10*(1). https://doi.org/10.1186/s40359-022-00762-3

Mohamad Azmi, N. A., Abdullah, N. N. A. A., Mohd Salaha, Z. F., & Ramlee, M. H. (2024). Convergence Study of Three-Dimensional Upper Skull Model: A Finite Element Method. *Communications in Computer and Information Science*, *1912 CCIS*, 351–361. https://doi.org/10.1007/978-981-99-7243-2_30

Mosconi, L., Cavagnaro, L., Zanirato, A., Quarto, E., Lontaro Baracchini, M., & Formica, M. (2021). Long-term follow-up of a low profile, coated, press-fit cup: the trabeculae oriented pattern (T.O.P.) acetabular system. *European Journal of Orthopaedic Surgery and Traumatology*, *31*(7), 1515–1521. https://doi.org/10.1007/s00590-021-02917-1

Oltean-Dan, D., Apostu, D., Tomoaia, G., Kerekes, K., Paiusan, M. G., Bardas, C. A., & Benea, H. R. C. (2022). Causes of revision after total hip arthroplasty in an orthopedics and traumatology regional center. *Medicine and Pharmacy Reports*, *95*(2), 179–184. https://doi.org/10.15386/mpr-2136

Olugbade, T. O. (2022). *Corrosion Resistance, Evaluation Methods, and Surface Treatments of Stainless Steels*. www.intechopen.com

Oshkour, A. A., Davoodi, M. M., Abu Osman, N. A., Yau, Y. H., Tarlochan, F., & Abas, W. A. B. W. (2013). Finite element analysis of circumferential crack behavior in cement-femoral prosthesis interface. *Materials and Design*, *49*, 96–102. https://doi.org/10.1016/j.matdes.2013.01.037

Panwar, K., Cutter, B., Holmboe, M., Card, R., Pistel, W., & Law, J. I. (2023). Instability in Total Hip Arthroplasty. In Alessandro Rozim Zorzi, Hechmi Toumi, & Eric Lespessailles (Eds.), *Arthroplasty - Advanced Techniques and Future Perspectives*. https://doi.org/10.5772/intechopen.105801

Patel, I., Nham, F., Zalikha, A. K., & El-Othmani, M. M. (2023). Epidemiology of total hip arthroplasty: demographics, comorbidities and outcomes. *Arthroplasty*, *5*(1). https://doi.org/10.1186/s42836-022-00156-1

Paulo Amorim, Moraes, T., Silva, J., & Pedrini, H. (2015). *InVesalius: An Interactive Rendering Framework for Health Care Support* (G. Bebis, R. Boyle, B. Parvin, D. Koracin, I. Pavlidis, R. Feris, T. McGraw, M. Elendt, R. Kopper, E. Ragan, Z. Ye, & G. Weber, Eds.; Lecture Notes in Computer Science, Vol. 9474). Springer International Publishing. https://doi.org/10.1007/978-3-319-27857-5

Queen, R. M., Campbell, J. C., & Schmitt, D. (2019). Gait Analysis Reveals that Total Hip Arthroplasty Increases Power Production in the Hip during Level Walking and Stair Climbing. *Clinical Orthopaedics and Related Research*, *477*(8), 1839–1847. https://doi.org/10.1097/CORR.0000000000000809

Ravi, B., Jenkinson, R., Austin, P. C., Croxford, R., Wasserstein, D., Escott, B., Paterson, J. M., Kreder, H., & Hawker, G. A. (2014). Relation between surgeon volume and risk of complications after total hip arthroplasty: Propensity score matched cohort study. *BMJ (Online)*, *348*. https://doi.org/10.1136/bmj.g3284

Ruppert, G. C. S., Reis, L. O., Amorim, P. H. J., de Moraes, T. F., & da Silva, J. V. L. (2012). Touchless gesture user interface for interactive image visualization in urological surgery. *World Journal of Urology*, *30*(5), 687–691. https://doi.org/10.1007/s00345-012-0879-0

Saadoon, M. Z., Adam, D. I., Saadoon, Z. Z., & Al-Kamali, R. K. (2021). Impact of Hip Arthroplasty Stiffness on the Biocompatibility. *International Journal of Medical Science and Health Research*, *05*(02), 56–78. https://doi.org/10.51505/ijmshr.2021.5206

Shichman, I., Kurapatti, M., Roof, M., Christensen, T. H., Rozell, J. C., & Schwarzkopf, R. (2022). Impact of Indication for Revision THA on Resource Utilization. *Journal of Arthroplasty*, *37*(12), 2333–2339. https://doi.org/10.1016/j.arth.2022.06.007

Shichman, I., Roof, M., Askew, N., Nherera, L., Rozell, J. C., Seyler, T. M., & Schwarzkopf, R. (2023). Projections and Epidemiology of Primary Hip and Knee Arthroplasty in Medicare Patients to 2040-2060. *JBJS Open Access*, *8*(1). https://doi.org/10.2106/JBJS.OA.22.00112

Shuib, S., Romli, A. Z., Arrif, I. M., Hamizan, N. S., & Saeid, N. H. (2023). Relationship Between Various Cement Mixture, Cement Fixation and Gait Study for Total Hip Replacement Via Finite Element Analysis (FEA). *International Journal of Integrated Engineering*, *15*(3), 43–53. https://doi.org/10.30880/ijie.2023.15.03.004

Simões, J. A., Vaz, M. A., Blatcher, S., & Taylor, M. (2000). Influence of head constraint and muscle forces on the strain distribution within the intact femur. In *Medical Engineering & Physics* (Vol. 22). www.elsevier.com/locate/medengphy

Singh, G., Kahlon, S., a, S., Arya, G., Vashishth, R., Asar, V., Sran, S., & Paul, A. (2023). Anthropometricstudy Of Proximal End Of Dried Adult Human Femur: A Cross Sectional Study. *International Journal of Advanced Research*, *11*(01), 1667–1671. https://doi.org/10.21474/ijar01/16191

Singh, S., & Harsha, A. P. (2016). Analysis of Femoral Components of Cemented Total Hip-Arthroplasty. *Journal of The Institution of Engineers (India)*, *Series D*(97), 113–120. https://doi.org/https://doi.org/10.48550/arXiv.1403.1867

Sirignano, M. N., Nessler, J. M., Rhea, E. B., Ong, K. L., Watson, H. N., Yakkanti, M. R., & Malkani, A. L. (2023). Incidence of Instability Following Primary Total Hip Arthroplasty Continues to Decline in the Medicare Population. *Journal of Arthroplasty*, *38*(7), S89-S94.e1. https://doi.org/10.1016/j.arth.2023.04.035

Sofuoglu, H., & Cetin, M. E. (2015). An investigation on mechanical failure of hip joint using finite element method. *Biomedizinische Technik*, *60*(6), 603–616. https://doi.org/10.1515/bmt-2014-0173

Stasi, S., Sarantis, M., Papathanasiou, G., Evaggelou-Sossidis, G., Stamou, M., Tzefronis, D., & Macheras, G. (2023). Stair Climbing Ability and Identification of the Nine Stairs Ascent and Descent Test Cut-Off Points in Hip Osteoarthritis Patients: A Retrospective Study. *Cureus*. https://doi.org/10.7759/cureus.41095

Stocco, T. D., Silva, M. C. M., Corat, M. A. F., Lima, G. G., & Lobo, A. O. (2022). Towards Bioinspired Meniscus-Regenerative Scaffolds: Engineering a Novel 3D Bioprinted Patient-Specific Construct Reinforced by Biomimetically Aligned Nanofibers. *International Journal of Nanomedicine*, *17*, 1111–1124. https://doi.org/10.2147/IJN.S353937

Thejeel, B., & Endo, Y. (2022a). Imaging of total hip arthroplasty: Part I – Implant design, imaging techniques, and imaging of component wear and fracture. In *Clinical Imaging*. Elsevier Inc. https://doi.org/10.1016/j.clinimag.2022.09.008

Thejeel, B., & Endo, Y. (2022b). Imaging of total hip arthroplasty: part II – imaging of component dislocation, loosening, infection, and soft tissue injury. In *Clinical Imaging* (Vol. 92, pp. 72–82). Elsevier Inc. https://doi.org/10.1016/j.clinimag.2022.09.011

Todo, M., & Fukuoka, K. (2020). Biomechanical Analysis of Femur with THA and RHA implants using CT-Image Based Finite Element Method. *Journal of Orthopaedics and Sports Medicine*, *02*(02). https://doi.org/10.26502/josm.511500024

Toh, S. M. S., Ashkanfar, A., English, R., Rothwell, G., Langton, D. J., & Joyce, T. J. (2023). How does bicycling affect the longevity of Total Hip Arthroplasty? A finite element wear analysis. *Journal of the Mechanical Behavior of Biomedical Materials*, *139*. https://doi.org/10.1016/j.jmbbm.2023.105673

Torini, A. P., Barsotti, C. E., Andrade, R. M., Nali, L. H. da S., & Ribeiro, A. P. (2023). Effect of Total Hip Arthroplasty with Ceramic Acetabular Component on Clinical, Radiographic and Functional Parameters in Older Patients with Hip Osteoarthritis: Two-Year Follow-Up. *Journal of Clinical Medicine*, *12*(2). https://doi.org/10.3390/jcm12020670

Upfill-Brown, A., Hsiue, P. P., Sekimura, T., Patel, J. N., Adamson, M., & Stavrakis, A. I. (2021). Instability Is the Most Common Indication for Revision Hip Arthroplasty in the United States: National Trends From 2012 to 2018. *Arthroplasty Today*, *11*, 88–101. https://doi.org/10.1016/j.artd.2021.08.001

Vogel, D., Wehmeyer, M., Kebbach, M., Heyer, H., & Bader, R. (2021). Stress and strain distribution in femoral heads for hip resurfacing arthroplasty with different materials: A finite element analysis. *Journal of the Mechanical Behavior of Biomedical Materials*, *113*. https://doi.org/10.1016/j.jmbbm.2020.104115

Wera, G. D., Ting, N. T., Moric, M., Paprosky, W. G., Sporer, S. M., & Della Valle, C. J. (2012). Classification and Management of the Unstable Total Hip Arthroplasty. *Journal of Arthroplasty*, *27*(5), 710–715. https://doi.org/10.1016/j.arth.2011.09.010

Xiao, Z., Wu, L., Wu, W., Tang, R., Dai, J., & Zhu, D. (2023). Multi-Scale Topology Optimization of Femoral Stem Structure Subject to Stress Shielding Reduce. *Materials*, *16*(8). https://doi.org/10.3390/ma16083151

Yavuz Solmaz, M., Hakki Sanliturk, I., Turgut, A., Dundar, S., & Topkaya, T. (2018). *Stress distribution in a femoral implant with and without bone cement and at different inclination angles*. 393–398. https://doi.org/10.3139/120.111163

Yee, A. H. F., Chan, V. W. K., Fu, H., Chan, P.-K., & Chiu, K. Y. (2024). Long- term follow- up of an uncemented proximally hydroxyapatite- coated femoral stem in total hip arthroplasty. *Bone Joint J*, *106*(3), 110–114. https://doi.org/10.1302/0301-620X.106B3

Yusof, M. S., Aznan, N., Fazli, N., Manan, A., Hisyam Marwan, S., Mazlan, M. H., & Abdullah, A. H. (2021). Effects of Varus and Sagittal Implant Positioning to the Stress Adaptation in Cementless Hip Arthroplasty. In *Malaysian Journal of Medicine and Health Sciences* (Vol. 17, Number SUPP13).

Zaghloul, A. (2018). Hip Joint: Embryology, Anatomy and Biomechanics. *Biomedical Journal of Scientific & Technical Research*, *12*(3). https://doi.org/10.26717/bjstr.2018.12.002267

Zhang, S., Chen, J. Y., Pang, H. N., Lo, N. N., Yeo, S. J., & Liow, M. H. L. (2021). Revision total hip arthroplasty is associated with poorer clinically meaningful improvements and patient satisfaction compared to primary total hip arthroplasty. *Journal of Orthopaedics*, *28*, 96–100. https://doi.org/10.1016/j.jor.2021.11.008

Zhu, Y., Li, H., Lyu, S., Shan, X., Jan, Y. K., & Ma, F. (2023). Stair-climbing wheelchair proven to maintain user's body stability based on AnyBody musculoskeletal model and finite element analysis. *PLoS ONE*, *18*(1 January). https://doi.org/10.1371/journal.pone.0279478

AUTHOR'S PROFILE

Zaitul Asyikin binti Aznan obtained Diploma in Biomedical Electronic Engineering from Kolej Kemahiran Tinggi MARA Ledang, Johor and Bachelor of Engineering (Biomedical) (Hons.) in 2017 from Flinders University, Australia. Her research interest includes Biomechanics and Finite Element Analysis.

LIST OF PUBLICATION:

Aznan, Z. A., Azahan, N. M. K., Marwan, S. H., Taufiqurrakhman, M., Pandit, H., Khan, T., & Abdullah, A. H. (2025). Effect of Implant Positioning in Cemented Hip Arthroplasty. Journal of Mechanical Engineering, 22(1), 90–103. https://doi.org/10.24191/jmeche.v22i1.2802

LAMPIRAN

JUDUL BAHAN:

EFFECTS OF SMALL ANGULAR VARIATIONS IN IMPLANT POSITIONING ON STABILITY OF CEMENTED TOTAL HIP ARTHROPLASTY